Doctoral Dissertation

Development of Vehicle Robots Based on System Modeling and System Identification

2014 July

Danai Phoaharuhansa

SHIBAURA INSTITUTE OF TECHNOLOGY

Dynamic Modeling and Motion Control on Holonomic and Non-holonomic Vehicle Robots

by

Danai Phaoharuhansa

A thesis submitted in partial fulfillment for the degree of
Doctoral degree

in the
Division of Functional Control Systems
Graduate School of Engineering and Science

September 2014

Abstract

Division of Functional Control Systems
Graduate School of Engineering and Science

Doctoral degree

by Danai Phaoharuhansa

This thesis investigates on development of advanced motion control system for mobile robots considering dynamic uncertainty, holonomic and non-holonomic problem, and multi-rate sampling problem, which remain in the current studies of literature. The mobile robots utilized in this research are a two wheeled inverted pendulum robot and a four wheeled omni-directional robot. Then, the development of the mobile robots in this thesis is all-around improvement relative to these problems. The problems, the contributions, the experiment and the results are described as follows;

Dynamic model is a mathematical model of a physical system in order to express locomotion of physical system. It is the most important part in motion control design. Then, this thesis considers the dynamic uncertainty effect to the control performance. To analysis the uncertainty, system modeling and system identification have been presented for improving and estimating the dynamic model. Considering the motion of wheeled inverted pendulum robot, the dynamic models in literature reviews are derive considering only rotation of wheel. In fact, the motion is produced by rotation of wheel and rotation of body with wheel. Thus, the presented dynamic model is derived with considering not only wheel-rotation but also body-rotation. Moreover, the system identification is introduced based on autoregressive with exogenous inputs model (ARX model), which does not concern about measurement uncertainty. It is an cause to make the error in the identification. For multiple input multiple output system (MIMO), the uncertainty on each degree of freedom effects to the identification result of other degrees of freedom.

To evaluate the control systems using odometry, Kinect is mounted in operating space in order to observe the locomotion of the robots so that the space can locate the locomotion of the robots. It is called intelligent space. By the way, the space can locate the robot locomotion precisely than the odometry based locomotion because some uncertainties may appear in the odometry such as slip motion and global positioning error. However, the uncertainties occur in the odometry but the robot position can be computed with high frequency than vision system. In additional, multi-rate control system has introduced to involve the locomotion from both sources such the intelligent space and the odometry based locomotion. The multi-rate control systems for holonomic and non-holonomic robots are dissimilar structure because the motion of non-holonomic robot is limited. Then, only position feedback is not enough to perform the robot on the trajectory. The trajectory tracking algorithm is included in the motion control to navigate non-holonomic robot on the trajectory. It is designed corresponding to non-holonomic constraint. Therefore, the multi-rate control systems for omni-directional robot and the inverted pendulum robot are contrast at the trajectory tracking algorithm.

Then, this thesis has introduced the new dynamic model of the inverted pendulum robot, the system identification considering low accuracy measurement, and the multi-rate control systems for holonomic and non-holonomic robots. The new dynamic model is improved by considering the rotation of body with wheel and autoregressive moving average with exogenous

and sensor disturbance model (ARMAXD model) was established in order to identify the linear model with low accuracy measurement. The sensor noise is assumed that it is the high frequency of the error between the output and the estimate output, which is derived by the estimate of the state matrix and the input matrix. Then, it is recognized as the members in the regressive vector so that the effective of the sensor noise is decreased in the identification result, which means that the identification accuracy is better. By the way, the multi-rate control systems were evaluated with the position estimators, which estimate the robot position by involving the robot positions from the intelligent space and the odometry. To track the trajectory, way point denotes desired position. It is slided on the trajectory, and then, the control system tracks the way point. It is called continuous tracking control (CT). For approaching the way point, omni-directional robot can perform on every degrees of freedom by sliding mode and the input torques of four wheels can be derived by the attractive force on world coordinate and Jacobian matrix. On the other hands, the inverted pendulum can not directly perform on sideway so that it approaches to the desired position by straight or curve motions in order to archive the way point at the flank of the robot. The trajectory tracking algorithm is evaluated to treat the curve motion. It transforms the distance error on world coordinate to the distance error on the vehicle fixed coordinate, and then the distance error is bounded by trigonometric functions. It seems the weight function that the priority of yawing is higher than the straight motion.

As the result, the presented dynamic model of the inverted pendulum robot is derived with considering new motion constraint and the new structure model is established as autoregressive moving average with exogenous and sensor disturbance (ARMAXD) model. The simulation of system identification and the experiment on friction compensation have corroborated that ARMAXD model can identify the robot system precisely than ARX model. Moreover, the experiment of the multi-rate control consists of the experiments of the multi-rate control for the omni-directional robot and the inverted pendulum robot. The simulation of trajectory tracking deals the tracking performance of vision feedback control and multi-rate control. It shows that the robot with the multi-rate control can approach to the end of the trajectory faster than vision feedback control. The experiment on the omni-directional robot and the inverted pendulum robot can track the trajectory successfully.

Acknowledgements

I would like to offer my special thanks to Prof. Shimada Akira, who is my supervisor. He has given many comments and supports during Doctoral course. My special thanks are also extended to Prof. Mizukawa Makoto, Prof. Matsuhira Nobuto, Prof. Uchimura Yutaka, Prof. Fujimoto Hiroshi, and also the officers at Shibaura Institute of Technology.

Contents

List of Figures

List of Tables

Chapter 1

Introduction

This thesis presents the motion control technology on the vehicle robots from the variety view points. Then this chapter consists of the background, the problems in literature reviews, the aim of the research, and technical contribution. The vehicle robots utilized in this research are a two wheeled inverted pendulum robot in Fig.2.1a and a four wheeled omni-directional robot in Fig.2.2a. They were selected to evaluate the presented control technologies as the suitable examples.

1.1 Background

Robotics is a branch of technology that it deals design, hardware construction, control, and application of robot. It requires the knowledge in several engineering fields such mechanical engineering, electronic engineering, and computer engineering. Thus, the knowledge in the field of robotics is variety and the aim of the development depends on developer viewpoint and proficient of developer. The development can classify to kinematic and dynamic system[1–8], motion control system[9–23], motion planning and trajectory tracking[24–33], intelligent task[34–39], and environment system[40–43]. The developers study about the kinematic and dynamic system, who focus on system modeling and system identification in order to improve the model corresponding to actual motion. To identify the dynamic model, the papers[1–8] introduces the identification method based on autoregressive exogenous model (ARX) with offline prediction[3–9]. It does not consider the uncertainty of the sensor measurements so that the identification results may not be high accuracy. By the way, the motion control systems are generally designed as feedback control system and vision system is used to perceive robot position[25, 26, 29, 32, 33] and it is often introduced to perform the robot in the space. It is called vision feedback control system or visual control system. Moreover, the motion planning and the trajectory tracking are rather essential parts of motion control system in order that the robots can

perform on the trajectory with obstacle avoidance. The intelligent task [19, 24, 29, 33, 42] is the functions of the robots in order that the robots can interact the human intention and they obtain the brilliant responsibility. Moreover, the environment system is designed to support humans and robots in the space. It obtains the function relative to localization, 3D map building, sharing information, and human interaction.

Generally, wheeled mobile robots can be classified to non-holonomic robots can beFtheef classified to non-holonomic robot [10, 16, 17, 21, 23, 26, 31] and holonomic robot[25, 32, 37, 38]. The development trend for the indoor wheeled mobile robot can be divided to two trends such intelligent robot trend[11, 12, 36] and service robot with intelligent space trend[19, 40, 42]. The intelligent robot is developed to service human in various purposes and it can interact with human directly. On the other hands, the service robot with intelligent space is that the robots are used in intelligent space [24, 29, 33, 41, 42, 44], which is evaluated to support the robot operation in the space as shown in Fig.1.1. It illustrates 3D structure of an intelligent space and concept idea of sharing information system of which the details are described in [19, 42], respectively. The activities in the space are observed by the space system, and then they are provided to each robot in the space so that the number of sensor in each robot can be reduced. Then, the trend of the service robots with intelligent spaces seems greater than general intelligent robot trend because the cost of each robot is reduced and the intelligent space can locate the locomotion of robots precisely than the odometry based locomotion.

To establish the intelligent space, camera is mounted at fixed-position in the space as shown in Fig.1.1, the camera presents space image in perspective view, which is non linear scale with actual position. Then, the robot position is identified in the image and it is converted to the actual space position by the perspective transformation, which is presented in [19, 42]. The advantage of vision feedback system is that the global position of the robot and other objects are identified precisely than odometry such as rotary encoder because the global position error may be occurred by wheel slip motion, which is included in the measurement data of rotary encoder. To solve this error, the papers[45–48] have introduced the other methodologies to estimate and suppress the wheel slip. The disadvantage is that the sampling interval of vision system is low, which effects to the responsibility and the performance of the robot.

1.2 Problem and Objective

According to literature papers[24–33], the problems in the literature reviews can be summarized to dynamic uncertainty, holonomic and non-holonomic problem, and multi-rate sampling problem. The problems can be classified to two sections as shown in Fig.1.2. They are dynamic uncertainty and multi-sampling rate.

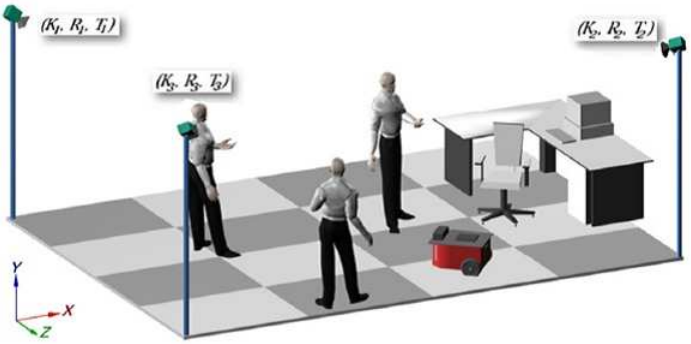

(A) 3D structure of the intelligent space[42].

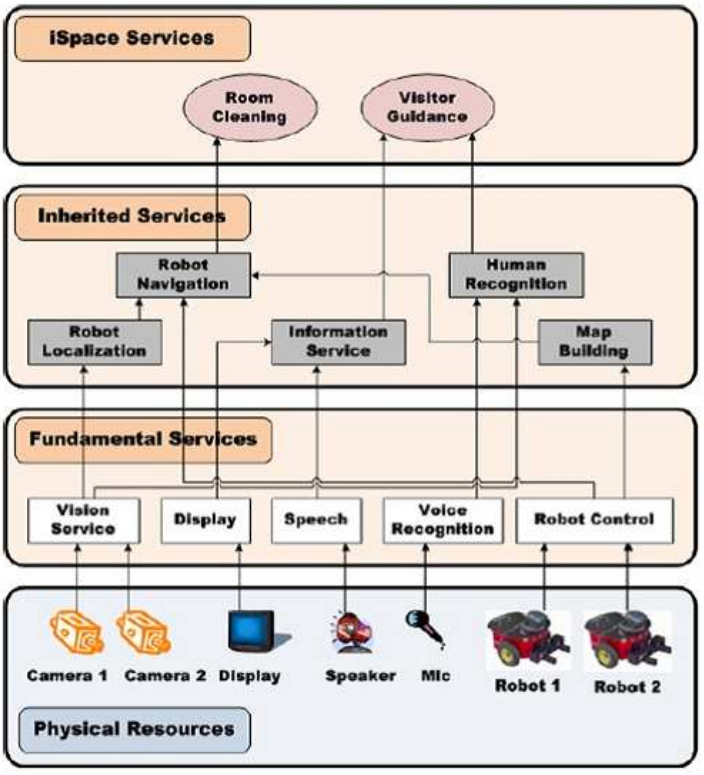

(B) The concept idea of sharing information in the intelligent space [19].

FIGURE 1.1: Concept of intelligent space in reference papers.

The dynamic uncertainty consists of system modeling error and system identification consider low accuracy sensor measurement. The motion of the inverted pendulum robot is considered that the straight motion is produced by rotation of wheel in Fig.1.3c and it can be measured by rotary encoder. In fact, the straight motion is generated by two rotations such as rotation of wheel relative to body in Fig.1.3c and rotation of wheel with body in Fig.1.3b, which can be measured by rotary encoder and IMU sensor, respectively. The summary of both rotations equals with the rotation of wheel relative to vertical axis. Then, the system modeling based on the assumption in the literatures is not precise model. By the way, the identification method in the literature is never considered the effectiveness of the sensor measurement, which exactly an important cause to make the error in the identification result.

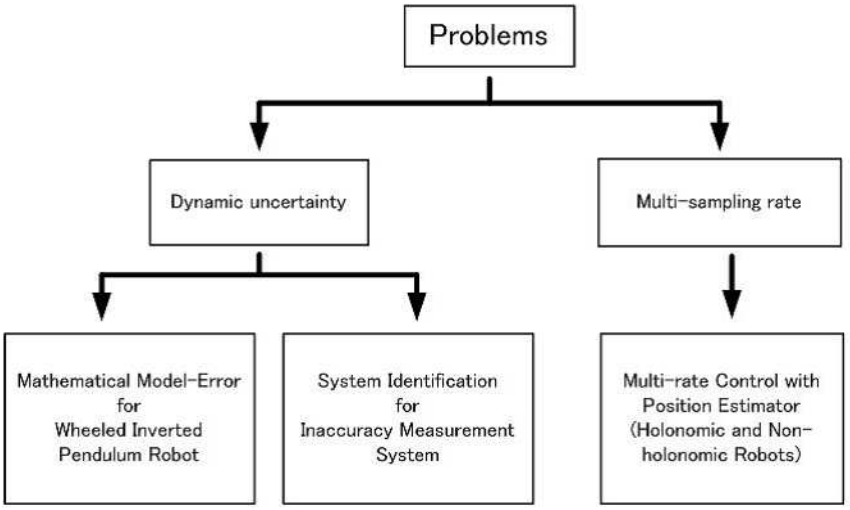

FIGURE 1.2: The figure illustrates the problems in the literature reviews.

Generally, sampling intervals of actuators and sensors are different intervals but many developers usually design control systems based on lowest sampling interval. For example, the control system is utilized with vision sensor, the control frequency is obtained as same as the frame rate of the vision system. However, the robot can approach the desired position but the performance may not be satisfied. To treat this problem, the control system is designed based on multi-rate control in order to treat the multiple sampled intervals. Moreover, the vehicle robots in this research are the inverted pendulum robot and the omni-directional robot, motions of which depends on non-holonomic and holonomic constraints. Thus, the multi-rate control systems for the both robots are designed considering the holonomic and non-holonomic constraints.

Therefore, this thesis aims to develop advanced motion control system for vehicle robots considering dynamic uncertainty, holonomic and non-holonomic problem, and multi-rate sampling problem. The dynamic models of the robots are improved by considering the actual motion and the system identification for inaccuracy sensor measurement is established to accurate the identification performance in practical. In additional, the control system for holonomic and non-holonomic robots are designed in view of multi-sampling interval.

1.3 Contribution

This thesis contributes to solve the problems of two types of vehicle robots such the dynamic modeling uncertainty, the system identification for the inaccuracy measurement system, and control system considering multi-sampling interval. The presented solution consists of theoretical analysis and experimental on friction compensation and multi-rate visual position control system for holonomic and non-holonomic robots. Therefore, the presented dynamic model of

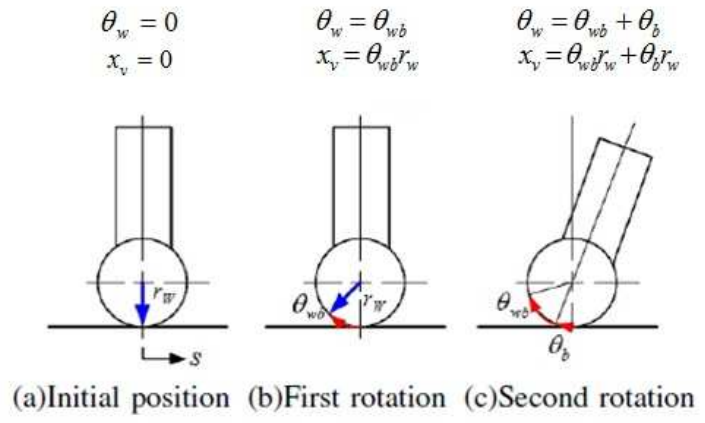

FIGURE 1.3: The straight motion of wheeled inverted pendulum robot.

the inverted pendulum robot is derived with considering not only wheel-rotation but also body-rotation. The consideration of their rotations directly effects to the dynamic uncertainty. By considering the both rotations, the dynamic model becomes the perfect dynamic model and the new structure model of system identification is created as autoregressive moving average with exogenous and sensor disturbance (ARMAXD) model in order to estimate the system concerning low accuracy sensor measurement. the estimate model is high accurate than autoregressive with exogenous (ARX) model, which is conventional and popular model. In additional, multi-rate control is created to solving the multi-sampling intervals. It becomes similar with the actual system and the performance is greater than vision feedback control.

1.4 Overview

The development in this thesis consists of system modeling and control system for holonomic and non holonomic robot. Then, the omni-directional robot and the inverted pendulum robots are suitable example to demonstrate the presented system modeling and the motion control technologies. The hardware construction of the robots are presented in Chapter 2 and Fig.1.4 expresses the content in this thesis to four parts such as system modeling, intelligent space, experiment on friction compensation, and experiment on multi-rate control for two types of vehicle robots.

The system modeling introduces the theoretical analysis relative to dynamic modeling and system identification in Chapter 2 and 3, subsequently. The dynamic models in literature reviews are derive considering only rotation of wheel. In fact, the motion is produced by rotation of wheel and rotation of body with wheel. Thus, the presented dynamic model is derived with considering not only wheel-rotation but also body-rotation. It seems nearby the actual dynamic than the dynamic model in the literature. The linear dynamic models of the both robots are

used to design the feedback gain by linear quadratic method. By the way, the system identification in the literature reviews have been introduced using autoregressive with exogenous inputs model (ARX), which does not concern about the sensor uncertainty, which is an cause to make the error in the identification. For multiple input multiple output system (MIMO), the uncertainty on each degree of freedom effects to the identification result of other degrees of freedom. Then, the thesis establishes autoregressive moving average with exogenous and sensor disturbance (ARMAXD) model, which is designed with concerning the effectiveness of the sensor disturbance. The structure and the derivation of ARMAXD model are modified based on two conventional models structures such autoregressive with exogenous inputs (ARX) model and autoregressive moving average with exogenous inputs (ARMAX) model. The prediction algorithm of ARMAXD model is minor modification of weight least mean square method to feedback the estimate sensor noise. The accuracy of ARMAXD model is compared with ARX model by simulation as shown in Chapter 3.

Secondly, the experiment on friction compensation control is designed to satisfy the identification results of ARMAXD model as presented in Chapter 4. It demonstrates by the inverted pendulum robot and the impulse response of the friction compensation controls, which are used the estimate friction coefficient of ARX and ARMAXD models. The controller is designed using the dynamic model without the friction so that the control performance can be indicated by the accuracy of the estimate friction. The result deals the performance of the friction compensation control using the estimate friction of ARX and ARMAXD models.

Thirdly, intelligent space is established to derive location of robot in the space as presented in Chapter 5. Kinect is mounted at the fixed position on the space and the host computer in the space will process Kinect's data by localization method, and then the result will be sent to the vehicle robots via rs-232 platform. The color marker is mounted at the robots for deriving the position and orientation so that the localization will identify the position and orientation of the vehicle robots by image processing technique and the distance vectors of the depth data are derived by projective vector in order to observe the size of the robots and other objects in the space.

Finally, multi-rate control systems are developed for two types of the robots such as the omni directional robot and the inverted pendulum robot. They are described in Chapter 6 and their motion constraints are holonomic and non-holonomic constraints, respectively. By the way, the omni directional robot can directly performs on all degrees of freedom but the inverted pendulum robot can perform only straight, pitching and yawing motions because the motion is bounded as described in non-holonomic constraint. Thus, the trajectory tracking algorithm is designed with considering non-holonomic constraint. Moreover, the operating space is covered by the soft material so that the huge slip motion appears in the odometry. Thus, the position

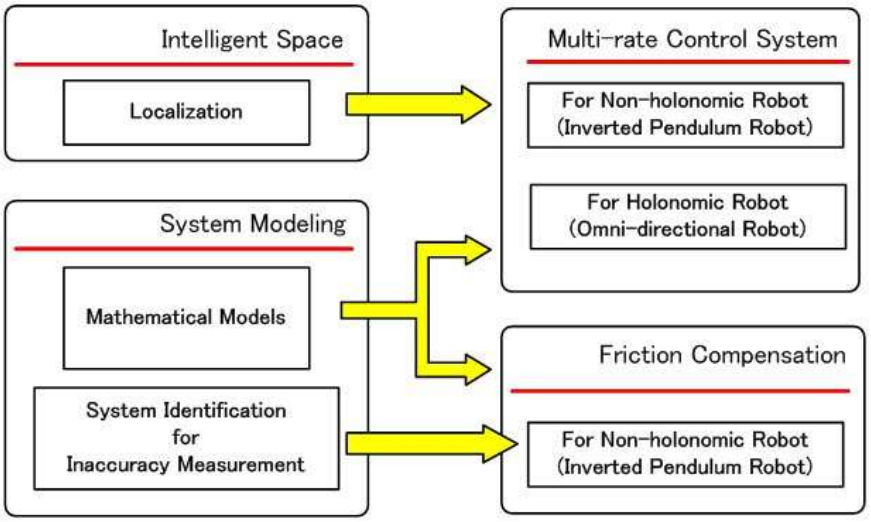

FIGURE 1.4: Overview of research.

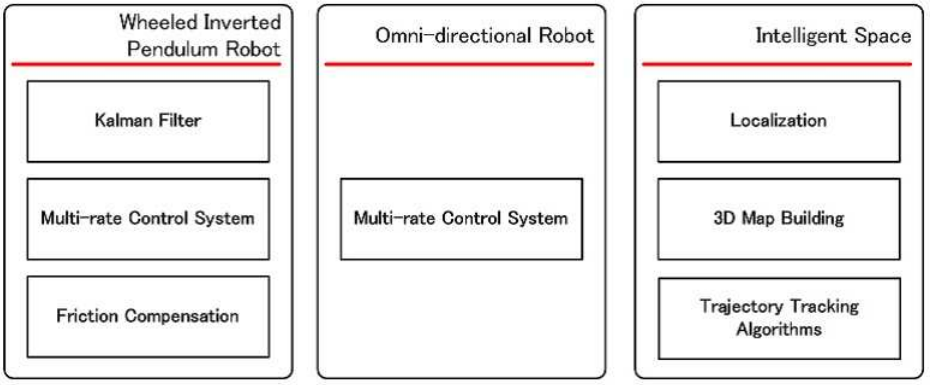

FIGURE 1.5: Task of wheeled inverted pendulum robot, omni-directional robot, and intelligent space.

estimator is also developed to predict the global position of the robots with high sampling rate. The result is satisfied by the simulation and the experiment, which are presented in Chapter 6.

As above sentences, Fig.1.5 describes the software task for the omni-directional robot, the inverted pendulum robot, and intelligent space. The inverted pendulum robot consists of three tasks such Kalman filter, multi-rate control system, and friction compensation. Kalman filter is basic task to estimate the tilt and angular velocity of body. Then, it is always used with the friction compensation and multi-rate control in chapter 3 and 5, respectively. By the way, the omni-directional robot is installed only multi-rate control to experiment in chapter 5. For intelligent space, it is mainly designed to navigate the robot position in the space. The function to navigate the robot consists of two tasks that localization is presented to derive the robot position and the trajectory tracking algorithm is the algorithm to determine the motion the non-holonomic robot.

Chapter 2

Dynamics

2.1 Introduction

This chapter introduces properties of vehicle robot in our experiment such as inverted pendulum robot and omni-directional robot. It is organized as follows; principal properties, hardware construction, kinematic and Jacobian matrix, equation of motion, state space model.

2.2 Hardware Construction

This section describes the construction for the two wheeled inverted pendulum robot, the omni-directional robot, and the intelligent space.

2.2.1 Two wheeled inverted pendulum robot

Two wheeled inverted pendulum robot is developed as shown in Fig.2.1a and the physical parameters of the robot is presented in Fig.2.1. The electronic system is presented in Fig.2.1b. IMU sensor consists of low-cost 3-axis accelerometer and gyro sensor. The data from IMU sensor is processed to derive tilt and angular velocity of body by Kalman filter. By the way, the data from rotary encoders are computed to locate the position of robot in a space. To perform the robot the 32-bit microprocessor generate digital command to DA converter in order to control the torque of motor by analog motor driver.

Fig.2.1 illustrates wheeled inverted pendulum robot and hardware configuration. The value of physical parameters for inverted pendulum robot in Fig.2.1(a) are presented in Table.2.1. To perform the robot, two rotary encoders and an inertial measurement unit (IMU) sensor are mounted at the robot. Rotary encoders detect the rotation of wheels and IMU sensor consists of

3-axis accelerometer and 3-axis gyro sensor, which measure acceleration and angular velocity of body of robot. Their data are sent to 32-bit microprocessor and it processes acceleration and angular velocity to derive tilt angle and pitching rate. Rotary encoder data are used to compute the position of robot in space. After that these data are feedback data for controller and sent the command to motor driver for controlling input torque. To treat tilt and pitching rate, we studied some papers[13, 49, 50], they investigated on how to reduce sensor uncertainty using complementary and Kalman filter. Then, we applied Kalman filter to estimate the tilt and pitching rate.

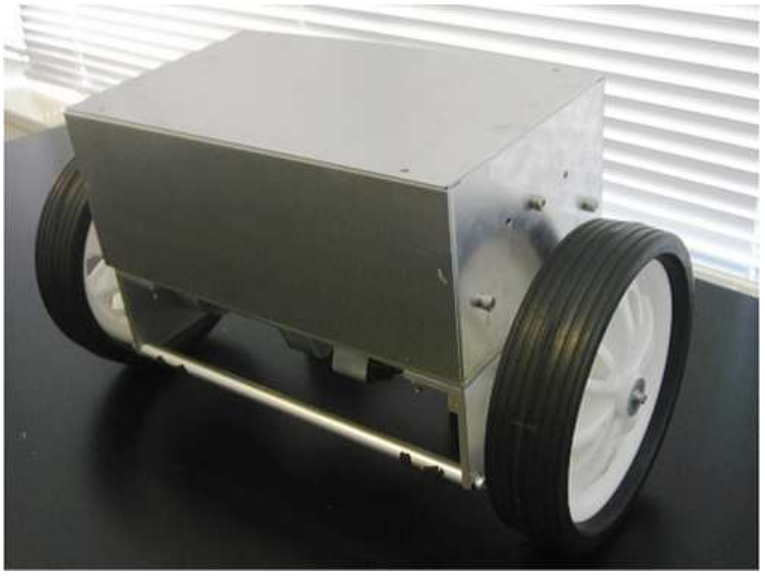

(A) Two wheeled inverted pendulum robot.

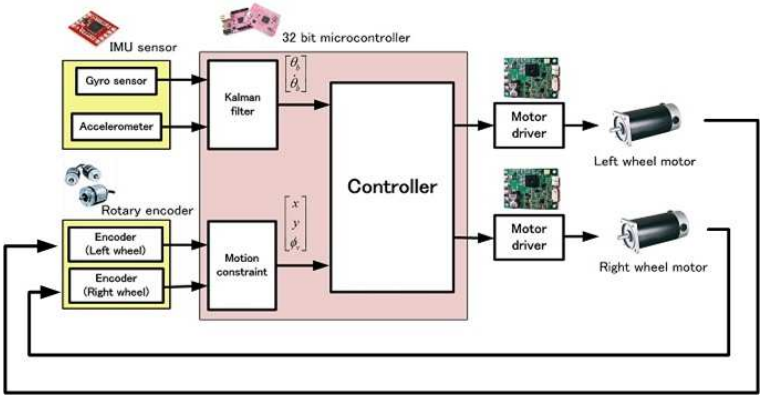

(B) Electronic system of the inverted pendulum robot.

FIGURE 2.1: Development of the non-holonomic robot in an intelligent space.

2.2.2 Omni-directional Robot

Omni-directional robot is developed as shown in Fig.2.2a and the physical parameters of the robot is presented in Fig.2.1. The electronic system is presented in Fig.2.2b. The data from

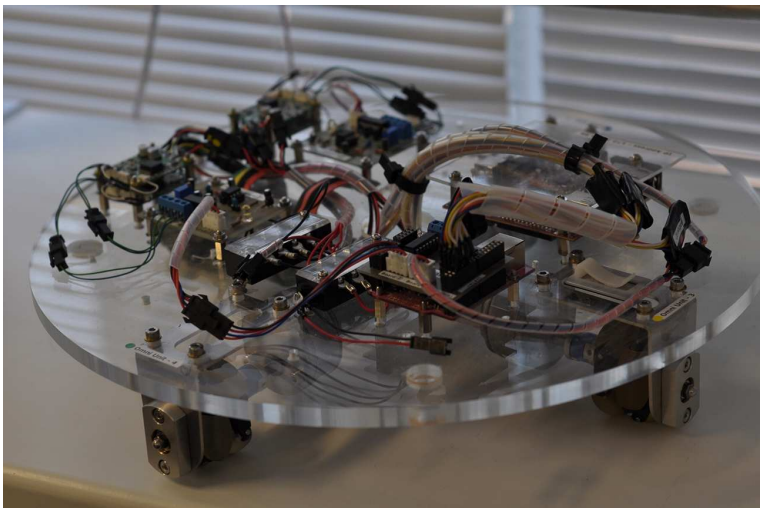

(A) Omni-directional robot.

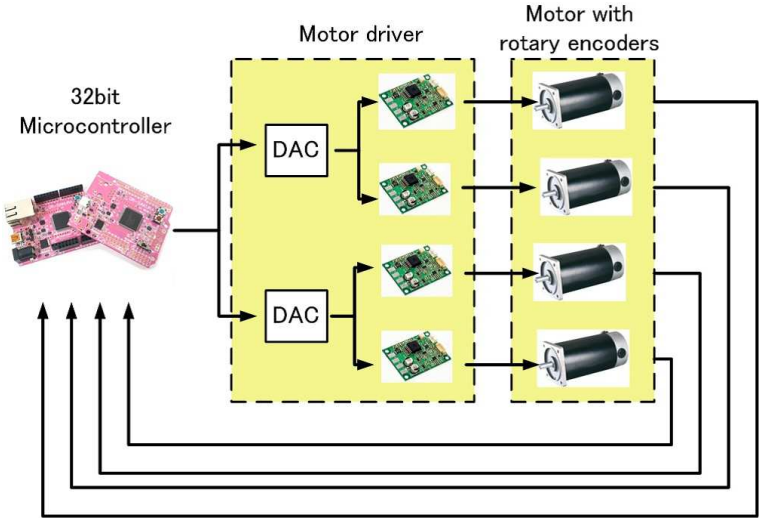

(B) Electronic system of omni-directional robot.

FIGURE 2.2: Development of the holonomic robot in an intelligent space.

TABLE 2.1: Physical parameters of the inverted pendulum robot

Parameters	Value	Unit
Body's mass (m_b)	3.5	$kg.$
Wheel's mass (m_w)	0.25	$kg.$
Inertia of body about pitching (I_{yy})	8.5×10^{-4}	$kg. \cdot m^2$
Inertia of body about yawing (I_{zz})	0.0255	$kg. \cdot m^2$
Inertia of wheel (I_w)	0.0013	$Kg.$
Inertia of rotor (I_r)	1.6×10^{-5}	$Kg.$
Distance of center of gravity (z)	0.04	$m.$
Width of robot (b)	0.4	$m.$
Radius of wheel (r_w)	0.08	$m.$
Gear ratio (n)	1/400	

rotary encoders are computed to locate the position of robot. To perform the robot the 32-bit microprocessor generate digital command to DA converter in order to control the torque of

motor by analog motor driver.

Omni-directional robot is four wheeled-type robot as shown in Fig.2.2(a) and it consists of omni-directional wheels, motors, motor drivers, digital/analog converters (DAC), and 32-bit microcontroller. To perform omni-directional robot, the microcontroller receives data from rotary encoders and compute global position and it send command to control motors via motor drivers. For the value of physical parameters, they are shown in Table.2.2.

TABLE 2.2: Physical parameters of omni-directional robot

Part	Value	Unit
Total weight (M_t)	7.31	$kg.$
Body width (B)	0.40	$m.$
Distance between wheel (b)	0.36	$m.$
Radius of wheel (r_w)	0.024	$m.$
Mass moment of inertia of robot (I_ϕ)	$7.29x10^{-5}$	$kg./m^2$
Mass moment of inertia of wheel (I_w)	$0.1x10^{-5}$	$kg./m^2$
Gear ratio (n)	1/9	-
Pulse number per round (G_c)	12	pulse/round

2.3 Two Wheeled Inverted Pendulum Mobile-type Robot

A two wheeled inverted pendulum mobile-type robot is classified in vehicle robot, which is used in our experiment. Then, this section introduces inverted pendulum system, hardware construction, equation of motion, and state space model.

2.3.1 Inverted Pendulum System

Principle of the robot is similar with inverted pendulum system and some kinds of inverted pendulum system are presented in Fig.2.3 such as prismatic-type, cart-type, and wheeled-type. However, position (x_v) is moved by the difference kind of actuator, but dynamic of them are similar and wheeled-type is developed to be mobile robot. In Fig.2.3, they are expressed in two dimensional degrees such x_v and θ_b. Equation of motion is well known as

$$\begin{bmatrix} M_c + m_b & m_b g l \cos\theta_b \\ m_b g l \cos\theta_b & J_T \end{bmatrix} \begin{bmatrix} \ddot{x}_v \\ \ddot{\theta}_b \end{bmatrix} + \begin{bmatrix} -m_b l \dot{\theta}_b^2 \sin\theta_b \\ -m_b g l \sin\theta_b \end{bmatrix} = \begin{bmatrix} 1 \\ 0 \end{bmatrix} f \tag{2.1}$$

where, f denotes input force. M_c and m_b denote mass of cart and inverted pendulum, respectively. J_T is mass moment of inertia about pitching axis. l denotes distance from pivot to center of gravity. x_v and θ_b are distance and tilt angle.

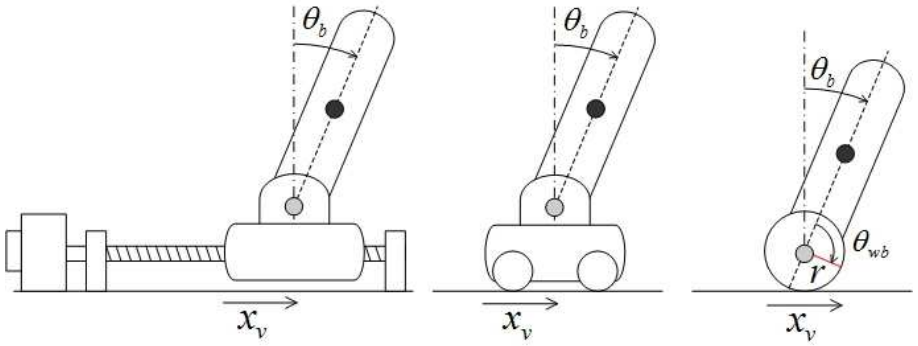

(a) Prismatic-type (b) Cart-type (c) Wheeled-type

FIGURE 2.3: Some kinds of inverted pendulum system.

2.3.2 Equation of Motion

As *S. Jeong and T. Takahashi* [11, 12] presented the method to derive equation of motion (EOM) by Lagrangian unknown multiplier. At first step, EOM is treated on generalized coordinate (q), $q = \begin{bmatrix} x & y & \phi_v & \theta_b & \theta_{wr} & \theta_{wl} \end{bmatrix}^T$, and then it is converted to a new coordinate using Lagrangian multiplier, which is introduced as an actual control variables so that it is called control coordinate (ν), $\nu = \begin{bmatrix} \dot{s} & \dot{\phi}_v & \dot{\theta}_b \end{bmatrix}^T$. Where, x and y denote position on x-axis and y-axis. ϕ_v denotes the yaw angle of the robot. θ_b denotes tilt angle of the body. θ_{wr} and θ_{wl} are rotation angle of the right and left wheels. s and $\dot{s}$ denote distance of the robot belong to trajectory and forwarding velocity, subsequently. The components of q are referred to world coordinate frame (Σ_W) and the components of ν are referred to the vehicle-fixed frame (Σ_V). Then, this section is organized as follow: kinematic constraints, Jacobian matrix, and the relationship of robot motion between world coordinate frame (Σ_W) and vehicle coordinate frame (Σ_V) are derived.

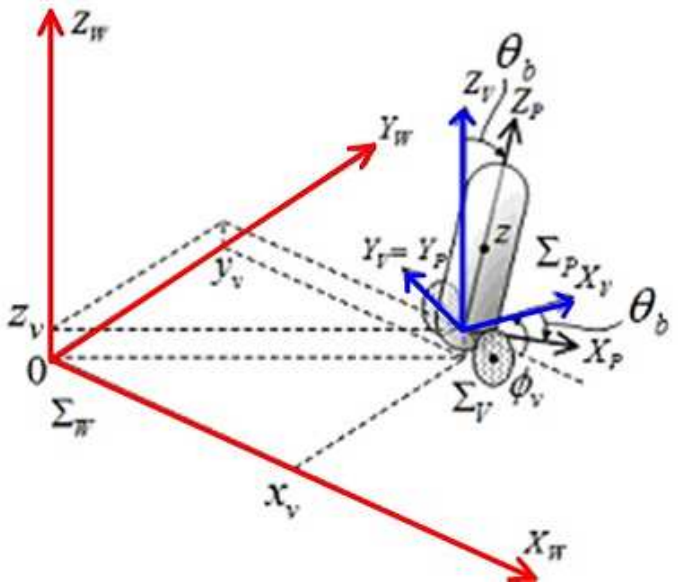

FIGURE 2.4: Two wheeled inverted pendulum robot on world coordinate frame (Σ_W) and vehicle coordinate frame (Σ_V).

2.3.2.1 Position and Velocity on World Coordinate Frame

Fig.2.4 exhibits motion of an inverted pendulum robot on Σ_W. The velocity of robot is derived by homogeneous transformation between Σ_W and Σ_V that

$$
\begin{aligned}
H_b^w &= H_v^w \cdot H_b^v \\
&= Trans(x_v, y_v, r)Rot(Z_v, \phi_v)Rot(Y_v, \theta_b) \\
&= \begin{bmatrix} 1 & 0 & 0 & x_v \\ 0 & 1 & 0 & y_v \\ 0 & 0 & 1 & z_v \\ 0 & 0 & 0 & 1 \end{bmatrix} \begin{bmatrix} \cos\phi_v & -\sin\phi_v & 0 & 0 \\ \sin\phi_v & \cos\phi_v & 0 & 0 \\ 0 & 0 & 1 & 0 \\ 0 & 0 & 0 & 1 \end{bmatrix} \begin{bmatrix} \cos\theta_b & 0 & \sin\theta_b & 0 \\ 0 & 1 & 0 & 0 \\ -\sin\theta_b & 0 & \cos\theta_b & 0 \\ 0 & 0 & 0 & 1 \end{bmatrix} \\
&= \begin{bmatrix} \cos\phi_v\cos\theta_b & -\sin\phi_v & \cos\phi_v\sin\theta_b & x_v \\ \sin\phi_v\cos\theta_b & \cos\phi_v & \sin\phi_v\sin\theta_b & y_v \\ -\sin\theta_b & 0 & \cos\theta_b & z_v \\ 0 & 0 & 0 & 1 \end{bmatrix} \\
&= \begin{bmatrix} R_b^w & p_v^w \\ 0_{1\times 3} & 1 \end{bmatrix} \in R^{4\times 4}
\end{aligned} \tag{2.2}
$$

where, p_v^w denotes position of robot based on Σ_W and R_b^w denotes rotation matrix of body. In additional, position of center of gravity based on Σ_W ($\bar{p}_c^w$) is given by

$$\begin{aligned}
\bar{p}_c^w &= H_b^w \cdot \bar{p}_c^b \\
&= \begin{bmatrix} \cos\phi_v\cos\theta_b & -\sin\phi_v & \cos\phi_v\sin\theta_b & x_v \\ \sin\phi_v\cos\theta_b & \cos\phi_v & \sin\phi_v\sin\theta_b & y_v \\ -\sin\theta_b & 0 & \cos\theta_b & r \\ 0 & 0 & 0 & 1 \end{bmatrix} \begin{bmatrix} 0 \\ 0 \\ z \\ 1 \end{bmatrix} \\
&= \begin{bmatrix} x_v + z \cdot \cos\phi_v\sin\theta_b \\ y_v + z \cdot \sin\phi_v\sin\theta_b \\ z \cdot \cos\theta_b + r \\ 1 \end{bmatrix} \in R^4
\end{aligned} \tag{2.3}$$

Translation velocity of body (v_b^w) at center of gravity is derived by

$$v_c^w = \begin{bmatrix} \dot{x}_v - z \cdot \sin\phi_v\sin\theta_b\dot{\phi}_v + z \cdot \cos\phi_v\cos\theta_b\dot{\theta}_b \\ \dot{y}_v + z \cdot \cos\phi_v\sin\theta_b\dot{\phi}_v + z \cdot \sin\phi_v\cos\theta_b\dot{\theta}_b \\ -z \cdot \sin\theta_b\dot{\theta}_b \end{bmatrix} \in R^3 \tag{2.4}$$

To derive angular velocity of body (ω_b^w) at center of gravity, it is computed by rotation matrix by

$$\omega_b^w = (\dot{R}_b^w R_b^{wT})^\vee \in R^3 \tag{2.5}$$

V operator is presented in [2] that

$$\begin{bmatrix} 0 & -\omega_z & \omega_y \\ \omega_z & 0 & \omega_x \\ -\omega_y & \omega_x & 0 \end{bmatrix}^\vee = \begin{bmatrix} \omega_x \\ \omega_y \\ \omega_z \end{bmatrix} \in R^3 \tag{2.6}$$

Thus, the angular velocity (ω_b^w) is

$$\begin{aligned}
\omega_b^w &= (\dot{R}_b^w R_b^{wT})^\vee \\
&= \begin{bmatrix} 0 & -\dot{\phi}_v & \cos\phi_v\dot{\theta}_b \\ \dot{\phi}_v & 0 & \sin\phi_v\dot{\theta}_b \\ -\cos\phi_v\dot{\theta}_b & -\sin\phi_v\dot{\theta}_b & 0 \end{bmatrix}^\vee \\
&= \begin{bmatrix} -\sin\phi_v\dot{\theta}_b \\ \cos\phi_v\dot{\theta}_b \\ \dot{\phi}_v \end{bmatrix} \in R^3
\end{aligned} \tag{2.7}$$

As summary, we know velocity of Σ_V, velocity of body (v_c^w) and angular velocity (ω_b^w) based on Σ_W as follows;

$$v_v^w = \begin{bmatrix} x_v \\ y_v \\ \phi_v \end{bmatrix} \tag{2.8}$$

$$v_b^w = \begin{bmatrix} \dot{x}_v - z \cdot \sin\phi_\mathrm{v}\sin\theta_\mathrm{b}\dot{\phi}_\mathrm{v} + \mathrm{z} \cdot \cos\phi_\mathrm{v}\cos\theta_\mathrm{b}\dot{\theta}_\mathrm{b} \\ \dot{y}_v + z \cdot \cos\phi_\mathrm{v}\sin\theta_\mathrm{b}\dot{\phi}_\mathrm{v} + \mathrm{z} \cdot \sin\phi_\mathrm{v}\cos\theta_\mathrm{b}\dot{\theta}_\mathrm{b} \\ -z \cdot \sin\theta_\mathrm{b}\dot{\theta}_\mathrm{b} \end{bmatrix} \tag{2.9}$$

$$\omega_b^w = \begin{bmatrix} -\sin\phi_\mathrm{v}\dot{\theta}_\mathrm{b} \\ \cos\phi_\mathrm{v}\dot{\theta}_\mathrm{b} \\ \dot{\phi}_v \end{bmatrix} \tag{2.10}$$

2.3.2.2 Mass Moment of Inertia

Generally, mass moment of inertia can computed by shape of mass but it refers on vehicle-fixed coordinate frame (Σ_V). In order to derive equation of motion based on world coordinate frame (Σ_W), it has to converted the reference frame to Σ_W as follows;

Mass moment of inertia of body (I_{cm}^w) at center of gravity based on Σ_W :

$$\begin{aligned} I_{cm}^w &= R_b^w I_{cm}^b R_b^{wT} \\ &= \begin{bmatrix} \mathrm{c}\phi_\mathrm{v}\mathrm{c}\theta_\mathrm{b} & -\mathrm{s}\phi_\mathrm{v} & \mathrm{c}\phi_\mathrm{v}\mathrm{s}\theta_\mathrm{b} \\ \mathrm{s}\phi_\mathrm{v}\mathrm{c}\theta_\mathrm{b} & \mathrm{c}\phi_\mathrm{v} & \mathrm{s}\phi_\mathrm{v}\mathrm{s}\theta_\mathrm{b} \\ -\mathrm{s}\theta_\mathrm{b} & 0 & \mathrm{c}\theta_\mathrm{b} \end{bmatrix} \begin{bmatrix} I_{xx} & 0 & 0 \\ 0 & I_{yy} & 0 \\ 0 & 0 & I_{zz} \end{bmatrix} \begin{bmatrix} \mathrm{c}\phi_\mathrm{v}\mathrm{c}\theta_\mathrm{b} & \mathrm{s}\phi_\mathrm{v}\mathrm{c}\theta_\mathrm{b} & -\mathrm{s}\theta_\mathrm{b} \\ -\mathrm{s}\phi_\mathrm{v} & \mathrm{c}\phi_\mathrm{v} & 0 \\ \mathrm{c}\phi_\mathrm{v}\mathrm{s}\theta_\mathrm{b} & \mathrm{s}\phi_\mathrm{v}\mathrm{s}\theta_\mathrm{b} & \mathrm{c}\theta_\mathrm{b} \end{bmatrix} \\ &= \begin{bmatrix} I_{11}^w(\phi_v,\theta_b) & I_{12}^w(\phi_v,\theta_b) & I_{13}^w(\phi_v,\theta_b) \\ I_{21}^w(\phi_v,\theta_b) & I_{22}^w(\phi_v,\theta_b) & I_{23}^w(\phi_v,\theta_b) \\ I_{31}^w(\phi_v,\theta_b) & I_{32}^w(\phi_v,\theta_b) & I_{33}^w(\phi_v,\theta_b) \end{bmatrix} \end{aligned} \tag{2.11}$$

here, I_{cm}^b denotes moment of inertia based on vehicle-fixed coordinate,
$I_{cm}^b = \begin{bmatrix} I_{xx} & 0 & 0 \\ 0 & I_{yy} & 0 \\ 0 & 0 & I_{zz} \end{bmatrix} \in R^{3\times3}$. I_{xx},I_{yy},I_{zz} denote moment of inertia about X, Y, and Z axis, respectively. $I_{x-z} = I_{xx} - I_{zz}$,

$I_{11}^w(\phi_v,\theta_b) = I_{xx}\mathrm{c}^2\phi_\mathrm{v}\mathrm{c}^2\theta_\mathrm{b} + \mathrm{I}_{yy}\mathrm{s}^2\phi_\mathrm{v} + \mathrm{I}_{zz}\mathrm{c}^2\phi_\mathrm{v}\mathrm{s}^2\theta_\mathrm{b}$,

$\mathrm{I}_{12}^w(\phi_\mathrm{v},\theta_\mathrm{b}) = \mathrm{I}_{21}^w(\phi_\mathrm{v},\theta_\mathrm{b}) = \mathrm{c}\phi_\mathrm{v}\mathrm{s}\phi_\mathrm{v}\left(\mathrm{I}_{xx}\,\mathrm{c}^2\theta_\mathrm{b} - \mathrm{I}_{yy} + \mathrm{I}_{zz}\mathrm{s}^2\theta_\mathrm{b}\right)$,

$\mathrm{I}_{22}^w(\phi_\mathrm{v},\theta_\mathrm{b}) = \mathrm{I}_{xx}\mathrm{s}^2\phi_\mathrm{v}\mathrm{c}^2\theta_\mathrm{b} + \mathrm{I}_{yy}\mathrm{c}^2\phi_\mathrm{v} + \mathrm{I}_{zz}\mathrm{s}^2\phi_\mathrm{v}\mathrm{s}^2\theta_\mathrm{b}$,

$\mathrm{I}_{13}^w(\phi_\mathrm{v},\theta_\mathrm{b}) = \mathrm{I}_{31}^w(\phi_\mathrm{v},\theta_\mathrm{b}) = -\mathrm{I}_{x-z}\mathrm{c}\phi_\mathrm{v}\mathrm{c}\theta_\mathrm{b}\mathrm{s}\theta_\mathrm{b}$,

$\mathrm{I}_{23}^w = \mathrm{I}_{32}^w = -\mathrm{I}_{x-z}\mathrm{s}\phi_\mathrm{v}\mathrm{c}\theta_\mathrm{b}\mathrm{s}\theta_\mathrm{b}$,

$\mathrm{I}_{33}^{\mathrm{w}}(\phi_{\mathrm{v}}, \theta_{\mathrm{b}}) = \mathrm{I}_{\mathrm{xx}}\mathrm{s}^2\theta_{\mathrm{b}} + \mathrm{I}_{\mathrm{zz}}\mathrm{c}^2\theta_{\mathrm{b}}$

Mass moment of inertia of wheel (I_{wh}^{w}) at center of gravity based on Σ_w :

$$I_{wh}^{w} = R_b^w I_{wh}^b R_{wh}^{wT} = R_v^w (R_b^v I_{wh}^b R_b^{vT}) R_v^{wT} = R_v^w I_{wh}^v R_v^{wT} \tag{2.12}$$

$$I_{wh}^{w} = R_v^w I_{wh}^v R_v^{wT} = \begin{bmatrix} \mathrm{c}\phi_{\mathrm{v}} & -\mathrm{s}\phi_{\mathrm{v}} & 0 \\ \mathrm{s}\phi_{\mathrm{v}} & \mathrm{c}\phi_{\mathrm{v}} & 0 \\ 0 & 0 & 1 \end{bmatrix} \begin{bmatrix} I_{wx} & 0 & 0 \\ 0 & I_{wy} & 0 \\ 0 & 0 & I_{wz} \end{bmatrix} \begin{bmatrix} \mathrm{c}\phi_{\mathrm{v}} & \mathrm{s}\phi_{\mathrm{v}} & 0 \\ -\mathrm{s}\phi_{\mathrm{v}} & \mathrm{c}\phi_{\mathrm{v}} & 0 \\ 0 & 0 & 1 \end{bmatrix}$$

$$= \begin{bmatrix} I_{wx}\mathrm{c}^2\phi_{\mathrm{v}} + \mathrm{I}_{\mathrm{wy}}\mathrm{s}^2\phi_{\mathrm{v}} & (I_{wx} - I_{wy})\mathrm{s}\phi_{\mathrm{v}}\mathrm{c}\phi_{\mathrm{v}} & 0 \\ (I_{wx} - I_{wy})\mathrm{s}\phi_{\mathrm{v}}\mathrm{c}\phi_{\mathrm{v}} & I_{wx}\mathrm{s}^2\phi_{\mathrm{v}} + \mathrm{I}_{\mathrm{wy}}\mathrm{c}^2\phi_{\mathrm{v}} & 0 \\ 0 & 0 & I_{wz} \end{bmatrix} \tag{2.13}$$

here, I_{wh}^b denotes moment of inertia relative to body, $I_{wh}^b = \begin{bmatrix} I_{wx} & 0 & 0 \\ 0 & I_{wy} & 0 \\ 0 & 0 & I_{wz} \end{bmatrix} \in R^{3\times3}$. I_{wx},I_{wy},I_{wz} denote moment of inertia of wheel about X, Y, and Z axis, respectively and $I_{wx} = I_{wz}$.

Mass moment of inertia of rotor (I_r^w) at center of gravity based on Σ_W :

$$I_r^w = \begin{bmatrix} I_{rx}\mathrm{c}^2\phi_{\mathrm{v}} + \mathrm{I}_{\mathrm{ry}}\mathrm{s}^2\phi_{\mathrm{v}} & (I_{rx} - I_{ry})\mathrm{s}\phi_{\mathrm{v}}\mathrm{c}\phi_{\mathrm{v}} & 0 \\ (I_{rx} - I_{ry})\mathrm{s}\phi_{\mathrm{v}}\mathrm{c}\phi_{\mathrm{v}} & I_{rx}\mathrm{s}^2\phi_{\mathrm{v}} + \mathrm{I}_{\mathrm{ry}}\mathrm{c}^2\phi_{\mathrm{v}} & 0 \\ 0 & 0 & I_{rz} \end{bmatrix} \tag{2.14}$$

here, I_{rx},I_{ry},I_{rz} denote moment of inertia of rotor about X, Y, and Z axis.

2.3.2.3 Equation of Motion Based on World Coordinate Frame

As above sentences, we know the position, velocity, mass moment of inertia of each part relative to world coordinate frame. Then, equation of motion can be derived by Lagrangian equation as follows;

$$L = T - U \tag{2.15}$$

$$\frac{d}{dt}\frac{\partial L}{\partial \dot{q}} - \frac{\partial L}{\partial q} = \frac{\partial W}{\partial q}\tau \tag{2.16}$$

where, L denotes Lagrangian equation. T and U denote kinetic and potential energies of system. $q = \begin{bmatrix} x & y & \phi_v & \theta_b & \theta_{wr} & \theta_{wl} \end{bmatrix}^T$ and inertia matrix (M_{bw}) is defined as $M_{bw} = \begin{bmatrix} m_{bw} & 0 & 0 \\ 0 & m_{bw} & 0 \\ 0 & 0 & m_{bw} \end{bmatrix} \in R^{3\times3}$, m_{bw} denotes mass of body and wheels.

Kinetic Energy : It consists of four parts that kinetic energy of translation for wheel and body and kinetic energy of rotation for for wheel and body . Kinetic energy of wheels considering at the middle of both wheels is given by

$$\begin{aligned} K_{wt} = & \quad \frac{1}{2}\dot{p}_v^{wT} M_{bw} \dot{p}_v^w \\ = & \quad \frac{1}{2} m_{bw}(\dot{x}_v^2 + \dot{y}_v^2 \end{aligned} \tag{2.17}$$

Kinetic energy of body for translation motion is derived as

$$\begin{aligned} K_{pt} = & \quad \frac{1}{2} v_c^{wT} M_{bw} v_c^w \\ = & \quad \frac{1}{2} m_{bw}(\dot{x}_v^2 + \dot{y}_v^2 + z^2\dot{\theta}_b^2 + z^2 \mathrm{s}^2\theta_\mathrm{b}\dot{\phi}_\mathrm{v}^2) + \mathrm{m_{bw}} z \mathrm{c}\theta_\mathrm{b}\dot{\theta}_\mathrm{b}(\dot{\mathrm{x}}_\mathrm{v}\mathrm{c}\phi_\mathrm{v} + \dot{\mathrm{y}}_\mathrm{v}\mathrm{s}\phi_\mathrm{v}) \\ & + m_{bw} z \mathrm{s}\theta_\mathrm{b}\dot{\phi}_\mathrm{v}(-\dot{\mathrm{x}}_\mathrm{v}\mathrm{s}\phi_\mathrm{v} + \dot{\mathrm{y}}_\mathrm{v}\mathrm{c}\phi_\mathrm{v}) \end{aligned} \tag{2.18}$$

Kinetic energy of body for rotation motion is derived as

$$\begin{aligned} K_{pb} = & \quad \frac{1}{2} \omega_b^{wT} I_{cm}^w \omega_b^w \\ = & \quad \frac{1}{2} \begin{bmatrix} -\mathrm{s}\phi_\mathrm{v}\dot{\theta}_\mathrm{b} \\ \mathrm{c}\phi_\mathrm{v}\dot{\theta}_\mathrm{b} \\ \dot{\phi}_v \end{bmatrix}^T \begin{bmatrix} I_{11}^w(\phi_v,\theta_b) & I_{12}^w(\phi_v,\theta_b) & I_{13}^w(\phi_v,\theta_b) \\ I_{21}^w(\phi_v,\theta_b) & I_{22}^w(\phi_v,\theta_b) & I_{23}^w(\phi_v,\theta_b) \\ I_{31}^w(\phi_v,\theta_b) & I_{32}^w(\phi_v,\theta_b) & I_{33}^w(\phi_v,\theta_b) \end{bmatrix} \begin{bmatrix} -\mathrm{s}\phi_\mathrm{v}\dot{\theta}_\mathrm{b} \\ \mathrm{c}\phi_\mathrm{v}\dot{\theta}_\mathrm{b} \\ \dot{\phi}_v \end{bmatrix} \\ = & \quad \frac{1}{2} I_{yy}\dot{\theta}_b^2 + \frac{1}{2}(I_{xx}\mathrm{s}^2\theta_\mathrm{b} + \mathrm{I_{zz}}\mathrm{c}^2\theta_\mathrm{b})\dot{\phi}_\mathrm{v}^2 \end{aligned} \tag{2.19}$$

where, I^w_{cm} denotes mass moment of inertia of body based on world coordinate frame. Kinetic energy of right wheel (K_{pwr}) and left wheel (K_{pwl}) is derived as

$$\begin{aligned}
K_{pwr} &= \frac{1}{2}\omega^{wT}_{whr} I^w_{wh} \omega^w_{whr} \\
&= \frac{1}{2}\begin{bmatrix} -\mathrm{s}\phi_v(\dot{\theta}_{wbr}+\dot{\theta}_b) \\ \mathrm{c}\phi_v(\dot{\theta}_{wbr}+\dot{\theta}_b) \\ \dot{\phi}_v \end{bmatrix}^T \begin{bmatrix} I_{wx}\mathrm{c}^2\phi_v + I_{wy}\mathrm{s}^2\phi_v & (I_{wx}-I_{wy})\mathrm{s}\phi_v\mathrm{c}\phi_v & 0 \\ (I_{wx}-I_{wy})\mathrm{s}\phi_v\mathrm{c}\phi_v & I_{wx}\mathrm{s}^2\phi_v + I_{wy}\mathrm{c}^2\phi_v & 0 \\ 0 & 0 & I_{wz} \end{bmatrix} \begin{bmatrix} -\mathrm{s}\phi_v(\dot{\theta}_{wbr}+\dot{\theta}_b) \\ \mathrm{c}\phi_v(\dot{\theta}_{wbr}+\dot{\theta}_b) \\ \dot{\phi}_v \end{bmatrix} \\
&= \frac{1}{2}\{I_{wy}\mathrm{s}^2\phi_v^2(\dot{\theta}_{wbr}+\dot{\theta}_b)^2 + I_{wy}\mathrm{c}^2\phi_v^2(\dot{\theta}_{wbr}+\dot{\theta}_b)^2 + I_{wz}\dot{\phi}_v^2\} \qquad (2.20) \\
&= \frac{1}{2}\{I_{wy}(\dot{\theta}_{wbr}+\dot{\theta}_b)^2 + I_{wz}\dot{\phi}_v^2\} \qquad (2.21) \\
K_{pwl} &= \frac{1}{2}\{I_{wy}(\dot{\theta}_{wbl}+\dot{\theta}_b)^2 + I_{wz}\dot{\phi}_v^2\} \qquad (2.22) \\
& \qquad (2.23)
\end{aligned}$$

Summary of kinetic energy is computed by

$$\begin{aligned}
K_p &= K_{pt} + K_{pb} + (K_{pwr} + K_{pwl}) + (K_{prr} + K_{prl}) \\
&= \frac{1}{2}m_{bw}(\dot{x}_v^2 + \dot{y}_v^2 + z^2\dot{\theta}_b^2 + z^2 s^2\theta_b\dot{\phi}_v^2) + m_{bw}z\mathrm{c}\theta_b\dot{\theta}_b(\dot{x}_v\mathrm{c}\phi_v + \dot{y}_v s\phi_v) + m_{bw}zs\theta_b\dot{\phi}_v(-\dot{x}_v\mathrm{s}\phi_v + \dot{y}_v\mathrm{c}\phi_v) \\
&\quad + \frac{1}{2}I_{yy}\dot{\theta}_b^2 + \frac{1}{2}(I_{xx}s^2\theta_b + I_{zz}c^2\theta_b)\dot{\phi}_v^2 \\
&\quad + \frac{1}{2}\{I_{wy}(\dot{\theta}_{wbr}+\dot{\theta}_b)^2 + I_{wz}\dot{\phi}_v^2\} + \frac{1}{2}\{I_{wy}(\dot{\theta}_{wbl}+\dot{\theta}_b)^2 + I_{wz}\dot{\phi}_v^2\} \\
&\quad + \frac{1}{2}\{I_{ry}(n\dot{\theta}_{wbr}+\dot{\theta}_b)^2 + I_{rz}\dot{\phi}_v^2\} + \frac{1}{2}\{I_{ry}(n\dot{\theta}_{wbl}+\dot{\theta}_b)^2 + I_{rz}\dot{\phi}_v^2\} \\
&= \frac{1}{2}m_{bw}(\dot{x}_v^2 + \dot{y}_v^2 + z^2\dot{\theta}_b^2 + z^2 s^2\theta_b\dot{\phi}_v^2) + m_{bw}z\mathrm{c}\theta_b\dot{\theta}_b(\dot{x}_v\mathrm{c}\phi_v + \dot{y}_v s\phi_v) + m_{bw}zs\theta_b\dot{\phi}_v(-\dot{x}_v\mathrm{s}\phi_v + \dot{y}_v\mathrm{c}\phi_v) \\
&\quad + \frac{1}{2}I_{yy}\dot{\theta}_b^2 + \frac{1}{2}(I_{xx}s^2\theta_b + I_{zz}c^2\theta_b)\dot{\phi}_v^2 \\
&\quad + \frac{1}{2}(I_{wy} + n^2 I_{ry})(\dot{\theta}_{wbr}^2 + \dot{\theta}_{wbl}^2) + (I_{wy} + I_{ry})\dot{\theta}_b^2 + (I_{wy} + nI_{ry})\dot{\theta}_b(\dot{\theta}_{wbr} + \dot{\theta}_{wbl}) + (I_{wz} + I_{rz})\dot{\phi}_v^2 \\
&= \frac{1}{2}m_{bw}(\dot{x}_v^2 + \dot{y}_v^2) + \frac{1}{2}\{m_{bw}z^2 + I_{yy} + 2(I_{wy} + I_{ry})\}\dot{\theta}_b^2 \\
&\quad + \frac{1}{2}\{(m_{bw}z^2 + I_{xx})s^2\theta_b + I_{zz}c^2\theta_b + (I_{wz} + I_{rz})\}\dot{\phi}_v^2 \\
&\quad + m_{bw}z\mathrm{c}\theta_\mathrm{b}\dot{\theta}_\mathrm{b}(\dot{\mathrm{x}}_\mathrm{v}\mathrm{c}\phi_\mathrm{v} + \dot{\mathrm{y}}_\mathrm{v}\mathrm{s}\phi_\mathrm{v}) + \mathrm{m}_\mathrm{bw}\mathrm{zs}\theta_\mathrm{b}\dot{\phi}_\mathrm{v}(-\dot{\mathrm{x}}_\mathrm{v}\mathrm{s}\phi_\mathrm{v} + \dot{\mathrm{y}}_\mathrm{v}\mathrm{c}\phi_\mathrm{v}) \\
&\quad + \frac{1}{2}(I_{wy} + n^2 I_{ry})(\dot{\theta}_{wbr}^2 + \dot{\theta}_{wbl}^2) + (I_{wy} + nI_{ry})\dot{\theta}_b(\dot{\theta}_{wbr} + \dot{\theta}_{wbl}) \qquad (2.24)
\end{aligned}$$

Potential Energy : Potential of body at center of gravity is

$$U_{pb} = m_b(r + z\mathrm{c}\theta_\mathrm{b})\mathrm{g} \qquad (2.25)$$

Lagrangian equation : According to Eq. (2.24) and (2.25), Lagrangian equation is

$$\begin{aligned} L_p &= K_p - U_{pb} = K_{pt} + K_{pb} + (K_{pwr} + K_{pwl}) + (K_{prr} + K_{prl}) - U_{pb} \\ &= \frac{1}{2}m_{bw}(\dot{x}_v^2 + \dot{y}_v^2) + \frac{1}{2}\{m_{bw}z^2 + I_{yy} + 2(I_{wy} + I_{ry})\}\dot{\theta}_b^2 \\ &\quad + \frac{1}{2}\{(m_{bw}z^2 + I_{xx})\mathrm{s}^2\theta_b + I_{zz}\mathrm{c}^2\theta_b + (I_{wz} + I_{rz})\}\dot{\phi}_v^2 \\ &\quad + m_{bw}z\mathrm{c}\theta_b\dot{\theta}_b(\dot{x}_v\mathrm{c}\phi_v + \dot{y}_v s\phi_v) + m_{bw}z s\theta_b\dot{\phi}_v(-\dot{x}_v\mathrm{s}\phi_v + \dot{y}_v\mathrm{c}\phi_v) \\ &\quad + \frac{1}{2}(I_{wy} + n^2 I_{ry})(\dot{\theta}_{wbr}^2 + \dot{\theta}_{wbl}^2) + (I_{wy} + nI_{ry})\dot{\theta}_b(\dot{\theta}_{wbr} + \dot{\theta}_{wbl}) - m_b(r + z\mathrm{c}\theta_\mathrm{b})\mathrm{g} \end{aligned} \tag{2.26}$$

From Eq.(2.67), equation of motion based on q variables can be expressed by

$$M\ddot{q} + V(q, \dot{q}) + G(q) = E\tau \tag{2.27}$$

$$\begin{bmatrix} m_{bw} & 0 & m_{13} & m_{14} & 0 & 0 \\ 0 & m_{bw} & m_{23} & m_{24} & 0 & 0 \\ m_{31} & m_{32} & m_{33} & 0 & 0 & 0 \\ m_{41} & m_{42} & 0 & m_{44} & m_{45} & m_{46} \\ 0 & 0 & 0 & m_{54} & m_{55} & 0 \\ 0 & 0 & 0 & m_{64} & 0 & m_{66} \end{bmatrix} \begin{bmatrix} \ddot{x} \\ \ddot{y} \\ \ddot{\phi}_v \\ \ddot{\theta}_b \\ \ddot{\theta}_{wbr} \\ \ddot{\theta}_{wbl} \end{bmatrix} + \begin{bmatrix} v_1(q, \dot{q}) \\ v_2(q, \dot{q}) \\ v_3(q, \dot{q}) \\ v_4(q, \dot{q}) \\ 0 \\ 0 \end{bmatrix} + \begin{bmatrix} 0 \\ 0 \\ 0 \\ g_4(q) \\ 0 \\ 0 \end{bmatrix} = \begin{bmatrix} 0 & 0 \\ 0 & 0 \\ 0 & 0 \\ 0 & 0 \\ 1 & 0 \\ 0 & 1 \end{bmatrix} \begin{bmatrix} \tau_{wbr} \\ \tau_{wbl} \end{bmatrix} \tag{2.28}$$

where, $m_{13} = m_{31} = -m_{bw}z\mathrm{s}\theta_b\mathrm{s}\phi_v$,

$m_{14} = m_{41} = m_{bw}z\mathrm{c}\theta_b\mathrm{c}\phi_v$,

$m_{23} = m_{32} = m_{bw}z\mathrm{s}\theta_b\mathrm{c}\phi_v$,

$m_{24} = m_{42} = m_{bw}z\mathrm{c}\theta_b\mathrm{s}\phi_v$,

$m_{33} = (m_{bw}z^2 + I_{xx})\mathrm{s}^2\theta_b + I_{zz}\mathrm{c}^2\theta_b + (I_{wz} + I_{rz})$,

$m_{44} = m_{bw}z^2 + I_{yy} + 2(I_{wy} + I_{ry})$,

$m_{45} = m_{46} = m_{54} = m_{64} = I_{wy} + nI_{ry}$,

$m_{55} = m_{66} = I_{wy} + n^2 I_{ry}$,

$v_1(q, \dot{q}) = -m_{bw}z\mathrm{s}\theta_b\mathrm{c}\phi_v(\dot{\theta}_b^2 + \dot{\phi}_v^2) - 2m_{bw}z\mathrm{c}\theta_b\mathrm{s}\phi_v\dot{\theta}_b\dot{\phi}_b$,

$v_2(q, \dot{q}) = -m_{bw}z\mathrm{s}\theta_b\mathrm{s}\phi_v(\dot{\theta}_b^2 + \dot{\phi}_v^2) + 2m_{bw}z\mathrm{c}\theta_b\mathrm{c}\phi_v\dot{\theta}_b\dot{\phi}_b$,

$v_3(q, \dot{q}) = 2\mathrm{s}\theta_b\mathrm{c}\theta_b(m_{bw}z^2 + I_{xx} - I_{zz})\dot{\theta}_b\dot{\phi}_v$,

$v_4(q, \dot{q}) = -\mathrm{s}\theta_b\mathrm{c}\theta_b(m_{bw}z^2 + I_{xx} - I_{zz})\dot{\phi}_v^2$

$g_4(q) = -m_{bw}gz\mathrm{s}\theta_b$

To derive input matrix E, it considers that it is produced by the torque of right motor (τ_{wbr}) and torque of left motor (τ_{wbl}). Therefore, work input (W) is function of τ_{wbr}, τ_{wbl}, θ_{wbr} and θ_{wbl} then work input can be defined as

$$W = \theta_{wbr}\tau_{wbr} + \theta_{wbl}\tau_{wbl} \tag{2.29}$$

Controlled torque can be shown as

$$E\tau = \begin{bmatrix} 0 & 0 \\ 0 & 0 \\ 0 & 0 \\ 0 & 0 \\ \partial W/\partial\theta_{wbr} & 0 \\ 0 & \partial W/\partial\theta_{wbl} \end{bmatrix} \begin{bmatrix} \tau_{wbr} \\ \tau_{wbl} \end{bmatrix} \tag{2.30}$$

where, $E = \begin{bmatrix} 0 & 0 & 0 & 0 & 1 & 0 \\ 0 & 0 & 0 & 0 & 0 & 1 \end{bmatrix}^T$, $\tau = \begin{bmatrix} \tau_{wbr} & \tau_{wbl} \end{bmatrix}^T$.

2.3.2.4 Motion Constraints

In order to design the control system, the dynamic model should be improved to refer vehicle coordinate frame(Σ_V), it is that $\nu = \begin{bmatrix} \dot{s} & \dot{\phi}_v & \dot{\theta}_b \end{bmatrix}^T$, where, s and $\dot{s}$ denote length of the robot motion and straight velocity, respectively. ϕ_v and θ_b denote yaw and tilt angles. Lagrangian multiplier (λ) is used to transform the generalized coordinate (q) to the controlled coordinate (ν). Generally, the motion of a two-wheeled mobile robot on horizontal plan as shown in Fig.2.5 is assumed that the wheels does not slip. Thus, it has the motion constraints as same as the constraints of the inverted pendulum robot. The velocity on generalized coordinate (q)can be denoted as

$$\dot{x} = v\cos\phi_v \tag{2.31}$$

$$\dot{y} = v\sin\phi_v \tag{2.32}$$

$$\dot{\phi} = \frac{r_w}{2b}(\dot{\theta}_{wr} - \dot{\theta}_{wl}) \tag{2.33}$$

Eq.(2.31)-(2.32) can be arranged to constraint equations as follows;

$$\dot{x}\sin\phi_v - \dot{y}\cos\phi_v = 0 \tag{2.34}$$

$$\dot{x}\cos\phi_v + \dot{y}\sin\phi_v = \frac{r_w}{2}(\dot{\theta}_{wr} + \dot{\theta}_{wl}) \tag{2.35}$$

$$\dot{\phi}_v = \frac{r_w}{2b}(\dot{\theta}_{wr} - \dot{\theta}_{wl}) \tag{2.36}$$

Here, Eq.(2.34) and Eq.(2.35) are non-holonomic constraints and Eq.(2.36) is holonomic constraint.$v = \dot{s}$, r_w denotes radius of wheels and b is a half of distance between both wheels.

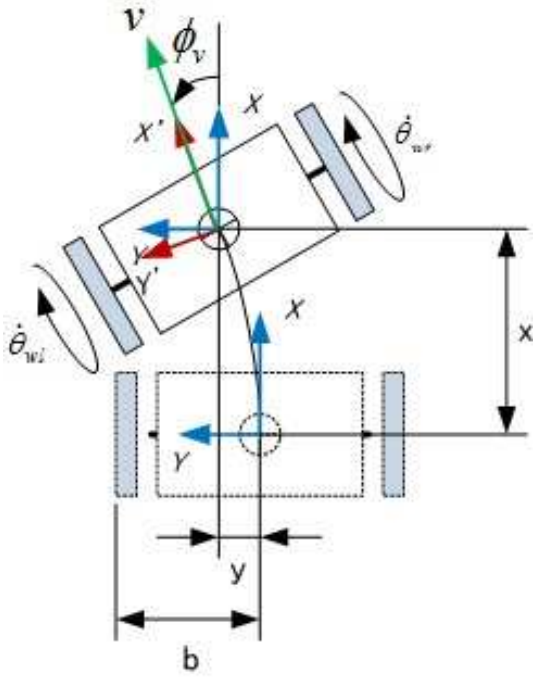

FIGURE 2.5: Two wheeled inverted pendulum robot on world coordinate frame (Σ_W) and vehicle coordinate frame (Σ_V).

According to consider constraints in section 5.3, Eq.(2.34-2.36) can be represented as follows;

$$\dot{x}\sin\phi_v - \dot{y}\cos\phi_v = 0 \tag{2.37}$$

$$\dot{x}\cos\phi_v + \dot{y}\sin\phi_v = \frac{r_w}{2}(\dot{\theta}_{wbr} + \dot{\theta}_{wbl} + 2\dot{\theta}_{bl}) \tag{2.38}$$

$$\dot{\phi}_v = \frac{r_w}{2b}(\dot{\theta}_{wbr} - \dot{\theta}_{wbl}) \tag{2.39}$$

Then, the constraint matrix ($A(q)$) represents the constraints of a two-wheeled mobile robot. Their equations are expressed as $A(q)\dot{q} = 0$ then $A(q)$ is given as

$$A(q) = \begin{bmatrix} \sin\phi_v & -\cos\phi_v & 0 & 0 & 0 & 0 \\ \cos\phi_v & \sin\phi_v & b & -r_w & -r_w & 0 \\ \cos\phi_v & \sin\phi_v & -b & -r_w & 0 & -r_w \end{bmatrix} \tag{2.40}$$

Here, we define a matrix $S(q)$, which is composed of linear independent vector in the null-space of $A(q)$ as

$$S(q) = \begin{bmatrix} \cos\phi_v & 0 & 0 \\ \sin\phi_v & 0 & 0 \\ 0 & 1 & 0 \\ 0 & 0 & 1 \\ \frac{1}{r_w} & \frac{b}{r_w} & -1 \\ \frac{1}{r_w} & -\frac{b}{r_w} & -1 \end{bmatrix} \tag{2.41}$$

$S(q)$ included in the null-space of $A(q)$ and $\ddot{q}$ always exists in the null-space of $A(q)$ and the relation of both coordinates can be satisfied as

$$A(q)S(q) = 0 \tag{2.42}$$

$$\dot{q} = S(q)\dot{\nu} \tag{2.43}$$

$$\ddot{q} = \dot{S}(q)\dot{\nu} + S(q)\ddot{\nu} \tag{2.44}$$

2.3.2.5 Equation of Motion Based on Vehicle Coordinate Frame

To derive equation of motion based on vehicle coordinate frame (Σ_V), Eq.(2.28) is transformed by Lagrangian unknown multiplier (λ)

$$M\ddot{q} + V(q,\dot{q}) + G(q) + A^T(q)\lambda = E\tau \tag{2.45}$$

Consequently, Eq.(2.42) - Eq.(2.44) are substituted in Eq.(2.45), Eq.(2.45) is represented by new coordinate that

$$S^T(q)M(\dot{S}(q)\dot{\nu} + S(q)\ddot{\nu}) + S^T(q)V(q,\dot{q}) + S^T(q)G(q) + S^T(q)A^T(q)\lambda = S^T(q)E\tau \tag{2.46}$$

$$S^T(q)M(\dot{S}(q)\dot{\nu} + S(q)\ddot{\nu}) + S^T(q)V(q,\dot{q}) + S^T(q)G(q) + (A(q)S(q))^T\lambda = S^T(q)E\tau \tag{2.47}$$

Therefore, $(A(q)S(q))^T$ equal zero and the factor of unknown multiplier is canceled, and then a new equation of motion is given as follows;

$$\bar{M}\ddot{\nu} + \bar{H}(\nu)\dot{\nu} + \bar{V}(\nu,\dot{\nu}) + \bar{G} = \bar{E}\tau \tag{2.48}$$

Where, $\bar{M} = S^T(q)MS(q) = \begin{bmatrix} \bar{m}_{11} & 0 & \bar{m}_{13} \\ 0 & \bar{m}_{22} & 0 \\ \bar{m}_{31} & 0 & \bar{m}_{33} \end{bmatrix}$, $\bar{H}(\nu) = S^T(q)M\dot{S}(q) = \begin{bmatrix} 0 & 0 & 0 \\ m_{bw}z\mathrm{s}\theta_b\dot{\phi}_v & 0 & 0 \\ 0 & 0 & 0 \end{bmatrix}$,

$\bar{V}(\nu,\dot{\nu}) = S^T(q)V(q,\dot{q}) = \begin{bmatrix} -m_{bw}z\mathrm{s}\theta_b(\dot{\theta}_b^2 + \dot{\phi}_v^2) \\ 2\mathrm{s}\theta_b\mathrm{c}\theta_b(m_{bw}z^2 + I_{xx} - I_{zz})\dot{\theta}_b\dot{\phi}_v \\ -\mathrm{s}\theta_b\mathrm{c}\theta_b(m_{bw}z^2 + I_{xx} - I_{zz})\dot{\phi}_v^2 \end{bmatrix}$, $\bar{G} = S^T(q)G(q) = \begin{bmatrix} 0 \\ 0 \\ -m_{bw}gz\mathrm{s}\theta_b \end{bmatrix}$,

$\bar{E} = S^T(q)E = \begin{bmatrix} \frac{1}{r_w} & \frac{1}{r_w} \\ \frac{b}{r_w} & -\frac{b}{r_w} \\ -1 & -1 \end{bmatrix}$, $\bar{m}_{13} = \bar{m}_{31} = 2\frac{(n-n^2)I_{ry}}{r_w^2}$, $\bar{m}_{11} = m_{bw} + 2\frac{I_{wy}+n^2I_{ry}}{r_w^2}$,

$\bar{m}_{22} = (m_{bw}z^2 + I_{xx})\mathrm{s}^2\theta_b + I_{zz}\mathrm{c}^2\theta_b + (I_{wz} + I_{rz}) + 2(\frac{b}{r_w})^2(I_{wy} + n^2I_{ry})$, $\bar{m}_{33} = m_{bw}z^2 + I_{yy} + 2((1 + n^2 - n)I_{ry} - I_{wy})$.

2.3.3 State Space Model

State space model is necessary model to derive controller gain using linear control theory such as linear quadratic regulator, pole placement, and limited pole placement. In order to treat state space model, Eq.(2.48) is linearized using Taylor's series that Taylor's series is

$$f(x) = \sum_{i=1}^{n} \frac{f^n}{n!}(x - x_0) \quad : \quad f^n = \frac{d^n f}{dt} \tag{2.49}$$

Then, linear model can be derived by Taylor's series and it is obtained as

$$M_L\dot{\nu} + G_L\nu = E\tau \tag{2.50}$$

$$M_L = \begin{bmatrix} m_{l,11} & 0 & m_{l,13} \\ 0 & m_{l,22} & 0 \\ m_{l,31} & 0 & m_{l,33} \end{bmatrix} \tag{2.51}$$

$$G_L = \begin{bmatrix} 0 & 0 & 0 \\ 0 & 0 & 0 \\ 0 & 0 & -m_{bw}gz \end{bmatrix} \tag{2.52}$$

$$E = \begin{bmatrix} \frac{1}{r_w} & \frac{1}{r_w} \\ \frac{b}{r_w} & -\frac{b}{r_w} \\ -1 & -1 \end{bmatrix} \tag{2.53}$$

where, $m_{l,11} = m_{bw} + 2\frac{I_{wy}+n^2I_{ry}}{r_w^2}$, $m_{l,22} = I_{zz} + (I_{wz} + I_{rz}) + 2(\frac{b}{r_w})^2(I_{wy} + n^2I_{ry})$, $m_{l,13} = m_{l,31} = 2\frac{(n-n^2)I_{ry}}{r_w^2}$, and $m_{l,33} = m_{bw}z^2 + I_{yy} + 2((1 + n^2 - n)I_{ry} - I_{wy})$.

Therefore, state space model is

$$\dot{x}_{ss} = A_{ss}x_{ss} + B_{ss}\tau \tag{2.54}$$

$$A_{ss} = \begin{bmatrix} 0_{3\times3} & I_{3\times3} \\ -M_L^{-1}G_L & 0_{3\times3} \end{bmatrix} \tag{2.55}$$

$$B = \begin{bmatrix} 0_{3\times2} \\ M_L^{-1}E \end{bmatrix} \tag{2.56}$$

$$x_{ss} = \begin{bmatrix} s & \phi_v & \theta_b & \dot{s} & \dot{\phi}_v & \dot{\theta}_b \end{bmatrix}^T \tag{2.57}$$

where, s and $\dot{s}$ denote length of the robot motion and straight velocity, respectively. ϕ_v and θ_b denote yaw and tilt angles.

2.4 Omni-directional Robot

This section introduces properties of omni-directional robot such as hardware construction, physical parameter, equation of motion, state space model. It is basis necessary information to design control system based on modern control system.

2.4.1 Velocity Constraints and Jacobian Matrix

To consider robot motion on world coordinate frame (Σ_W) in Fig.2.6, it consider by homogeneous transformation as follows:

$${}^0H_B = \begin{bmatrix} \mathrm{c}\phi & -\mathrm{s}\phi & 0 & x \\ \mathrm{s}\phi & \mathrm{c}\phi & 0 & y \\ 0 & 0 & 1 & 0 \\ 0 & 0 & 0 & 1 \end{bmatrix} \tag{2.58}$$

$$\begin{bmatrix} R_v^w & P_v^w \\ 0_{1\times3} & 1 \end{bmatrix} \tag{2.59}$$

Translation velocity based on Σ_W is given that

$$v_v^w \begin{bmatrix} \dot{x} & \dot{y} & \dot{\phi} \end{bmatrix}^T \tag{2.60}$$

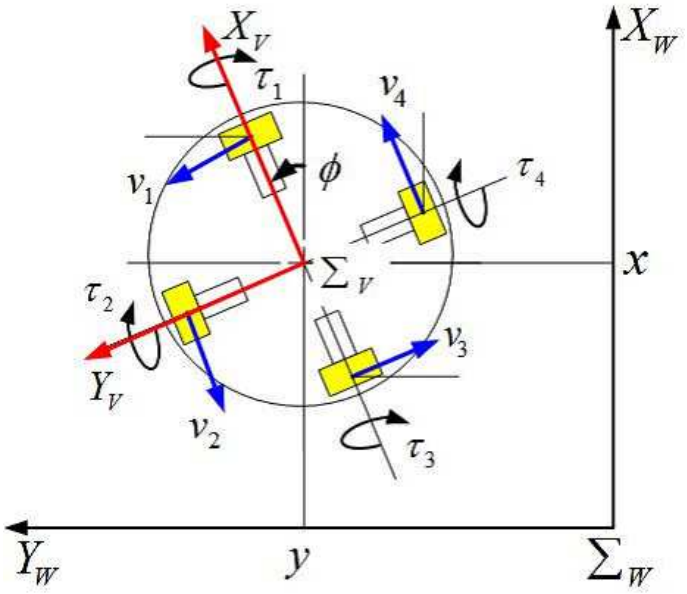

FIGURE 2.6: The motion of omni-directional robot in horizontal space.

where, v_1,v_2,v_3,v_4 denote translation velocities of wheels no. 1, 2, 3, 4, respectively. Angular velocity is derive by V operation as

$$\omega_v^w = (\dot{R}_v^w R_v^w)^V \tag{2.61}$$

$$= \begin{bmatrix} 0 & 0 & \dot{\phi} \end{bmatrix}^T \tag{2.62}$$

From velocity in Fig.2.6, the relationship of velocity between Σ_W and Σ_V is in domain of wheel velocities that

$$\begin{bmatrix} \dot{x} \\ \dot{y} \\ \dot{\phi} \end{bmatrix} = \begin{bmatrix} -\frac{1}{2}\mathrm{s}\phi & -\frac{1}{2}\mathrm{c}\phi & \frac{1}{2}\mathrm{s}\phi & \frac{1}{2}\mathrm{c}\phi \\ \frac{1}{2}\mathrm{c}\phi & -\frac{1}{2}\mathrm{s}\phi & -\frac{1}{2}\mathrm{c}\phi & \frac{1}{2}\mathrm{s}\phi \\ \frac{r_w}{2b} & \frac{r_w}{2b} & \frac{r_w}{2b} & \frac{r_w}{2b} \end{bmatrix} \begin{bmatrix} \dot{\theta}_1 \\ \dot{\theta}_2 \\ \dot{\theta}_3 \\ \dot{\theta}_4 \end{bmatrix} \tag{2.63}$$

Following Jacobian matrix (J) definition in [2], it can be derived from Eq.(2.63) that

$$v = J\omega \tag{2.64}$$

$$\tau = J^T F \tag{2.65}$$

$$J = \begin{bmatrix} -\frac{r_w}{2}\mathrm{s}\phi & -\frac{r_w}{2}\mathrm{c}\phi & \frac{r_w}{2}\mathrm{s}\phi & \frac{r_w}{2}\mathrm{c}\phi \\ \frac{r_w}{2}\mathrm{c}\phi & -\frac{r_w}{2}\mathrm{s}\phi & -\frac{r_w}{2}\mathrm{c}\phi & \frac{r_w}{2}\mathrm{s}\phi \\ \frac{r_w}{2b} & \frac{r_w}{2b} & \frac{r_w}{2b} & \frac{r_w}{2b} \end{bmatrix} \tag{2.66}$$

2.4.2 Equation of Motion

As velocity in Eq.(2.60) and (2.62), Lagrangian equation is derived based on Σ_W. The state variable q is defined as $[x, y, \phi, \theta_1, \theta_2, \theta_3, \theta_4]^T$ as follows:

$$
\begin{aligned}
L &= T - V && (2.67)\\
T &= \frac{1}{2}{}^0 V_B^T M_B^0 V_B + \frac{1}{2}{}^0 \omega_B^T I_B^0 \omega_B && (2.68)\\
&\quad + \frac{1}{2}{}^0 \omega_{w1}^T I_{w1}^0 \omega_{w1} + \frac{1}{2}{}^0 \omega_{w2}^T I_{w2}^0 \omega_{w2}\\
&\quad + \frac{1}{2}{}^0 \omega_{w3}^T I_{w3}^0 \omega_{w3} + \frac{1}{2}{}^0 \omega_{w4}^T I_{w4}^0 \omega_{w4}\\
V &= m_b g z && (2.69)
\end{aligned}
$$

where, ${}^0V_B = [\dot{x}, \dot{y}, 0]^T$, $M_B = \begin{bmatrix} m_b & 0 & 0 \\ 0 & m_b & 0 \\ 0 & 0 & m_b \end{bmatrix}$, $I_B = \begin{bmatrix} I_{bx} & 0 & 0 \\ 0 & I_{by} & 0 \\ 0 & 0 & I_{bz} \end{bmatrix}$, $I_{w1} = I_{w3} = \begin{bmatrix} I_w & 0 & 0 \\ 0 & I_{ws} & 0 \\ 0 & 0 & I_{ws} \end{bmatrix}$, $I_{w2} = I_{w4} = \begin{bmatrix} I_{ws} & 0 & 0 \\ 0 & I_w & 0 \\ 0 & 0 & I_{ws} \end{bmatrix}$. I_{bx},I_{by},I_{bz} denote mass moment of inertia of robot about X, Y, and Z axis, respectively.

2.4.2.1 Equation of Motion Based on World Coordinate Frame

As Lagrangian equation of motion in Eq.(2.69), equation of motion based on world coordinate frame is obtained as

$$M_I \ddot{q} + V(q, \dot{q}) + H(q)\dot{q} + G(q) = E\tau \tag{2.70}$$

where, $M_I = \begin{bmatrix} m_b & 0 & 0 & 0 & 0 & 0 & 0 \\ 0 & m_b & 0 & 0 & 0 & 0 & 0 \\ 0 & 0 & I_{33} & 0 & 0 & 0 & 0 \\ 0 & 0 & 0 & I_{44} & 0 & 0 & 0 \\ 0 & 0 & 0 & 0 & I_{55} & 0 & 0 \\ 0 & 0 & 0 & 0 & 0 & I_{66} & 0 \\ 0 & 0 & 0 & 0 & 0 & 0 & I_{77} \end{bmatrix}$, $V(q, \dot{q}) = \begin{bmatrix} 0 \\ 0 \\ 0 \\ (I_w - I_{ws})\mathrm{s}\phi\mathrm{c}\phi\dot{\phi}\dot{\theta}_1 \\ -(I_w - I_{ws})\mathrm{s}\phi\mathrm{c}\phi\dot{\phi}\dot{\theta}_2 \\ (I_w - I_{ws})\mathrm{s}\phi\mathrm{c}\phi\dot{\phi}\dot{\theta}_3 \\ -(I_w - I_{ws})\mathrm{s}\phi\mathrm{c}\phi\dot{\phi}\dot{\theta}_4 \end{bmatrix}$, $H(q)\dot{q} = 0$, $G(q) = 0$, $I_{33} = I_{bz} + 4I_{ws}$, $I_{44} = I_{66} = I_w\mathrm{s}^2\phi + I_{ws}\mathrm{c}^2\phi$. $I_{55} = I_{77} = I_w\mathrm{c}^2\phi + I_{ws}\mathrm{s}^2\phi$. Considering the input torque (τ) is $\tau = [\tau_1, \tau_2, \tau_3, \tau_4]^T$, work of omni-directional robot system is expressed

that

$$W = \tau_1\theta_1 + \tau_2\theta_2 + \tau_3\theta_3 + \tau_4\theta_4 \tag{2.71}$$

Then, the input matrix (E) for omni-directional robot is given

$$E = \begin{bmatrix} 0 & 0 & 0 & 0 \\ 0 & 0 & 0 & 0 \\ 0 & 0 & 0 & 0 \\ 1 & 0 & 0 & 0 \\ 0 & 1 & 0 & 0 \\ 0 & 0 & 1 & 0 \\ 0 & 0 & 0 & 1 \end{bmatrix} \tag{2.72}$$

2.4.2.2 Equation of Motion Based on Vehicle Coordinate Frame

To transform reference coordinate frame, the constraint matrix $A(q)$ and $S(q)$ are computed as follow;

$$A(q) = \begin{bmatrix} -1 & 0 & 0 & -\frac{r_w \mathrm{s}\phi}{2} & -\frac{r_w \mathrm{c}\phi}{2} & \frac{r_w \mathrm{s}\phi}{2} & \frac{r_w \mathrm{c}\phi}{2} \\ 0 & -1 & 0 & \frac{r_w \mathrm{c}\phi}{2} & -\frac{r_w \mathrm{s}\phi}{2} & -\frac{r_w \mathrm{c}\phi}{2} & \frac{r_w \mathrm{s}\phi}{2} \\ 0 & 0 & -1 & \frac{r_w}{2b} & \frac{r_w}{2b} & \frac{r_w}{2b} & \frac{r_w}{2b} \end{bmatrix}$$

and

$$S(q) = \begin{bmatrix} 1 & 0 & 0 \\ 0 & 1 & 0 \\ 0 & 0 & 1 \\ -\frac{\mathrm{s}\phi}{r_w} & \frac{\mathrm{c}\phi}{r_w} & \frac{b}{2r_w} \\ -\frac{\mathrm{c}\phi}{r_w} & -\frac{\mathrm{s}\phi}{r_w} & \frac{b}{2r_w} \\ \frac{\mathrm{s}\phi}{r_w} & -\frac{\mathrm{c}\phi}{r_w} & \frac{b}{2r_w} \\ \frac{\mathrm{c}\phi}{r_w} & \frac{\mathrm{s}\phi}{r_w} & \frac{b}{2r_w} \end{bmatrix}$$

Therefore, the equation of motion is derived by Lagrangian equation based on Σ_V, state variable of which is $\begin{bmatrix} x & y & \phi \end{bmatrix}^T$ and input is torque of four wheels (τ) as $\begin{bmatrix} \tau_1 & \tau_2 & \tau_3 & \tau_4 \end{bmatrix}^T$. Then, it is given as

$$\bar{M}\dot{\nu} + \bar{V}(\nu, \dot{\nu}) = \bar{E}\tau \tag{2.73}$$

$$\bar{M} = \begin{bmatrix} M_t + \frac{2}{r_w^2} I_w & 0 & 0 \\ 0 & M_t + \frac{2}{r_w^2} I_w & 0 \\ 0 & 0 & I_\phi + \frac{b^2}{r_w^2} I_w \end{bmatrix} \tag{2.74}$$

$$\bar{V}(\nu, \dot{\nu}) = \begin{bmatrix} 0 & \frac{2}{r_w^2} I_w \dot{\phi} \dot{y} & 0 \\ -\frac{2}{r_w^2} I_w \dot{\phi} \dot{x} & 0 & 0 \\ 0 & 0 & 0 \end{bmatrix} \tag{2.75}$$

$$\bar{E} = \begin{bmatrix} -\frac{1}{r_w} \mathrm{s}\phi & -\frac{1}{r_w} \mathrm{c}\phi & \frac{1}{r_w} \mathrm{s}\phi & \frac{1}{r_w} \mathrm{c}\phi \\ \frac{1}{r_w} \mathrm{c}\phi & -\frac{1}{r_w} \mathrm{s}\phi & -\frac{1}{r_w} \mathrm{c}\phi & \frac{1}{r_w} \mathrm{s}\phi \\ \frac{b}{2r_w} & \frac{b}{2r_w} & \frac{b}{2r_w} & \frac{b}{2r_w} \end{bmatrix} \tag{2.76}$$

where, M_t denotes total mass of body and wheel. I_ϕ is mass moment of inertial of the robot about vertical axis. b is the distance between the wheels. r_w denotes radius of wheel. The value of physical parameters are presented in Table.2.2.

2.4.3 State Space Model

From Eq.(2.73), the equation is linearized by Taylor's series that

$$\bar{M} \dot{\nu} = \bar{E} \tau \tag{2.77}$$

and it is transformed to state space model as

$$\dot{x}_{ss} = A_{ss} x_{ss} + B_{ss} \tau \tag{2.78}$$

$$A_{ss} = \begin{bmatrix} 0_{3\times3} & I_{3\times3} \\ 0_{3\times3} & 0_{3\times3} \end{bmatrix} \tag{2.79}$$

$$B = \begin{bmatrix} 0_{3\times2} \\ \bar{M}^{-1} E \end{bmatrix} \tag{2.80}$$

$$x_{ss} = \begin{bmatrix} x & y & \phi_v & \dot{x} & \dot{y} & \dot{\phi}_v \end{bmatrix}^T \tag{2.81}$$

Chapter 3

System Identification for Inaccuracy Measurement

3.1 Introduction

System identification is well-known as the methodology for estimating the unknown system. To estimate the unknown, the input and output are measured, and the accuracy of measurement is an important factor to identification result. Therefore, this chapter introduces a method to identify the system with inaccuracy measurement and the identified system is the two wheeled inverted pendulum robot system, which is presented in Fig.2.1. The sensor in the robot is inaccuracy and noisy. The method consists of three parts that structure model, problem model, and prediction algorithms. The structure model is designed corresponding to actual system. Autoregressive exogenous (ARX) and autoregressive moving-average model with exogenous(ARMAX), and output error model (OE) models are suitable to the robot system, which are presented in [1, 3–6, 9, 51]. The most popular model for ARX model.

By the way, This chapter introduces principle knowledge about system identification, autoregressive moving average with exogenous and sensor disturbance (ARMAXD), prediction methodology and simulation. Principle knowledge about system identification consists of predicted model, model structure, and parameter estimation method. The simulation is comparison of original ARX model and the system identification with inaccuracy sensor measurement. It exhibits the accuracy of them for the inaccuracy sensor measurement system. Therefore, it is organized as follow;

3.2 Principle Knowledge about System Identification

3.2.1 Predicted Model

System is usually expressed by linear difference equation :

$$y(t) + a_1 y(t-1) + \ldots + a_n y(t-n) = b_1 u(t-1) + \ldots + b_m u(t-m) \tag{3.1}$$

To represent the system in discrete time, primarily since observed data are always collected by sampling. In Eq.(3.1), we assume sampling interval to be one unit. This is not essential, but it makes notation easier. Then, Eq.(3.1) can be called as discrete system and the output is given

$$y(t) = -a_1 y(t-1) + \ldots + a_n y(t-n) + b_1 u(t-1) + \ldots + b_m u(t-m) \tag{3.2}$$

It can be simplified as

$$y(k) = \Phi^T(t)\Theta \tag{3.3}$$

where,

$$\Phi(t) = \begin{bmatrix} -y(t-1) & \ldots & -y(t-n) & u(t-1) & \ldots & u(t-m) \end{bmatrix}^T \tag{3.4}$$

$$\Theta = \begin{bmatrix} a_1 & \ldots & a_2 & b_1 & \ldots & b_m \end{bmatrix} \tag{3.5}$$

If we express system by transfer function, we introduce forward shift operator q by

$$qu(t) = u(t+1) \tag{3.6}$$

and backward shift operator by

$$q^{-1}u(t) = u(t-1) \tag{3.7}$$

Then, transfer function of Eq.(3.1) can be derived as follow:

$$A(q)y(t) = B(q)u(t) \tag{3.8}$$

$$G(q) = \frac{y(t)}{u(t)} = \frac{B(q)}{A(q)} \tag{3.9}$$

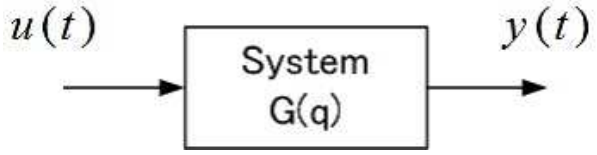

FIGURE 3.1: Original system

3.2.2 Characterization of Disturbance

Disturbance appears in most of system and it disturb the motion of mechanical system. The system with disturbance is shown in Fig.3.2. The value is not known beforehand. Thus, the characteristic is given

$$v(t) = H(q)e(t) \tag{3.10}$$

and output is derived as

$$y(t) = G(q)u(t) + H(q)e(t) \tag{3.11}$$

where,$v(t)$ denotes disturbance of system. $e(t)$ denotes white noise, which means a independent random signal.

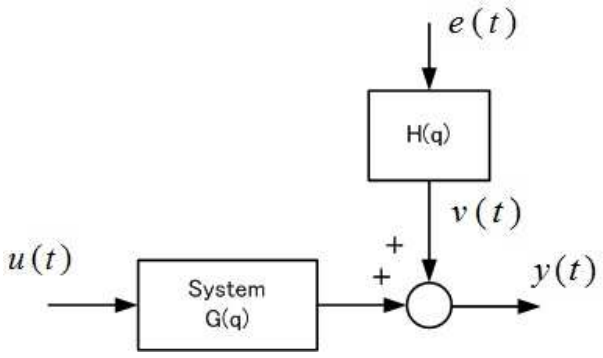

FIGURE 3.2: System with disturbance

3.2.3 Model Structure

This section introduces some principle model structures such as autoregressive exogenous (ARX) and autoregressive moving-average model with exogenous(ARMAX).

3.2.3.1 Autoregressive with exogenous inputs model

Autoregressive with exogenous inputs model (ARX model) in Fig.3.3 is the simplest input-output relationship model, where AR refers to the autoregressive part A(q)y(k) and X to extra input B(q)u(t), which are obtained by describing as linear difference equation:

$$A(q)y(t) = B(q)u(t) + e(t) \tag{3.12}$$

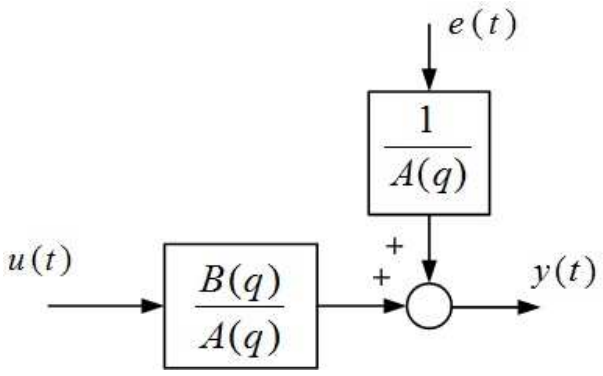

FIGURE 3.3: Autoregressive with exogenous inputs model (ARX model)

3.2.3.2 Autoregressive moving average with exogenous inputs model

Autoregressive moving average with exogenous inputs model (ARMAX model) in Fig.3.4 is obtained by a minor modification of ARX model, which is added flexibility to that by describing the equation error (e(k)) as moving average (MA) then it is given

$$A(q)y(t) = B(q)u(t) + C(q)e(t) \tag{3.13}$$

To compute the white noise, *Ljung* [1] introduces the white noise ($e(t)$) in ARMAX model is that

$$e(t) = C^{-1}(q)[B(q)u(t) - A(q)y(t)] \tag{3.14}$$

However, $e(t)$ can be derive by Eq.(3.14) in theoretical but $e(t)$ may not be derived for online prediction method because $C(q)$ may be singularity in sometimes.

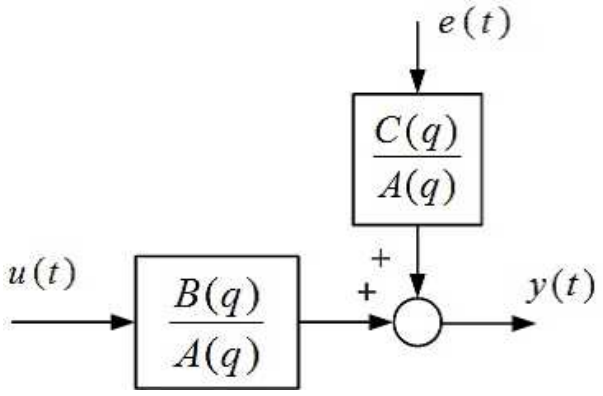

FIGURE 3.4: Block diagram of autoregressive moving average with exogenous inputs model (ARMAX model).

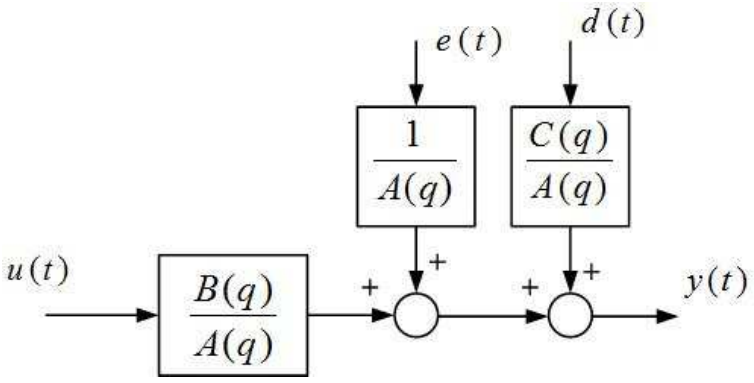

FIGURE 3.5: Block diagram autoregressive moving average with exogenous and sensor disturbance model (ARMAXD model).

3.2.3.3 Autoregressive moving average with exogenous and sensor disturbance model

Considering the robot system in Fig.3.8b, the white noise in the system is not only single white noise so that the existence models may not suitable to precise it. By the way, autoregressive moving average with exogenous and sensor disturbance model (ARMAXD) is designed based on two conventional models such as ARX and ARMAX models. The block diagram of ARMAXD is presented in Fig.3.5. $e(t)$ denotes white noise and $d(t)$ denotes sensor's uncertainty.

By the way, if I considers the white noises as the uncertainties of hardware, it will effects the prediction accuracy. Then, the white noises are assumed that their frequencies are equal with the sampling rate and the amplitudes are bounded corresponding to hardware specification. Thus, this study evaluates new method to compute $d(t)$ that the system equation is clarified in

Eq.(3.1). It is represented with white noise as

$$\begin{aligned} y(t) &= -a_1 y(t-1) + \ldots + a_n y(t-n) + b_1 u(t-1) + \ldots + b_m u(t-m) \\ &\quad + C_1 e(t-k) + \ldots + C_m e(t-k) \qquad (3.15) \\ y(t) &= A(q)y(t-1) + B(q)u(t) + C(q)e(t) \qquad (3.16) \end{aligned}$$

Then, the sensor noise ($d(t)$) is

$$d(t) = C^{-1}(q)[y(t) - A(q)y(t) - B(q)u(t) + e(t)] \qquad (3.17)$$

Considering the prediction in realtime. $A(q)$ and $B(q)$are estimated. Eq.(3.17) can be revised as

$$\begin{aligned} d(t) &= C^{-1}(q)[y(t) - \hat{y}(t)] \qquad (3.18) \\ \hat{y}(t) &= \hat{A}(q)y(t) + \hat{B}(q)u(t) + e(t) \qquad (3.19) \end{aligned}$$

where, $\hat{y}(t)$ denotes estimate output at t. $\hat{A}(q)$ and $\hat{B}(q)$ denote estimate of $A(q)$ and $B(q)$, respectively. As the characteristic of the sensor noise, $C(q)$ can be fixed as frequency filter. The cut-off frequency depends on frequency of sampled data and maximum of sensor uncertainty.

3.2.4 Parameter Estimation Methods

This section introduces the estimation method, which focuses on weight least-mean square method. According to Eq.(3.3), we know definition of $\Phi(t)$, $\Theta(t)$, and $Y(t)$. Then, we define prediction model that

$$\hat{Y}(t \mid \Theta) = \Phi^T(t)\Theta(t-1) \qquad (3.20)$$

3.2.4.1 Weight Least-mean Square Methods

Weight least-mean square method is a identification method considering weight function. The error function is represented with forgetting factor (λ) that

$$V(N, \hat{\Theta}) = \sum_{k=1}^{N} \lambda^{N-1} \epsilon(k) \qquad (3.21)$$

$$\epsilon(k) = Y(k) - \hat{Y}(k \mid \hat{\Theta}) \qquad (3.22)$$

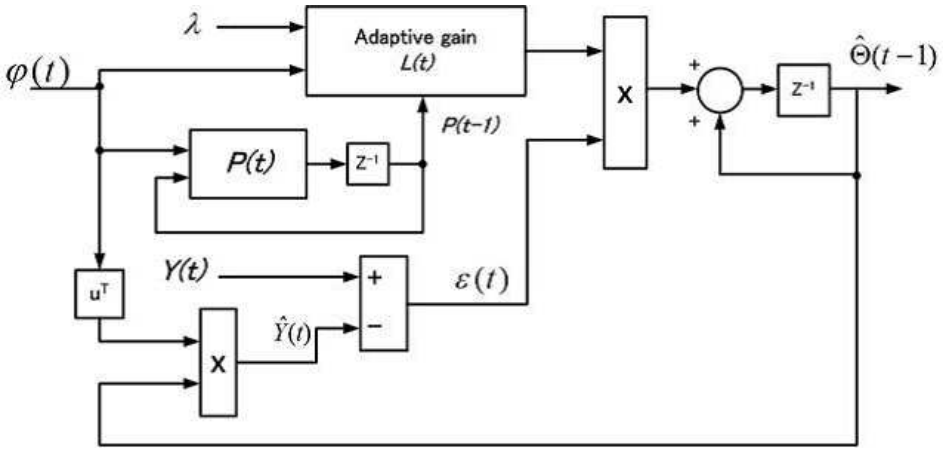

FIGURE 3.6: Block diagram of weight least-mean square.

Then, it is solved as same as the previous section. $P(N)$ and $(\Theta(N))$ are shown as follows;

$$P(N) = \left[\sum_{t=1}^{N} \lambda^{N-1}\Phi(k)\Phi(k)^T\right]^{-1} \tag{3.23}$$

$$= \left[P(N-1) + \lambda\Phi(N)\Phi(N)^T\right]^{-1} \tag{3.24}$$

$$= \frac{1}{\lambda}\left[P(N-1) - \frac{P(N-1)\Phi(N)\Phi^T(N)P(N-1)}{\lambda + \Phi^T(N)P(N-1)\Phi(N)}\right] \tag{3.25}$$

$$\hat{\Theta}(t) = \Theta(N-1) + \frac{P(N-1)\Phi(N)}{\lambda + \Phi^T(N)P(N-1)\Phi(N)} \tag{3.26}$$

3.2.4.2 Weight Least-mean Square Methods for Sensor Noise

This sections introduces weight least-mean square for ARMAXD model, which is modification of general WLS in Fig.3.6. It is added the separator in order to extract high and low frequencies of the error between the actual output and the estimate output following Eq.(3.18). It is presented in Fig.3.7. The cut-off frequency is defined slightly less than the frequency of sampled data. The high frequency denotes the sensor uncertainty and the low frequency denotes the error $(\epsilon(t))$.

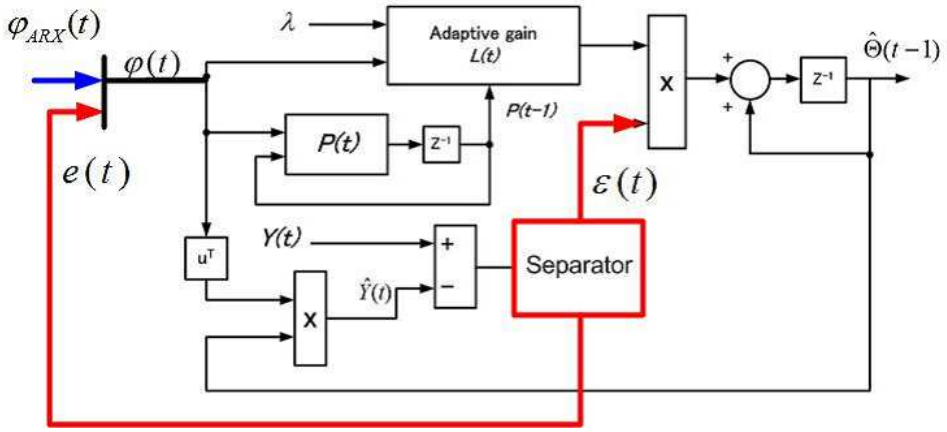

FIGURE 3.7: Block diagram of weight least-mean square for ARMAXD model.

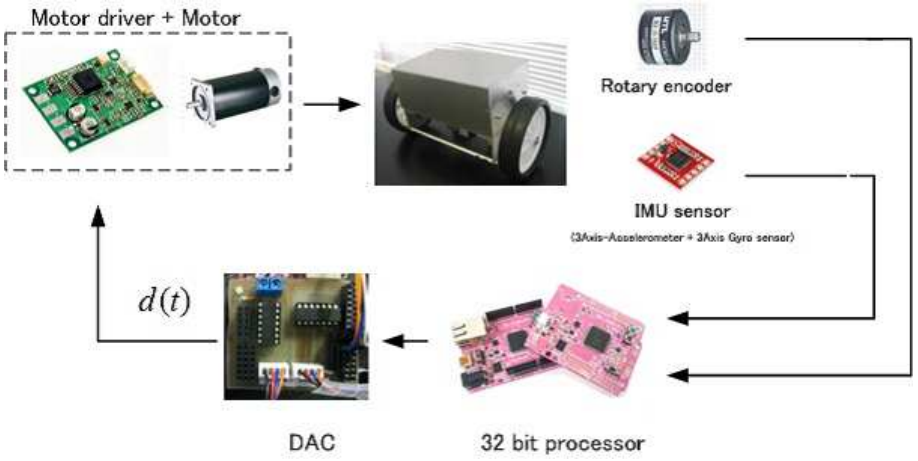

(A) Actual electronic system of two wheeled inverted pendulum robot.

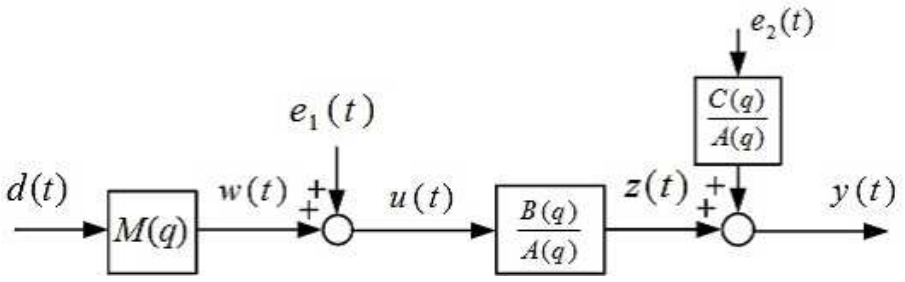

(B) Block diagram of wheeled inverted pendulum robot considering white actuator noise ($e_1(t)$) and white measurement noise ($e_2(t)$).

FIGURE 3.8: Two wheeled inverted pendulum system.

3.3 Robot Model

From Fig.3.8b, it consists of both white noises such as actuator and sensor measurement noises, The actual model can be expressed by

$$u(t) = M(q)d(t) + e_1(t) \tag{3.27}$$

$$A(q)y(t) = B(q)u(t) + C(q)e_2(t) \tag{3.28}$$

$$A(q)y(t) = B(q)\Big(M(q)d(t) + e_1(t)\Big) + C(q)e_2(t) \tag{3.29}$$

$$A(q)y(t) = B(q)M(q)d(t) + B(q)e_1(t) + C(q)e_2(t) \tag{3.30}$$

where, $d(t)$ denotes the digital signal to control motor torque. $w(t)$ is undisturbed motor torque and $u(t)$ is actual torque, which is input of robot system. $e_1(t)$ denotes white actuator noise and $e_2(t)$ is white sensor measurement noise.

If we assume that both white noises are random independent signal and the white actuator noise also effects to output. Then, white actuator noise can be combined with white output noise.

$$A(q)y(t) = B(q)M(q)d(t) + N(q)e(t) \tag{3.31}$$

It becomes similar with ARMAX model. Thus, ARMAX model suitable with actual system more than ARX model. White noise ($e(t)$) can not be measured. Therefore, Baillie [51] explains how to compute $e(t)$ for ARMAX that it is function in domain of regressive vector ($\Phi(t)$) and output error ($\epsilon(t)$).

In this study, we consider the noise that is high frequency noise and the value are bounded as same as uncertainty of measurement. Therefore, the error model can be given that

$$e(t) = H(q)\varepsilon(t) \tag{3.32}$$

where, $H(q)$ denotes high pass filter and $\varepsilon(t)$ is error between estimate plant and actual output. The passed frequency is over than 200-1000 Hz., which equals the sampling interval of control system.

3.3.1 System Model

Considering linear model of wheeled inverted pendulum robot, system model is given in difference equation that

$$\ddot{X}_1 = A_1X_1 + B_1(\tau_{c1} - \tau_{f1}) \tag{3.33}$$

where, $X_1 = \begin{bmatrix} s & \phi_v & \theta_b \end{bmatrix}^T$, $A_1 = \begin{bmatrix} 0 & 0 & -a_{13} \\ 0 & 0 & 0 \\ 0 & 0 & -a_{33} \end{bmatrix}$, $B_1 = \begin{bmatrix} \frac{1}{r_w} & \frac{1}{r_w} \\ \frac{b}{r_w} & \frac{b}{r_w} \\ -1 & -1 \end{bmatrix}$

Fiction torque (τ_f) is defined that it consists of viscous friction and coulomb friction. Then, τ_f is derived that

$$\tau_{f1} = \begin{bmatrix} \tau_{fwr} & \tau_{fwl} \end{bmatrix}^T \tag{3.34}$$

$$\tau_{f1} = C_{cu}\text{sgn}(\dot{\theta}_{wb}) + C_v\dot{\theta}_{wb} \tag{3.35}$$

$$\dot{\theta}_{wb} = \begin{bmatrix} \dot{\theta}_{wbr} & \dot{\theta}_{wbl} \end{bmatrix}^T \tag{3.36}$$

$$C_{cu} = \begin{bmatrix} c_{cu} & 0 \\ 0 & c_{cu} \end{bmatrix} \tag{3.37}$$

$$C_v = \begin{bmatrix} c_v & 0 \\ 0 & c_v \end{bmatrix} \tag{3.38}$$

where, τ_{wbr} and τ_{wbl} denote friction at right and left wheels. $\dot{\theta}_{wbr}$ and $\dot{\theta}_{wbl}$ denote angular velocity of right and left wheels, respectively. C_{cu} denote coulomb friction matrix and C_v denote viscous friction matrix.

Eq.(3.35) is substituted in Eq.(3.33), system model can be rearranged

$$\ddot{X}_1 = \bar{A}_1\bar{X}_1 + \bar{B}_1\tau_c \tag{3.39}$$

where, $\bar{X}_1 = \begin{bmatrix} \theta_b & \text{sgn}(\dot{\theta}_{wb}) & \dot{\theta}_{wb} \end{bmatrix}^T$, $\bar{A}_1 = \begin{bmatrix} A & -B_1C_{cu} & -B_1C_v \end{bmatrix}$, $\bar{B}_1 = B_1$

3.4 Simulation

To present the accuracy of system identification, the simulation deals the identification results of ARX and ARMAXD models on the inverted pendulum robot system. Generally, the regressive vector is defined as input and state variable but some components in the state variable are not appears in the state matrix so that we can neglect some components.

3.4.1 Preliminary

Defining the robot system with sensor noise ($d(t)$), it is identified while it is balancing. Then, servo control system is designed as shown in Fig.3.9. The plant denotes two dimensional system of the inverted pendulum robot, which is derived by the physical parameters in Table.2.1 and 3D linear model in Eq.(2.54)-(2.57). The noise is defined as sinusoid disturbance with high frequency, which consist of the noise of distance (s) and the noise of tilt angle (θ_b). The

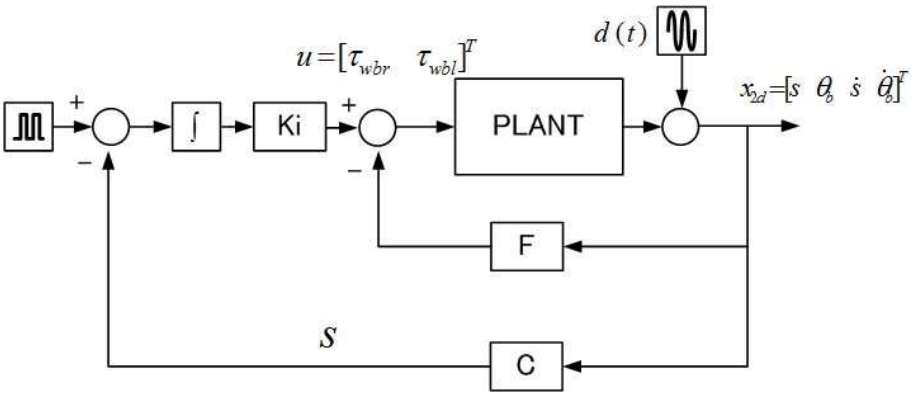

FIGURE 3.9: Servo control to balance the inverted pendulum robot.

frequencies are defined at 800 Hz. The amplitude is 0.001 m. and 0.05 rad., respectively. For ARMAXD model, the cut-off frequency is defined as 740 Hz., The 3D linear model of the inverted pendulum robot is represented that

$$\dot{x}_{ss} = A_{ss}x_{ss} + B_{ss}\tau \tag{3.40}$$

$$A_{ss} = \begin{bmatrix} 0 & 0 & 0 & 1 & 0 & 0 \\ 0 & 0 & 0 & 0 & 1 & 0 \\ 0 & 0 & 0 & 0 & 0 & 1 \\ 0 & 0 & 1.21 & 0 & 0 & 0 \\ 0 & 0 & 0 & 0 & 0 & 0 \\ 0 & 0 & -9.87 & 0 & 0 & 0 \end{bmatrix} \tag{3.41}$$

$$B_{ss} = \begin{bmatrix} 0 & 0 \\ 0 & 0 \\ 0 & 0 \\ -1.73 & -1.73 \\ 101.46 & -101.46 \\ 35.39 & 35.39 \end{bmatrix} \tag{3.42}$$

$$x_{ss} = \begin{bmatrix} s & \phi_v & \theta_b & \dot{s} & \dot{\phi}_v & \dot{\theta}_b \end{bmatrix}^T \tag{3.43}$$

The 2D linear model of the inverted pendulum robot can be presented that

$$\dot{x}_2 = A_2 x_2 + B_2 \tau \tag{3.44}$$

$$A_2 = \begin{bmatrix} 0 & 0 & 1 & 0 \\ 0 & 0 & 0 & 1 \\ 0 & 1.21 & 0 & 0 \\ 0 & -9.87 & 0 & 0 \end{bmatrix} \tag{3.45}$$

$$B_2 = \begin{bmatrix} 0 & 0 \\ 0 & 0 \\ -1.73 & -1.73 \\ 35.39 & 35.39 \end{bmatrix} \tag{3.46}$$

$$x_2 = \begin{bmatrix} s & \theta_b & \dot{s} & \dot{\theta}_b \end{bmatrix}^T \tag{3.47}$$

To identify the linear system, identification model is designed relative to Eq. (3.40) that

$$\dot{x}_{2d} = A_{2d} x_{2d} + B_{2d} \tau \tag{3.48}$$

$$A_{2d} = \begin{bmatrix} 0 & 1.21 \\ 0 & -9.87 \end{bmatrix} \tag{3.49}$$

$$B_{2d} = \begin{bmatrix} -1.73 & -1.73 \\ 35.39 & 35.39 \end{bmatrix} \tag{3.50}$$

$$x_{2d} = \begin{bmatrix} s & \theta_b \end{bmatrix}^T \tag{3.51}$$

Hence, x_{2d} is designed corresponding to real output of the practical system, components of which are directly measured by rotary encoders and IMU sensor, respectively.

3.4.2 Controller Design

The feedback gain (F) and servo gain (Ki) are designed based on extended linear model of Eq.(3.40), which is

$$\dot{x}_s = A_s x_s + B_s \tau + N r \tag{3.52}$$

$$A_s = \begin{bmatrix} A_2 & 0 \\ -C & 0 \end{bmatrix} \tag{3.53}$$

$$B_s = \begin{bmatrix} B_2 \\ 0_{1\times 2} \end{bmatrix} \tag{3.54}$$

$$x_s = \begin{bmatrix} s & \theta_b & \dot{s} & \dot{\theta}_b & \omega \end{bmatrix}^T \tag{3.55}$$

$$N = \begin{bmatrix} 0_{4\times 1} \\ 1 \end{bmatrix} \tag{3.56}$$

$$C = \begin{bmatrix} 1 & 0 & 0 & 0 & 0 \end{bmatrix} \tag{3.57}$$

$$\omega = r - C x_s \tag{3.58}$$

where, r denotes position reference, which is half pulse width signal. Then, (A_s) and input matrix (R) can be derived by the physical parameters in Table. I. The weight matrix Q and R are given as

$$Q = \mathrm{diag}\begin{bmatrix} 2\mathrm{x}10^5 & 8\mathrm{x}10^2 & 1\mathrm{x}10^2 & 6\mathrm{x}10^3 & 4\mathrm{x}10^3 \end{bmatrix} \tag{3.59}$$

$$R = \mathrm{diag}\begin{bmatrix} 4\mathrm{x}10^4 & 4\mathrm{x}10^4 \end{bmatrix} \tag{3.60}$$

Thus, feedback gain (F) and servo gain (Ki) are derived as

$$F = \begin{bmatrix} 6.7056 & 2.1560 & 6.0055 & 0.6502 \\ 6.7056 & 2.1560 & 6.0055 & 0.6502 \end{bmatrix} \tag{3.61}$$

$$Ki = \begin{bmatrix} 3.5355 \\ 3.5355 \end{bmatrix} \tag{3.62}$$

3.4.3 Regressive Vector Optimization

To define the regressive vector, it is generally recognized as input and state variable in Eq.(3.48). Then, the regressive vector of ARX model is defined such input ($u(t)$) and state

variable ($\begin{bmatrix} s(t) & \theta_b(t) \end{bmatrix}^T$). Thus, the problem model is defined that

$$\Phi_1(t) = \begin{bmatrix} s(t) & \theta_b(t) & u(t) \end{bmatrix}^T \tag{3.63}$$

$$Y(t) = \begin{bmatrix} \ddot{s}(t) & \ddot{\theta}_b(t) \end{bmatrix} \tag{3.64}$$

$$\Theta_1(t) = \begin{bmatrix} A_2 & B_2 \end{bmatrix}^T \tag{3.65}$$

By the way, the regressive vector of ARMAXD model is defined such input ($u(t)$), state variable ($\begin{bmatrix} s(t) & \theta_b(t) \end{bmatrix}^T$), and sensor disturbance ($d(t)$). Thus, the problem model is defined that

$$\Phi_2(t) = \begin{bmatrix} s(t) & \theta_b(t) & u(t) \end{bmatrix}^T \tag{3.66}$$

$$Y(t) = \begin{bmatrix} \ddot{s}(t) & \ddot{\theta}_b(t) \end{bmatrix} \tag{3.67}$$

$$\Theta_2(t) = \begin{bmatrix} A_2 & B_2 & C_2 \end{bmatrix} \tag{3.68}$$

where, C_2 denotes coefficient of disturbance.

3.4.4 Satisfaction

To satisfy the estimation parameter, the robot is performed and the position, the tilt angle, the input torque are collected and they are input to the prediction algorithm of ARX and ARMAXD models. The data is presented in Fig.3.10 and the estimate parameters are presented in Fig.3.11. Fig.3.11 presents that the estimate parameters are converge to constant values. It means the results is satisfaction result and the error of the results will be described in next section.

3.4.5 Results

As above sentences, the full state and the optimized regressive vectors are defined, and the components in A_{2d} and B_{2d} are predicted by ARX and ARMAXD models. The parameter in Fig.3.11 are presented as follows;

For $\hat{A}_{2d}$ and $\hat{B}_{2d}$ on ARX model :

$$\hat{A}_2 = \begin{bmatrix} 0.0173 & 1.166 \\ 1.262 & -12.71 \end{bmatrix} \tag{3.69}$$

$$\hat{B}_2 = \begin{bmatrix} -1.672 & -1.672 \\ 37.71 & 37.71 \end{bmatrix} \tag{3.70}$$

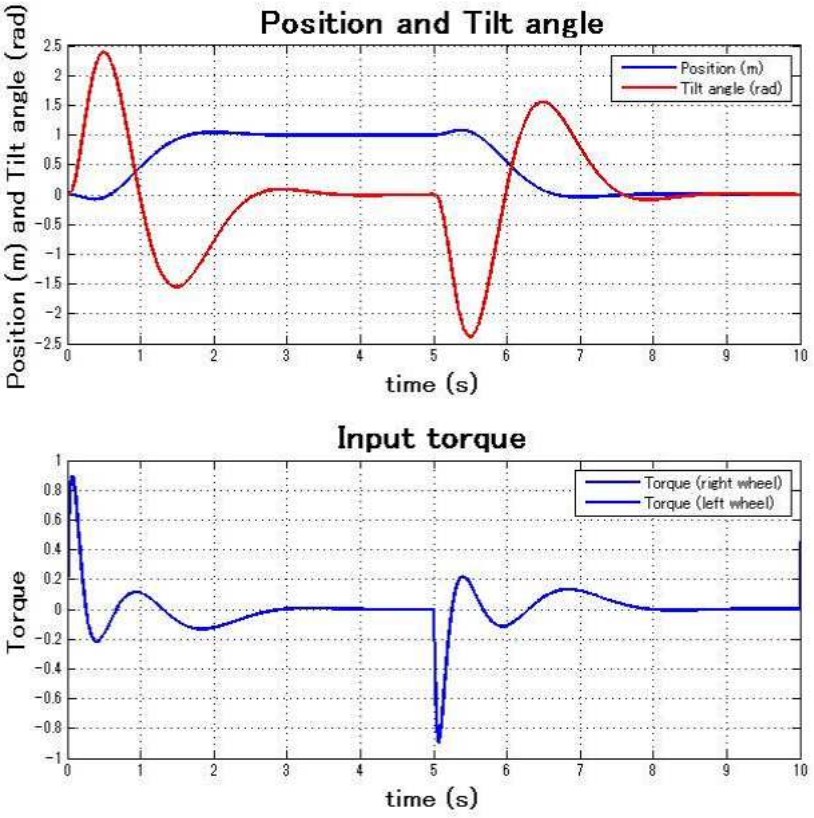

FIGURE 3.10: Data for system identification.

For $\hat{A}_{2d}$ and $\hat{B}_{2d}$ on ARMAXD model :

$$\hat{A}_2 = \begin{bmatrix} 0.0172 & 1.169 \\ 1.255 & -12.48 \end{bmatrix} \tag{3.71}$$

$$\hat{B}_2 = \begin{bmatrix} -1.697 & -1.697 \\ 36.08 & 36.08 \end{bmatrix} \tag{3.72}$$

$$\hat{C}_2 = \begin{bmatrix} 0.0005 & 0.0001 \\ 0.03796 & 0.008292 \end{bmatrix} \tag{3.73}$$

To indicate the accuracy of the predictions, the accuracy is indicated by the percentage of error between $\begin{bmatrix} \hat{A}_{2d} \hat{B}_2 \end{bmatrix}$ and $\begin{bmatrix} A_{2d} & B_2 \end{bmatrix}$. The actual result in Eq.(3.49)-(3.50). The accuracy is computed by

$$E_{er} = \frac{1}{n} \sum_{k=0}^{k=n} \left| \frac{P_{est} - P_{act}}{P_{act}} \times 100 \right| \tag{3.74}$$

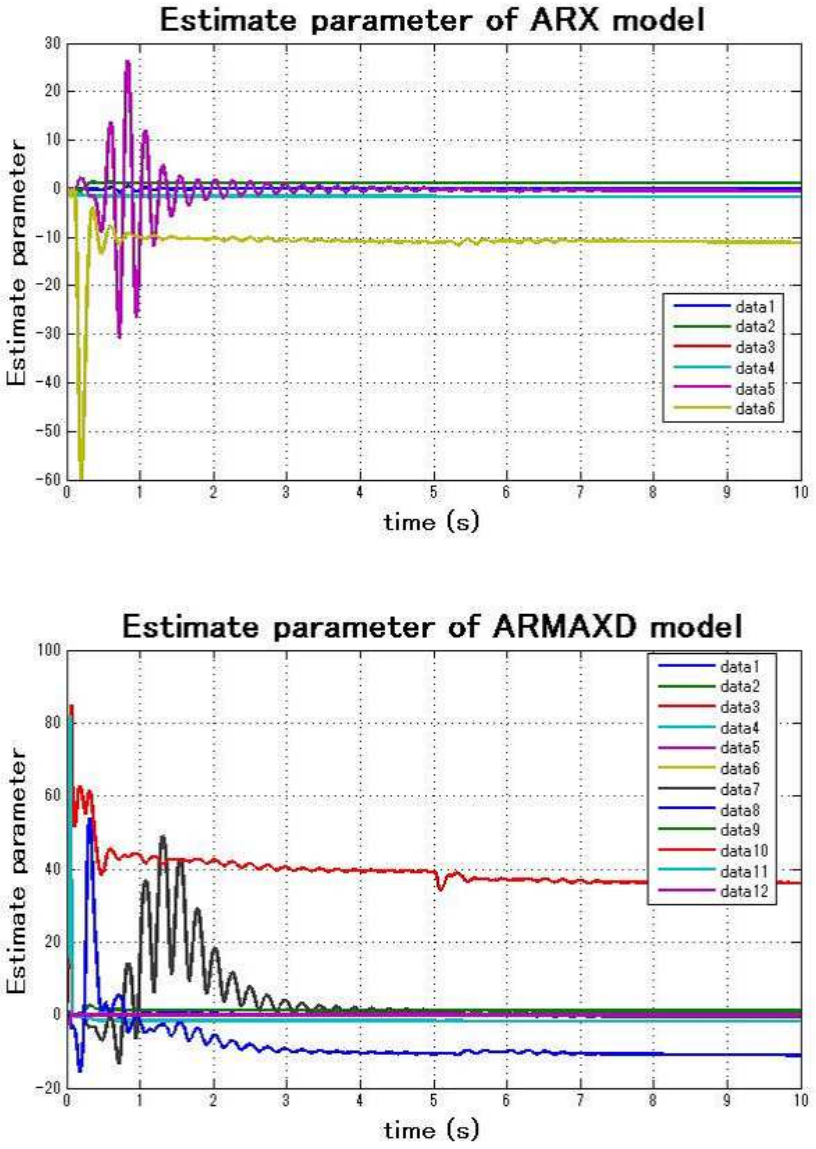

FIGURE 3.11: Satisfaction for estimate parameter by ARX and ARMAXD models.

where, P_{est} and P_{act} denote the estimate parameters and actual parameters of matrices A_{2d} and B_{2d}. n denotes the number of components in matrices A_{2d} and B_{2d}. If the component is zero, the denominator is one. Therefore, the error (E_{er}) of ARX and ARMAXD models are

$$E_{er,ARX} = 31.02 \tag{3.75}$$

$$E_{er,ARMAXD} = 26.5 \tag{3.76}$$

From the percentage of the errors, the identification result of ARMAXD model is greater than ARX model. Although, the errors are remained but the result shows the evaluation to precise

the identification.

Chapter 4

Friction Compensation

4.1 Introduction

Friction exists in almost mechanical systems and it disturbs the motion of mechanism so that it is a important factor to indicate the mechanical efficiency. As literature reviews[3–9], they focus on two topics with respect to identification accuracy [4, 7] and some applications such as friction compensation [5, 6, 8] and parameter tuning effects [9]. For friction compensation, it consists of two functions that friction estimation and compensation functions. Friction estimation methods have described in [3–6, 8, 9], the estimation based on system identification seems the best method to identify the friction in the actual system in practice because it not estimates only the friction but also the other parameters. Many developers usually select ARX model to identify the system in practice [4, 9], which is simplest model but the accuracy may not precise because it does not consider the white measurement noise so that it directly effects to the performance of friction compensation.

Considering wheeled inverted pendulum robot system in Fig.3.8a, we suppose that the robot system consists of several components such as software in 32-bit controller, digital-analog converter, motor driver, motor, rotary encoder, and IMU sensor. Each component remains some uncertainty such resolution and electronic disturbance. Then, the system should be written as shown in Fig.3.8b. It contains the uncertainties of actuator driving system and sensor measurement.

Therefore, this chapter develops friction compensation to treat the uncertainties of actuator and sensor measurement. It respects to a new model structure as shown in Fig.3.8a for wheeled inverted pendulum robot. Moreover, the adaptive friction compensation is approached by Lyapunov stability, which is used to satisfy the identification result in real time and the friction coefficients are adapted during stability period.

4.2 Friction Compensation by Constant Friction Coefficients

The aim of our study is to develop a friction compensation technique for two-wheeled inverted pendulum robot. The technique is based on on-line system identification method using ARX and actual models. The actual model seems similar with ARMAX model but it is concerned the uncertainties of hardware, and then definition of error is given as high frequency noise corresponding to the uncertainties. Therefore, it applied to identify friction coefficients of two-wheeled inverted pendulum robot, and then it is used to estimate the friction in real time. The new model is designed based on ARMAX model, which is called autoregressive moving average with exogenous and sensor disturbance model (ARMAXD). For the compensation methodology, it is separated to two steps. First step is the friction coefficient identification. The coefficients are derived by the estimate parameters using ARX and a new ARMAX models then the results are satisfied by considering the convergence of the estimate parameters in time domain. Second step is the friction estimation and compensation that the friction is predicted by the estimate friction coefficients in previous step. After that it is added with the input torque in order to compensate the actual friction. The experiment result shows the effectiveness of the presented method based on the on-line system identification for the both models. The impulse response of general feedback control, feedback control with friction compensation using the friction estimate of ARX and ARMAXD models are indexed. As result, the response of the estimate friction of a ARMAXD model is smoothly than ARX model and general feedback control. It exhibits that the friction compensation can treat the friction in the system successfully and ARMAXD model is suitable to estimate the friction better than ARX model.

4.2.1 Prediction Model

In this experiment, the system parameters are in identified by weight least mean square method (WLS method), which is a popular approach to deal with time-varying systems. We give a prediction model as

$$Y(n) = \Phi^T(n)\hat{\Theta}(n-1) \tag{4.1}$$

where, $Y(n)$ denotes sampled output data at step n. $\Phi(n)$ denotes regressive vector, which is variable parameters. $\hat{\Theta}(n)$ denotes estimate system parameters.

TABLE 4.1: Regression vector and unknown matrix

Model structure	Regressive vector (φ)	Unknown parameter matrix (Θ)
ARX	$[\bar{x}[k-1], u(k)]^T$	$\begin{bmatrix}\bar{A} & \bar{B}\end{bmatrix}^T$
ARMAXD	$[\bar{x}[k-1], u(k), e(k)]^T$	$\begin{bmatrix}\bar{A} & \bar{B} & C\end{bmatrix}^T$

To design prediction model for ARX model, Eq.(3.39) can be simplified in domain of regressive vector and unknown parameter matrix that

$$Y(n) = \ddot{X}_1 \tag{4.2}$$

$$\Phi(n) = \begin{bmatrix}\bar{X}_1 \\ \tau_c\end{bmatrix} \tag{4.3}$$

$$\hat{\Theta}(n-1) = \begin{bmatrix}\hat{\bar{A}}_1 & \bar{B}_1\end{bmatrix}^T \tag{4.4}$$

On the other hands, prediction model for original ARMAX model is given

$$Y(n) = \ddot{X}_1 \tag{4.5}$$

$$\Phi(n) = \begin{bmatrix}\bar{X}_1 \\ \tau_c \\ e(t)\end{bmatrix} \tag{4.6}$$

$$\hat{\Theta}(n-1) = \begin{bmatrix}\hat{\bar{A}}_1 & \bar{B}_1 & C\end{bmatrix}^T \tag{4.7}$$

where, $e(t)$ is high frequency white noise, which contrasts with the definition in [51] and it is given in Eq.(3.32).

According to previous chapter, ARX and ARMAXD models are described, and then Y, Φ, Θ in Eq.(4.2)-(4.7) are given as shown in Table.4.1.

4.2.2 Friction Compensation

This section introduces the feedback control with the friction compensation as shown in Fig.4.1. It illustrates the feedback control with friction compensation. It consists of friction estimation and feedback gain. The friction estimation and compensation describes the methodology to predict the friction estimate ($\hat{\tau}_f$). The controller design describes the method and parameters to design feedback gain (F). The friction estimation part is in the dashed line rectangular. It converted the data from the output of plant to angular velocity of wheels and it is used to compute the friction estimate ($\hat{\tau}_f$) corresponding to Eq.(3.35). Then, the friction estimate is added to with the control torque (τ_c) in order to cancel the real friction (τ_f).

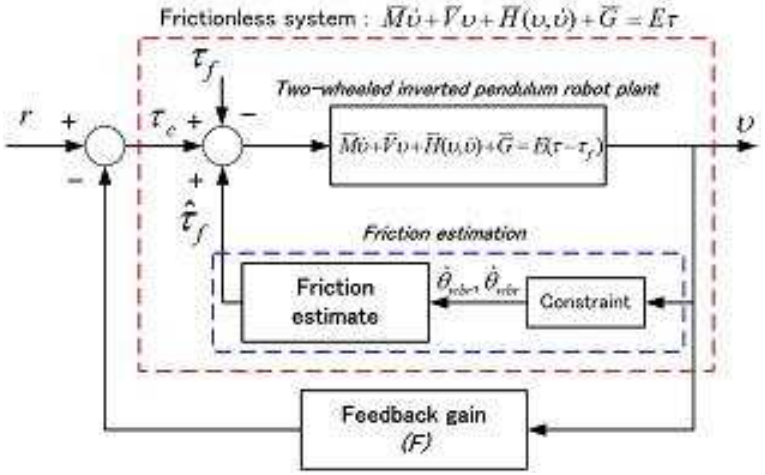

FIGURE 4.1: Block diagram of friction compensation with feedback control system.

4.2.2.1 Friction Coefficient Estimation

This experiment uses weight least-mean square method to estimate friction coefficients by sampled data in Fig.4.2. To estimate the coefficients, they are estimate by ARX and ARMAXD models, and then the estimate coefficients are used to compute the friction in real time relative to Eq.(3.34).

By the way, if $\hat{\bar{B}}_1$ is non singular matrix and $\bar{A}_1$ in Eq.(3.39) is identified, friction coefficient matrix can be extracted from the matrix $\bar{B}_1 C_{cu}$ and $\bar{B}_1 C_v$ by

$$\hat{C}_{cu} = \hat{\bar{B}}_1^{-1}(\hat{\bar{B}}_1 \hat{C}_{cu}) \tag{4.8}$$

$$\hat{C}_v = \hat{\bar{B}}_1^{-1}(\hat{\bar{B}}_1 \hat{C}_v) \tag{4.9}$$

4.2.2.2 Satisfaction

To satisfy the identification results, we consider on two points that convergence of identification result and non singularity of matrix $\hat{\bar{B}}_1$. The convergence of the estimate unknown parameter as shown in Fig.4.3. The upper graph shows the estimate parameters by ARX model and the lower graph show the estimate parameters by ARMAXD model. The parameters are converted to some values. It means that the friction coefficients are also satisfaction if they are derived from these estimate parameters. The result of friction coefficient estimation is shown in Table.4.2

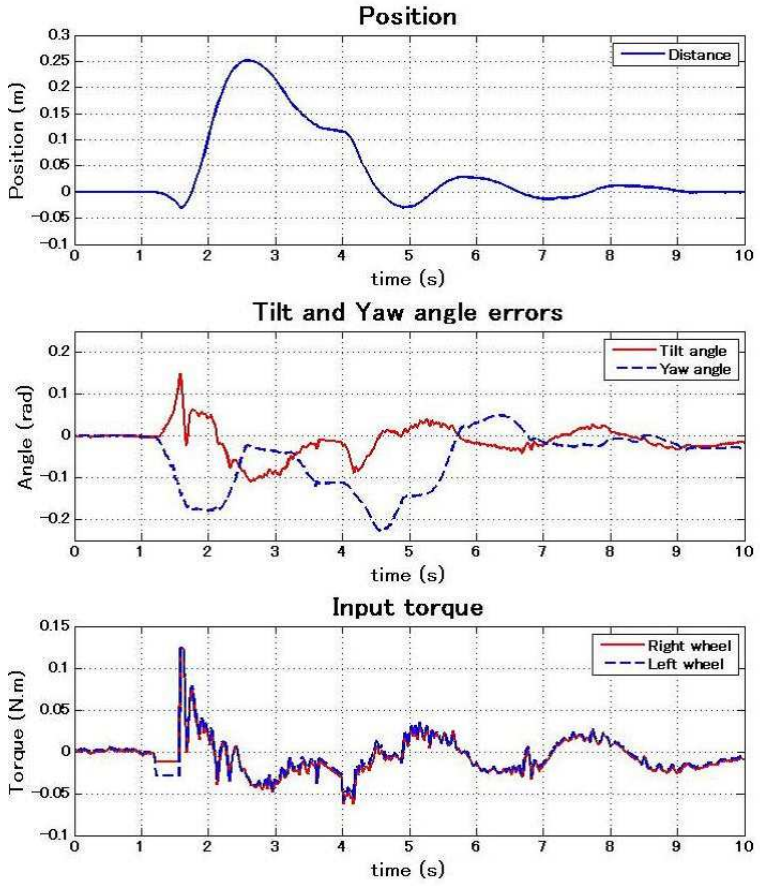

FIGURE 4.2: Position, tilt angle, yaw angle, and input torque data for friction coefficient estimation.

TABLE 4.2: System identification using ARX and ARMAXD models

ARX model	
Parameters	Value
Coulomb friction coefficient (c_{cu})	0.0067
Viscous friction coefficient (c_v)	0.0187
ARMAXD model	
Parameters	Value
Coulomb friction coefficient (c_{cu})	0.0061
Viscous friction coefficient (c_v)	0.0106

4.2.2.3 Controller Design

The feedback gain (F) is designed based on linear model in Eq.(3.33) and the friction (τ_f) is given as zero. It is used to derived the control torque (τ_c) in order to stabilize the robot. To define the feedback gain, linear quadratic regulator (LQR) method is used to design the feedback gain based on the dynamic model, which are derived by Eq.(3.33) and the parameters in Table. I. Hence, state matrix (A) and input matrix (R) can be derived by the physical parameters in

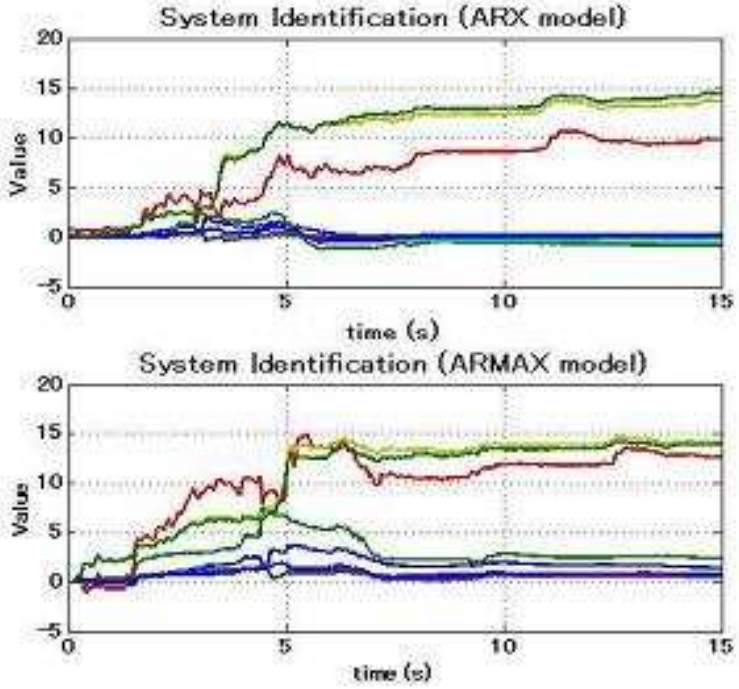

FIGURE 4.3: The identification results of the estimate unknown parameters by ARX and ARMAXD models.

Table. I. The weight matrix Q and R are given as

$$Q = \text{diag}\left[2\text{x}10^5 \quad 5\text{x}10^3 \quad 10^2 \quad 10^4 \quad 10^3 \quad 8\text{x}10^4\right] \tag{4.10}$$

Thus, feedback gain (F) is derived as

$$F = \begin{bmatrix} -0.3 & 0.05 & -1.0 & -0.49 & 0.03 & -0.2 \\ -0.3 & -0.05 & -1.0 & -0.49 & -0.03 & -0.2 \end{bmatrix} \tag{4.11}$$

4.3 Experiment Result

This section introduces the results of feedback controller with friction compensation and the assumption is given that the inverted pendulum robot is stabilizing then the disturbance is given at both wheels as impulse disturbance. The inverted pendulum robot has the response as follows: Fig.4.4 illustrates the input torque of right and left wheels in experiments, which consists of input torque of general feedback control, feedback control with the friction compensation using the friction estimate of ARX and ARMAXD models. The disturbances of three experiments are nearby and appear during 1.2-1.6 sec. Fig.4.5 presents the position errors and the tilt errors of the inverted pendulum robot. The solid line and first dash line show the position error of the robot for the friction compensation function, the friction coefficients of which are estimated by ARX and ARMAXD models, respectively. Another line exhibits the position error

of the robot for general feedback control. It expresses the ability of controller that the friction compensation is greater than general feedback control. The results of the friction compensation are greater than the result of general feedback control, however the position error remains a little for the compensation by the estimate friction of ARMAXD model.

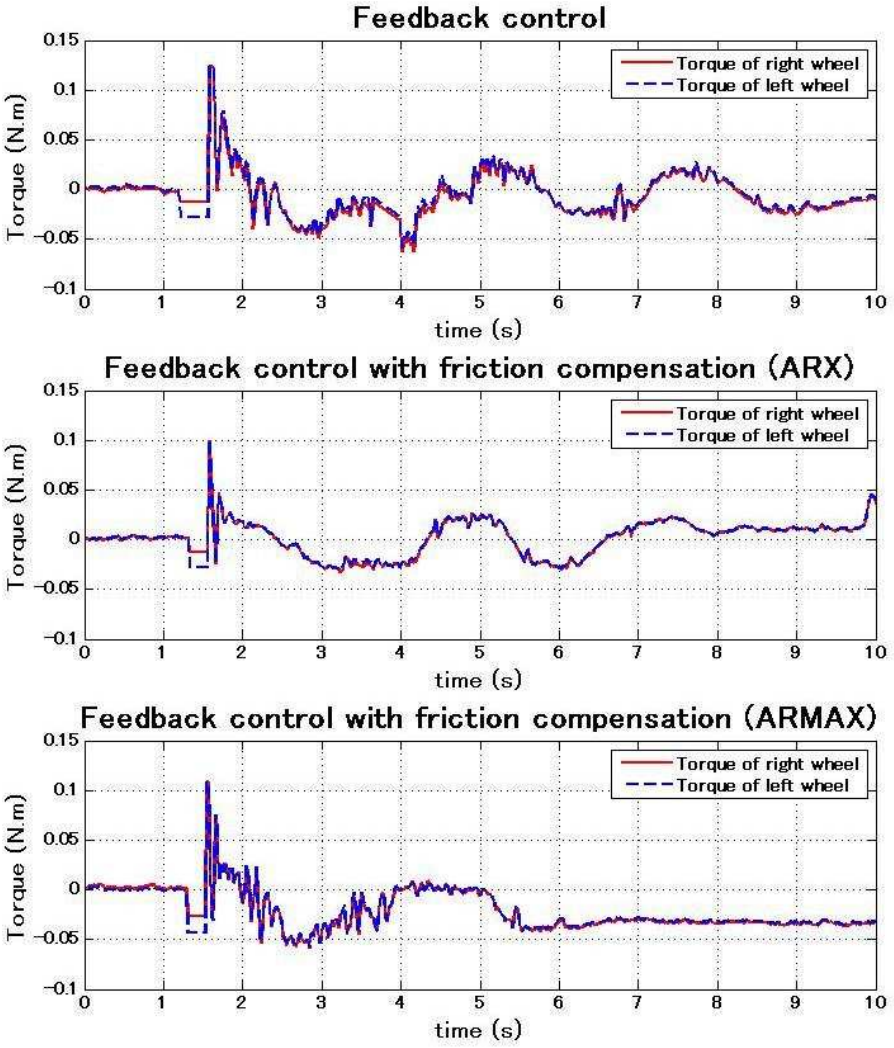

FIGURE 4.4: Input torque of the inverted pendulum robot for general feedback control, feedback control with friction compensation by the friction estimate using ARX and ARMAXD models.

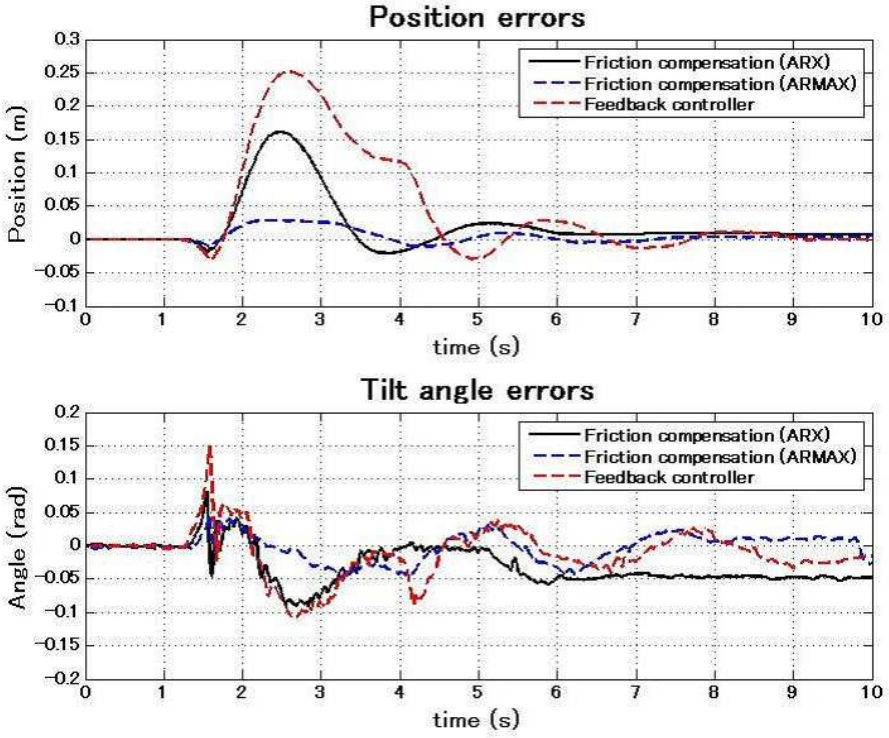

FIGURE 4.5: Position and tilt angle of the friction compensation to show impulse response of both friction models.

Chapter 5

Localization

5.1 Introduction

According to literature reviews, Kinect or camera is used as environment sensor and the space may be presented in perspective view. The scale of pixel per actual distance is nonlinearity. To treat this problem, the specific techniques such as SLAM[44], motion detection using color histogram[19], eight-points algorithm[42], and perspective projection method[40] are required to derive robot position with perspective view. On the other hands, other papers [29, 30, 40, 42] solves this problem by changing sensor location, which points to the area belong to vertical axis. Then, the area is presented in top view and the scale is linearity so that robot position can locate by simple method such threshold technique [29, 40, 42] and data fusion of environment and internal sensors[30].

In our study, the space is covered by carpet then wheel slip always occur. The position is computed by kinematic constraint[45], it can not provide the accuracy position because internal sensors such as rotary encoders cannot detected by internal sensors. Thus, Localization is required to observe the position and orientation of robot in space. Kinect is mounted at space in order to assist the robot in the space. Then, the space can be able to know the activity in space, which is called intelligent space [41]. For intelligent space, it requires two kinds of sensor data such camera and IR depth sensor. They are installed in Kinect. Camera is utilized to locate robot position and orientation. IR depth sensor is utilized to scan robot, obstacle, and available space. The combination of them exhibits 3D space information for motion planning. Thus, this section is organized as intelligent space installation, and data process.

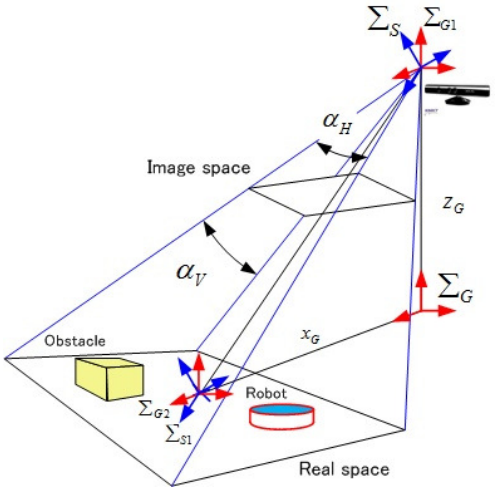

FIGURE 5.1: Kinect installation and coordinate frames in Intelligent space.

5.2 Kinect Installation

Fig.5.1 illustrates Kinect installation, orientation, and coordinate frames. Kinect is mounted on top and it points to space. Kinect specification is presented in Table.5.1 and color image presents the area in 3D view as perspective view and it is shown in Fig.5.4a. Coordinate frames are defined in Fig.5.1 as global coordinate frame (Σ_G), global coordinate frame at Kinect (Σ_{G1}), sensor coordinate frame (Σ_S), sensor coordinate frame at center of image (Σ_{S1}). Global coordinate frame (Σ_G) is defined at the space and it is under Kinect. x_G denotes distance from global coordinate frame to center of image, $x_G = 1.00$ m. z_G denotes height of sensor, $z_G = 2.78$ m.

To consider orientation of Kinect, homogeneous transformation from Σ_{G1} to Σ_S presents orientation of Kinect. Homogeneous transformation from Σ_{S1} to Σ_{G2} presents orientation of image viewpoint relative to the real space, and it is necessary part to transform the image to space's map. They are given as follows;

$$^{G1}H_S = \begin{bmatrix} R_z(\gamma)R_y(\alpha)R_x(\rho) & 0_{3\times1} \\ 0_{1\times3} & 1 \end{bmatrix} \tag{5.1}$$

$$^{S1}H_{G2} = \begin{bmatrix} R_z(\theta_z)R_y(\theta_y)R_x(\theta_x) & 0_{3\times1} \\ 0_{1\times3} & 1 \end{bmatrix} \tag{5.2}$$

where, R_x, R_y, and R_z denote rotation matrix about X, Y, and Z axis, respectively. ρ, α, and γ denote roll, pitch, and yaw angle of Kinect's orientation. They are given that $\rho = 0.059$ rad, $\alpha = 1.223$ rad, and $\gamma = 0.500$ rad. θ_x, θ_y, and θ_z are the rotation angle about X, Y, and Z axis of Σ_{S1}.

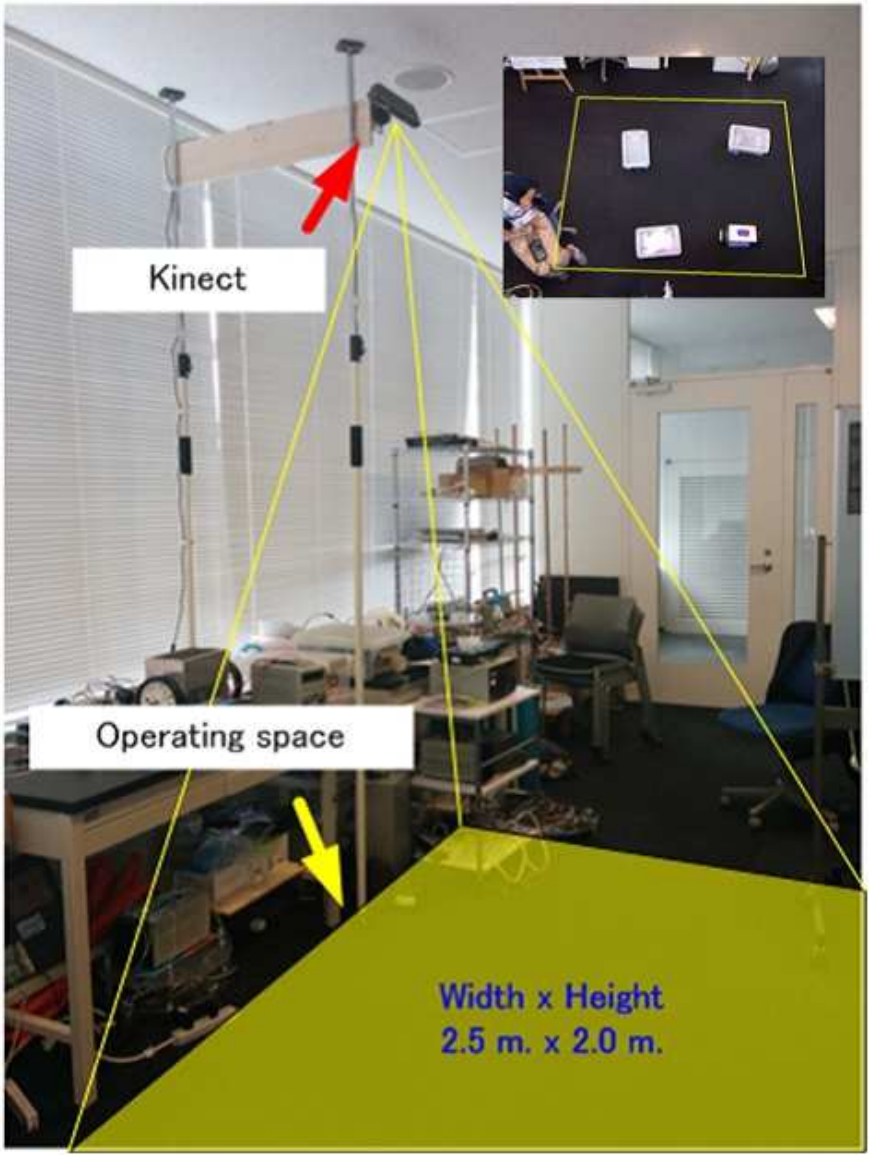

FIGURE 5.2: Structure of intelligent space.

TABLE 5.1: Kinect specification

Sensor	Value	Unit
Camera view angle in vertical (α_V)	0.7505	rad.
Camera view angle in horizontal (α_H)	0.9948	rad.
Resolution (P_H, P_V)	640x480	pixel.
Camera frame rate	30	fps.
Depth image sampling rate	30	fps.
Microphone	4	–
Audio input resolution	24-bit ADC	–
Audio format frequency	16000	Hz.
Audio format	24-bit	PCM
Accelerometer characteristics	2G/4G/8G	G

5.3 Data Process

To process Kinect data, it is separated to two processes as shown in Fig.5.3. It consists of camera process and depth data analysis. Color image from camera is processed to derive position and orientation of robot and depth data is projected to Σ_G. It is described space status and compute size of objects in space. For robot position, it is sent to local controller in robot by communication system.

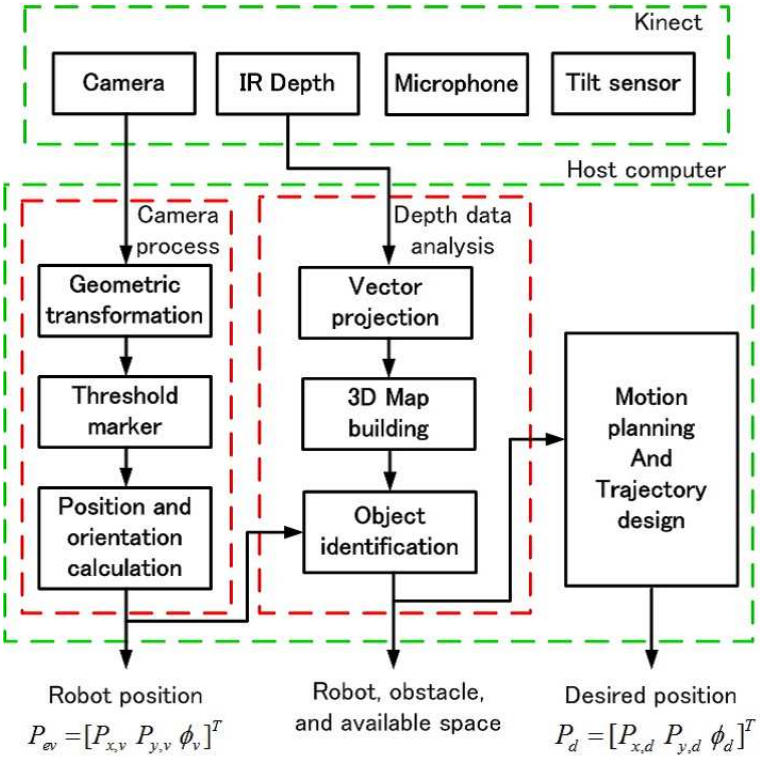

FIGURE 5.3: Flow chart to describe data fusion for color image and depth data.

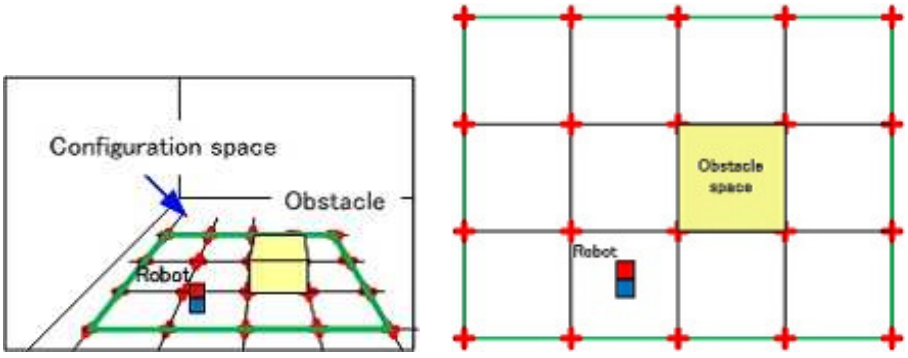

(a) perspective view image (b) top view image

FIGURE 5.4: Color image to present the intelligent space in perspective view and configuration space in top view.

5.3.1 Camera Process

This process consists of 3 steps that geometric transformation, threshold marker, and position and orientation calculation. Geometric transformation is introduced to transform perspective view in Fig.5.4(a) to top view image in Fig.5.4(b). It is a function in OpenCV library[52] and $C++$ program is presented as follows;

```
Mat Rmat;
Point2f old[4];
// Define position of trapezoid corner
Point2f new[4];
// Define the rectangle corner for top view image
Rmat = getPerspectiveTransform(old, new);
// Derive rotation matrix (Rmat)
warpPerspective(img, result, Rmat, size, flags, mode, value);
// Transform perspective view to top view
```

where, img and result denotes original perspective image and top view image, respectively. Rmat denotes rotation matrix of perspective view to top view. size is resolution of top view image. flags is the combination of interpolation methods. mode is the extrapolation method. value denotes the value used in case of a constant border, which is defined as 0 by default.

After that the marker on robot is separate from the screen and press into top view image as shown in Fig.5.4(b), and then it is derived the position and orientation, which denotes robot position in XY coordinate $[P_{x,v}, P_{y,v}]$ and yaw angle (ϕ_v).

5.3.2 Vector Projection Analysis

The depth data is the set of distance vector from Kinect to each position in the perspective image. By the way, the orientation of Kinect based on Σ_{G1} equals the orientation of depth data at the center of image. Then, the roll angle equals ρ in Eq.(5.1). The pitch angle (α_D) and yaw angle (γ_D) can be computed relative to the orientation of Kinect in Eq.(5.1) and the specification of Kinect in Table.5.1 are given that

$$\alpha_D = \alpha + \alpha_V \frac{(\frac{P_V}{2} - y)}{P_V} \tag{5.3}$$

$$\gamma_D = \alpha + \alpha_H \frac{(\frac{P_H}{2} - x)}{P_H} \tag{5.4}$$

where, x and y denote pixel number in horizontal and vertical axis, and then actual position of each pixel based on Σ_{G1} can be derived as follows;

$$\vec{d} = {}^{G1}R_S \vec{D} \tag{5.5}$$

$$\begin{bmatrix} \vec{d}_x \\ \vec{d}_y \\ \vec{d}_z \end{bmatrix} = \left[R_z(\gamma_D)R_y(\alpha_D)R_x(\rho)\right] \begin{bmatrix} D_x \\ 0 \\ 0 \end{bmatrix} \tag{5.6}$$

where, $\vec{d}$ and $\vec{D}$ denote distance vector based on Σ_{G1} and Σ_S, respectively. ${}^{G1}R_S$ denotes rotation matrix from orientation of vector $\vec{D}$ to $\Sigma G1$.$\vec{d}_x$,$\vec{d}_y$,$\vec{d}_z$ denote the distance vector from Kinect on X,Y,Z axis of Σ_{G1}. D_x is distance vector, which is measured by Kinect.

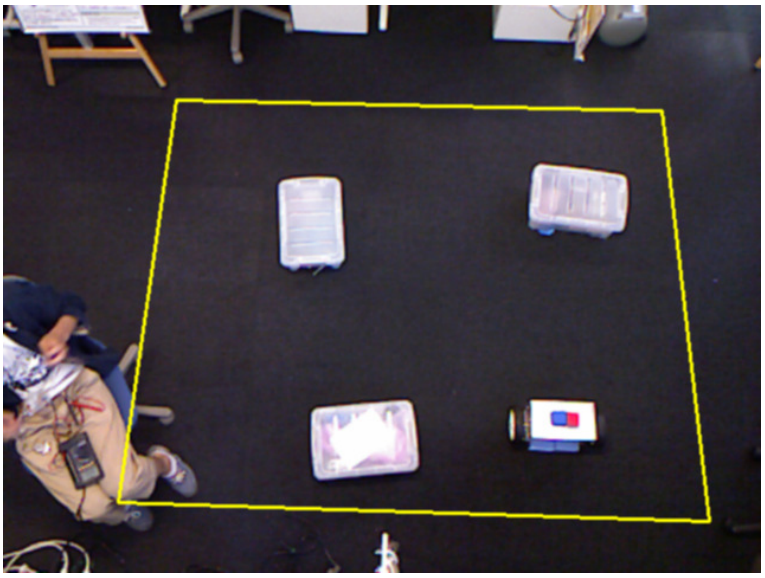

(a) Color image and configuration space in border.

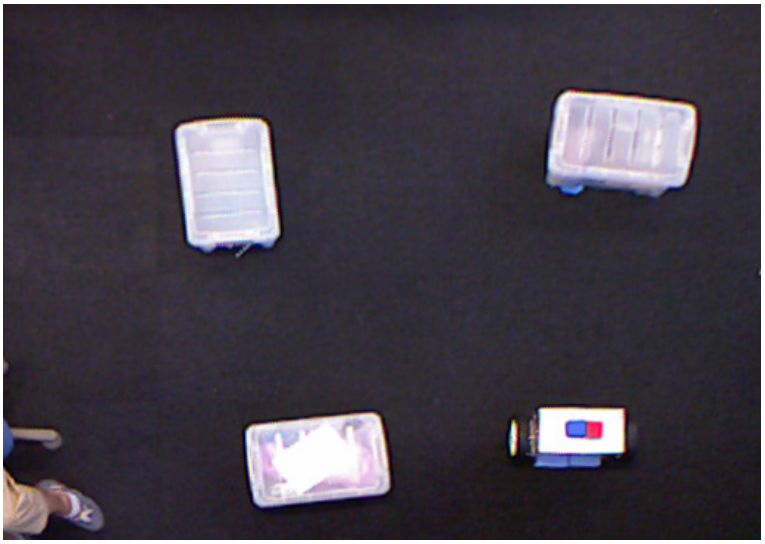

(b) Top view image of configuration space using image processing.

FIGURE 5.5: Color image to present the intelligent space in perspective view and configuration space in top view.

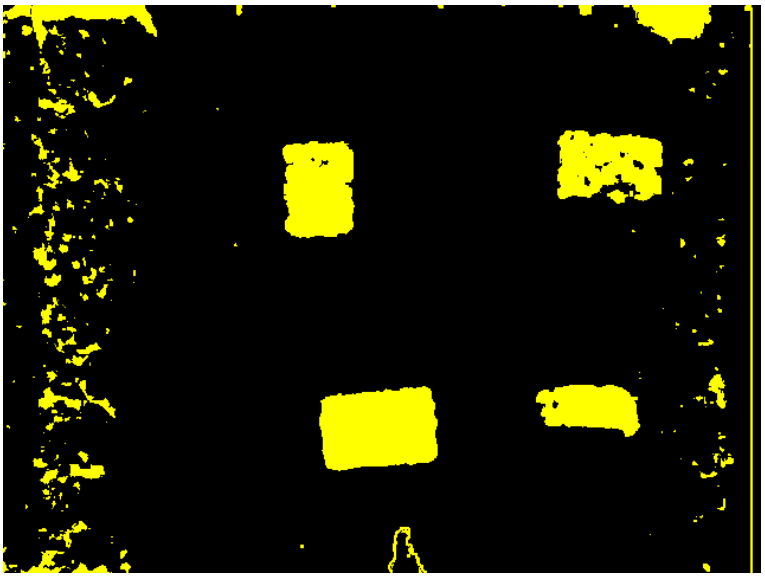

(a) Threshold image of depth data to detect object in intelligent space.

(b) Threshold image to present object in configuration space.

FIGURE 5.6: Threshold image to present object in intelligent space and configuration space using depth data.

5.4 Experiment Result

According to previous sections, the methodology has been described to perceive the information in horizontal plane using image processing and vector projective analysis. Therefore, this section shows the demonstration of the process in real situation as shown in Fig.5.5-5.7 .

Fig.5.5 illustrates perspective and top view images, which are detected by camera and geometric transformation process. The trapezoid in Fig.5.5(a) is defined as configuration space. It means the space to operate the robot and it equals with rectangular area in actual, size of which is high 2.0 m. and wide 2.5 m. After that, the area in trapezoid is transformed to top view image

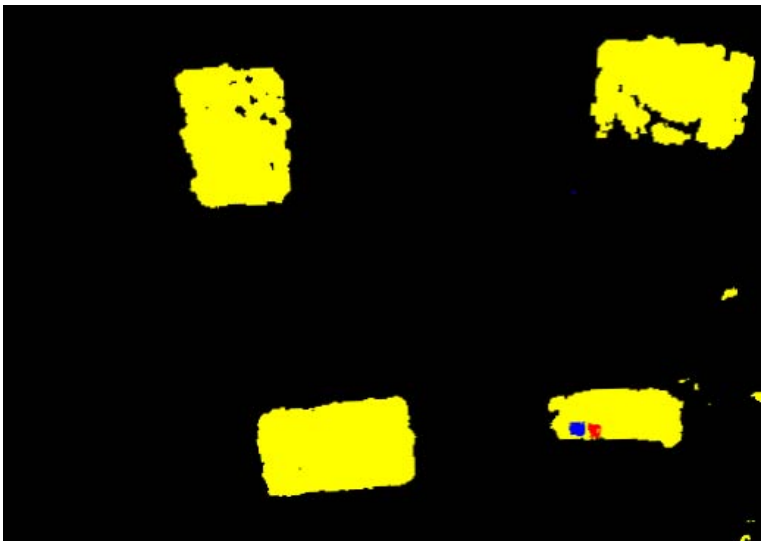

FIGURE 5.7: The configuration image in top view using data fusion technique.

as shown in Fig.5.5(b). The scales of Fig.5.5(b) seems linear than Fig.5.5(a). Horizontal scale is 0.00487 m./pixel and vertical scale is 0.00551 m./pixel. The robot position and orientation are identified by markers on the robot.

Moreover, Fig.5.6(a) shows the depth image, which is sort out only the objects from the screen. Black area denotes the available space and yellow area is the object area. It means that the robot can be perform only in the black area. After that, it is transform to configuration space as shown in Fig.5.6(b).

At summary, the robot can be identified by the marker and the objects can be sorted out from the screen. The orientation of the robot can be derived by the location of markers. From the combination image of the robot position in Fig.5.5(b) with the objects in Fig.5.6(b), we can identify the robot and the obstacles as shown in Fig.5.7 that the yellow areas are the obstacle areas and the yellow area with marker means the robot area. It is necessary information for motion planning.

Chapter 6

Multi-rate Discrete Control

6.1 Introduction

In last several years, intelligent space is introduced to assist humans and robots in a space and it is given the definition in [41] that it is room or area, where is equipped with sensors and they enable the space to perceive activities in the space. Then, this paper aims to develop localization and multi-rate discrete control system for omni-directional robot in space. The localization is a function of intelligent space to locate robot position in space. In general pattern to find the location, it is computed the position and orientation using internal sensor [45]. Multi-rate discrete control system is designed to derive global positioning error in feedback control system with internal sensors such as wheel slip.

In additional, vision feedback control system is often presented [19, 25, 29, 30, 40, 42] and the performance may not be high because the sampling rate of the vision sensor is low. Then, Multi-rate control (MRC) in [14, 18, 22, 33] seem suitable with actual system than vision feedback control. It is utilized to increase the sampling interval and it involves the sensor data with multiple sampling rates.

As above sentences, this study deals localization and multi-rate discrete control system. Kinect is used as an environment sensor. To locate robot position, geometric transformation using trapezoid corners is introduced to transform the perspective image to top view image and the depth image from IR depth sensor is projective to world coordinate frame. The combination of both data exhibits objects in space and 3D map information. After that robot position and orientation are identified by marker. In particular, this paper contrasts with previous studies on the control system that multi-rate discrete control system (MRDC) is applied to perform robot instead of vision control system. It treats global positioning error in feedback control system with internal sensors and low sampling rate vision system.

TABLE 6.1: The sampling interval of intelligent space's communication, internal sensors, and input torque.

Sampling period	time (*sec.*)
Intelligent space's communication (T_v)	0.095
Position output (T_y)	0.005
Input torque (T_u)	0.005

Therefore, this study improves the control systems in the previous studies[19, 25, 29, 30, 40, 42], which perform the robots by vision control system and multi-rate discrete control system is treated the multi-sampling rate problem. It is specialized for omni-system. This article is organized as follows: omni-directional robot, dynamic model, localization, localizing demonstration, multi-rate discrete control system, experiment result, and conclusion. It is divided MRCD control for non-holonimc robot and holonomic robot, which are two wheeled inverted pendulum robot in Fig.2.1a and four wheeled omni-directional robot in Fig.2.2a, respectively.

6.2 Multi-sampling rate System

The robot system of multi-rate system is shown in Fig.6.4(a), it obtains multiple sampling rates such as sampling interval of communication (T_v), position of internal sensors (T_y), and actuator (T_u). Intelligent space system derives the location of robot (P_{ev}) and desired position (P_d). Then, it is sent to the robot via communication system. The data from internal sensors such rotary encoder are computed to derive the location of robot (P_{lo}), $P_{lo} = \begin{bmatrix} P_{x,l} & P_{y,l} & \phi_l \end{bmatrix}^T$. However, the position of the robot by internal sensors can be computed with sampling interval T_y, the controller recognizes the position of the robot with T_u period. Then, the sampling interval of internal sensors may be configured that $T_u = T_y$. The sampling intervals are presented relationship with time domain as follows;

$$t = kT_y = kT_u \qquad : k = 0, 1, 2, ..., n \tag{6.1}$$

$$t = iT_v \qquad : i = 0, 1, 2, ..., m \tag{6.2}$$

$$i = k/N \qquad : N = \frac{T_v}{T_y} \tag{6.3}$$

where, $T_u = T_y = 0.005 sec.$, and $T_v = 0.095 sec.$.

6.3 Holonomic Robot vs Non-Holonomic Robot

The mobile robots utilized in this research are a two wheeled inverted pendulum robot in Fig.2.1a and a four wheeled omni-directional robot in Fig.2.2a. They obtains the properties of

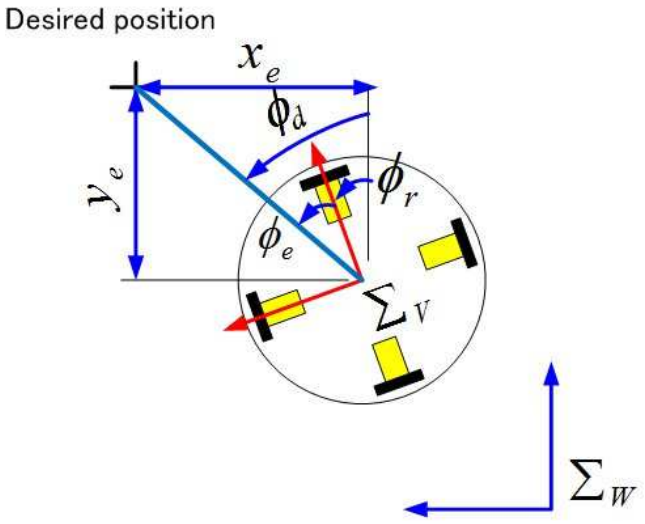

FIGURE 6.1: The motion of the omni-directional robot in the space.

non-holonomic and holonomic constraints, respectively. Fig.6.1 and Fig.6.2 illustrate the motion of the omni-directional robot and the inverted pendulum robot, respectively. Fig.6.1 presents that the omni-directional robot can directly perform on sliding mode belong to all degrees of freedom in world coordinate frame (Σ_W). The position control system can be designed using Jacobain matrix and the position error in world coordinate.

On the other hands, Fig.6.2 deals the motion of the inverted pendulum robot with the trajectory. The motion is stricted by non-holonomic constraint so that the robot cannot perform on sideway. The motion of robot consists of two types that the robot is performed by position feedback with Jacobian matrix, and position feedback with trajectory tracking. If the inverted pendulum robot is performed with Jacobian matrix, the trajectory will equal as solid blue line and the curve motion depends on the distance error and the yawing feedback gain (K_ϕ). If K_ϕ is huge and the distance error is constant, the curve motion becomes nearby the trajectory. However, the robot can successfully approach the desired positions but it can not be strict on the trajectory and the motion varies on several parameters. Thus, the trajectory tracking algorithm is required to fix the curve motion as shown in red line. It denotes the algorithm for ranking the priority of the error of each degree of freedom.

6.4 Wheel Slip Motion and Global Positioning Error

Wheel Slip is important factor to produce an effect of global positioning error and it is a critical cause of accident in vehicle. In [46, 47], the authors have introduced wheel slip constraint [46] and the method to control slip motion [47]. Generally, the floors are determined as flat and solid, but the space in our experiment is covered by carpet. It complicates to derive the slip model so that we purpose a development.

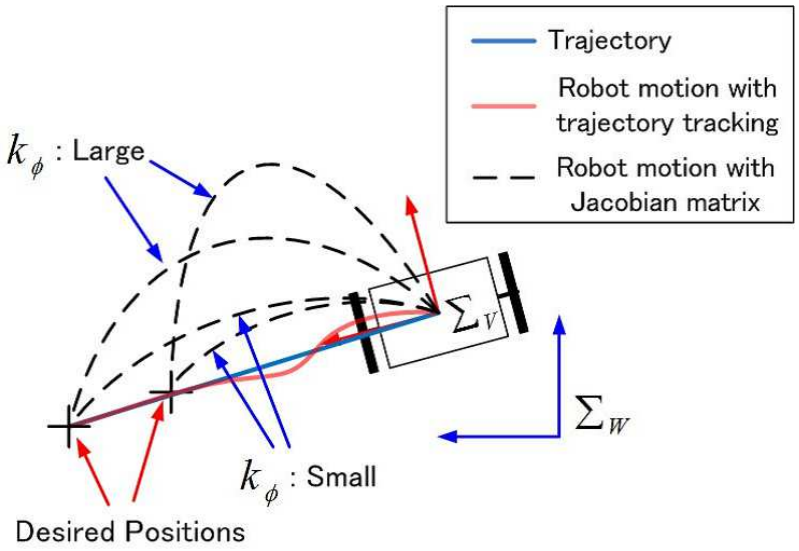

FIGURE 6.2: The motion of the inverted pendulum robot in the space.

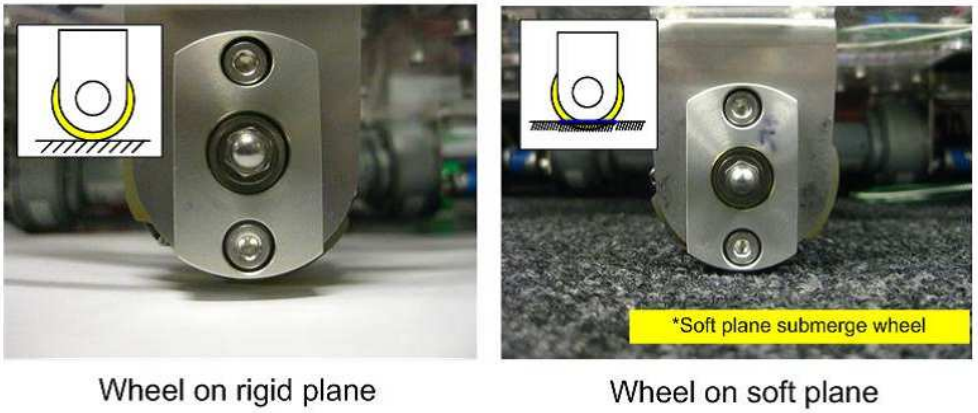

FIGURE 6.3: The figure illustrates the wheel on rigid plane and soft plane.

In this experiment space is cover by soft material so that the wheel is submerge in to the space as shown at right image in Fig.6.3. Then, the translation friction and slip motion are important factor to produce the global positioning error.

Generally, wheel slip usually appear relative to the dynamic friction between wheel and plane and the kind of plane. The wheel slip model is given that

$$s_L[k] = 1 - \frac{v_{actual}[k]}{v_{detect[k]}} \tag{6.4}$$

Then, the global positioning error (P_{er}) at k is given as step discrete function that

$$P_{er}[k] = P_{er}[k-1] + (I_{3\times3} s_L[k]) v_{detect}[k] T_y \tag{6.5}$$

where, $s_L[k]$ denotes the slip model based on world coordinate frame at step k, $I_{3\times3}$ denotes identity matrix of size 3. $s_L[k] = \begin{bmatrix} s_x[k] & s_y[k] & s_\phi[k] \end{bmatrix}^T$, $s_x[k]$ and $s_y[k]$ are slip model on X

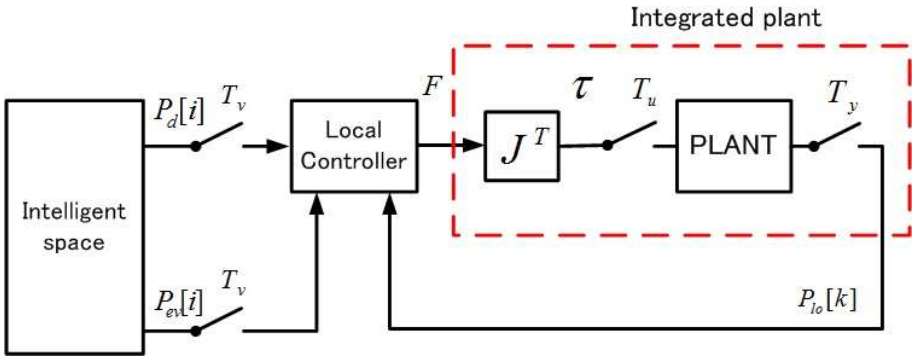

(a) Overview of robot system with multiple sampling intervals

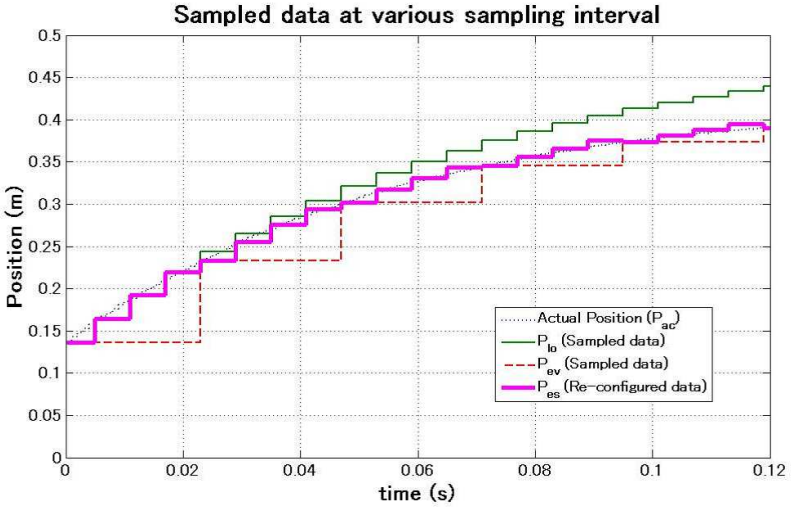

(b) Figure shows actual position and sampled position of T_y, T_u, and T_v.

FIGURE 6.4: Robot's system and sampled data.

and Y axis at step k. $s_\phi[k]$ denotes slip model of rotation about Z axis at step k. v_{actual} and v_{detect} are actual velocity and detected velocity based on world coordinate frame and $v_{detect} = J\dot{\theta}$. J denotes Jacobian matrix in Eq.(2.66). $P_{er}[k]$ is position and angle errors at step k and $P_{er}[k] = \begin{bmatrix} P_{e,x}[k] & P_{e,y}[k] & P_{e,\phi}[k] \end{bmatrix}^T$.

6.5 Multi-rate Control for Omni-directional Robot

6.5.1 Control Structure

The control system of the omni-directional robot is designed as shown in Fig.6.5 that it consists of plant, Jacobian matrix, position estimator and feedback gain. The plant denotes the dynamic of the omni-directional robot and Jacobian matrix of the robot is presented in Eq.(2.66). The combination of the robot position with different i and k intervals, which is called position

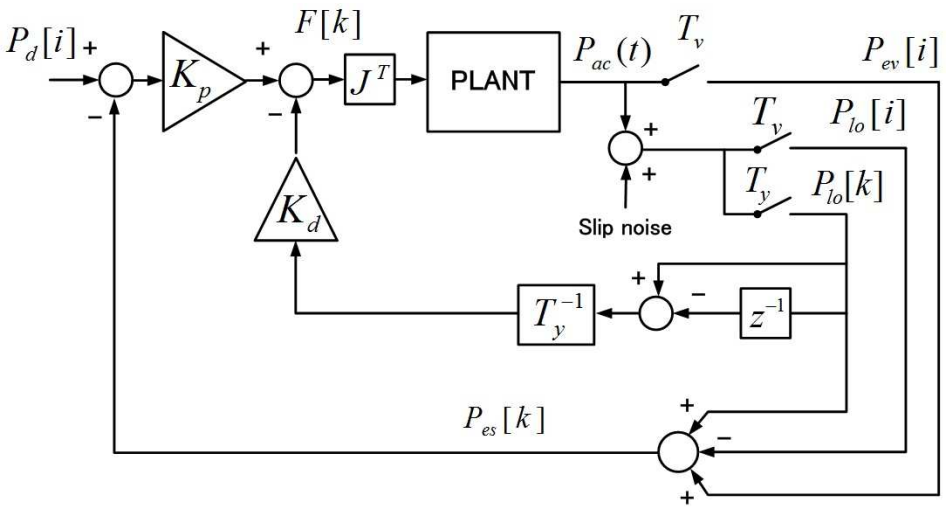

FIGURE 6.5: The multi-sampling rate control system in the local controller for holonomic robot.

estimator. The feedback gain is designed based on discrete system. The description of each part will present in next section.

6.5.2 Position estimator

To treat wheel slip error for the omni directional robot, Fig.6.4 (b) shows dot line denote ideal position, center line denotes actual position (P_{ac}). Thin solid line denotes sampled position from rotary encoders. Dash line denotes sampled position from environment system (P_{ev}) and position estimate(P_{es}) is configured by P_{ev} and P_{ac}. It describes that the actual position (P_{ac}) may be different with P_{lo} because rotary encoder measure rotation of wheel with slip motion. Then, position estimate (P_{es}) is approximated as the actual position. It is given that

$$P_{es}[i,k] \quad = \quad P_{ev}[i] + (P_{lo}[k] - P_{lo}[i]) \tag{6.6}$$

By the way, the different between P_{lo} at sampling interval T_y and T_v means distance of robot motion during interval T_v. In particular, sampled data of P_{ev} adjusts the reference of estimate position P_{es} corresponding to actual position. Thus, it effects to decrease the accumulated error from wheel slip.

6.5.3 Controller design

As the description of the multi-rate system, the equation of motion in Eq.(2.73) can be simplified as integrated plant. The dimension of input is redefined to force (F) corresponding to

Eq.(2.65). Then, linear system in time-invariant is given by

$$\dot{x}_{s1}(t) = Ax_{s1}(t) + BF(t) \tag{6.7}$$
$$y(t) = Cx_{s1}(t) \tag{6.8}$$

The discrete system is realized that

$$x_{s1}[i, k+1] = A_d x_{s1}[i, k] + B_d F[i, k] \tag{6.9}$$
$$y[i, k] = C_d x[i, k] \tag{6.10}$$

where, $A = \begin{bmatrix} 0_{3x3} & I_{3x3} \\ 0_{3x3} & 0_{3x3} \end{bmatrix}$, $B = \begin{bmatrix} 0_{3x3} \\ M^{-1}EJ^T \end{bmatrix}$, $A_d = e^{AT_u}$,
$B_d = \int e^{A\tau_s} d\tau_s B$, $C = C_d = \begin{bmatrix} I_{3x3} & 0_{3x3} \end{bmatrix}$. $x_{s1} = \begin{bmatrix} q & \dot{q} \end{bmatrix}^T \in R^6$

The control system is designed as shown in Fig.6.5 and it consists of double loops that inner loop is velocity feedback and outer loop is position error feedback. Then, state space in Eq.(6.9) is redefined that

$$\dot{x}_{s2}(t) = A_{s2}x_{s2}(t) + B_{s2}F(t) \tag{6.11}$$
$$x_{s2}(t) = \begin{bmatrix} x_1(t) & x_2(t) \end{bmatrix}^T \tag{6.12}$$
$$x_1 = P_{ev}(t) - P_d(t) \quad , \quad \dot{P}_d(t) = 0 \tag{6.13}$$
$$x_2 = \dot{P}_{ac}(t) \tag{6.14}$$

Therefore, state matrix (A_{s2}) and input matrix (A_{s2}) in time-variant are

$$A_{s2} = \begin{bmatrix} 0_{3\times3} & I_{3\times3} \\ 0_{3\times3} & 0_{3\times3} \end{bmatrix} \tag{6.15}$$
$$B_{s2} = \begin{bmatrix} 0_{3x3} \\ M^{-1}EJ^T \end{bmatrix} \tag{6.16}$$

Discrete state space model with sampling interval T_u is given by

$$x_{s2}[k+1] = A_{ds2}x_{s2}[k] + B_{ds2}F[k] \tag{6.17}$$
$$A_{ds2} = \begin{bmatrix} I_{3\times3} & T_u I_{3\times3} \\ 0_{3\times3} & I_{3\times3} \end{bmatrix} \tag{6.18}$$
$$B_{ds2} = \begin{bmatrix} 0_{3x3} \\ T_u M^{-1}EJ^T \end{bmatrix} \tag{6.19}$$

where, $EJ^T = I_{3\times3}$

$$x_{s2}[k] = \begin{bmatrix} x_1[k] & x_2[k] \end{bmatrix}^T \tag{6.20}$$

$$x_1[k] = P_d[k] - P_{ev}[k] \quad , \quad \frac{P_d[k] - P_d[k-1]}{T_u} = 0 \tag{6.21}$$

$$x_2[k] = \dot{P}_{ac}[k] \tag{6.22}$$

Considering the estimate position (P_{es}) in Eq.(6.6), it seems full state feedback as shown in Fig.6.5, and then input force is given that

$$F(t) = K_p(P_d(t) - P_{ev}(t)) - K_d(\dot{P}_{es}(t)) \tag{6.23}$$

where, K_p and K_d is proportional gain and derivative gain, respectively. $\dot{P}_{es}(t) = \dot{P}_{lo}(t)$, even if wheel slip is neglected, $P_{es}(t) = P_{lo}(t)$.

Controller gain is derived using digital linear quadratic regulator (*DLQR*) by

$$Q = \text{diag}[1.4, 1.4, 0.0975, 17.5, 17.55, 1] \times 10^4 \tag{6.24}$$

$$R = \text{diag}[23, 23, 5] \times 10^2 \tag{6.25}$$

and feedback gain K_p and K_d are

$$K_p = \begin{bmatrix} 2.45 & 0 & 0 \\ 0 & 2.45 & 0 \\ 0 & 0 & 1.23 \end{bmatrix} \tag{6.26}$$

$$K_d = \begin{bmatrix} 10 & 0 & 0 \\ 0 & 10 & 0 \\ 0 & 0 & 4 \end{bmatrix} \tag{6.27}$$

6.6 Multi-rate Control for Wheeled Inverted Pendulum Robot

6.6.1 Control structure

The control system is designed as shown in Fig.6.6 and the structure for non-holonomic robot contrasts with the structure of holonomic robot that the motion of non-holonomic robot may not perform on the trajectory to the desired position. Then, trajectory tracking algorithm is used to define the motion planning. In particular, the motion of the inverted pendulum robot not concern only non-holonomic constraint but also the stabilization of the body. The controller will be separated to two parts for the position tracking and the stabilizing. Thus, the control

system of the inverted pendulum robot consists of plant, position estimator, trajectory tracking and controller. The position estimator, trajectory tracking and controller design will be described in next section.

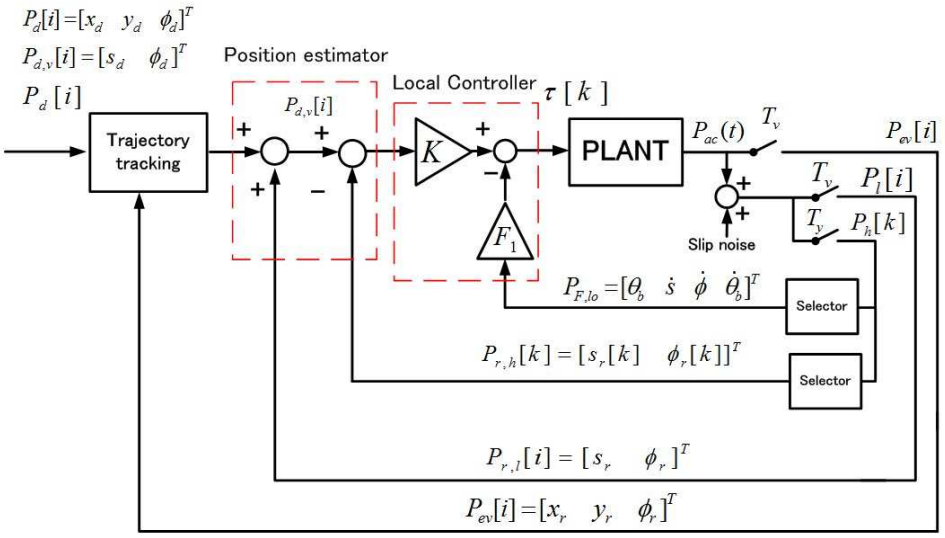

FIGURE 6.6: The multi-sampling rate control system in the local controller for non-holonomic robot.

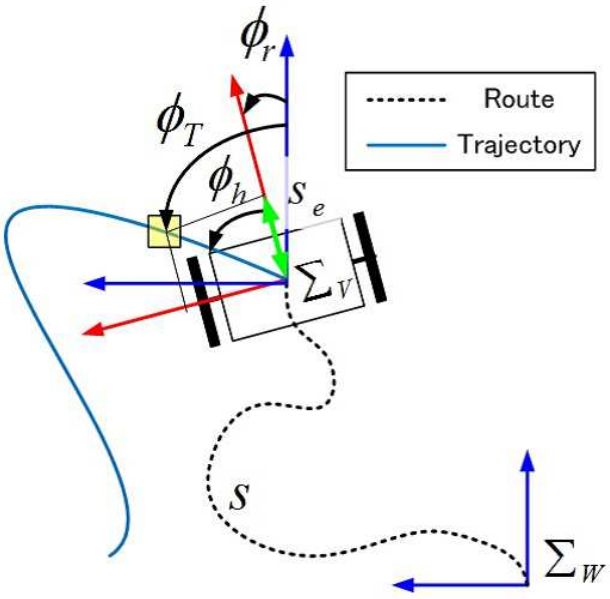

FIGURE 6.7: The motion of the inverted pendulum robot with the way point.

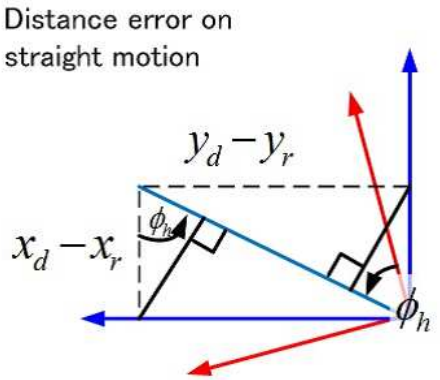

FIGURE 6.8: Figure to show distance error relative to world and vehicle coordinate frames.

6.6.2 Trajectory Tracking

The way point denotes the desired position ($P_d[i]$), which is defined based on world coordinate frame but it is not convenience information for performing the robot. Then, it is converted to the desired position based on vehicle coordinate frame ($P_{d,V}[i]$). Thus, trajectory tracking is designed to derive the distance error ($P_{d,V}[i]$). The error is shown in Fig.6.7 and Fig.6.8. The trajectory tracking algorithm is given that

$$P_e[i] = \begin{bmatrix} s_e & \phi_h \end{bmatrix}^T \tag{6.28}$$

$$\phi_h = \phi_T - \phi_r \tag{6.29}$$

$$\phi_T = \text{atan2}(y_d - y_r, x_d - x_r) \tag{6.30}$$

$$s_e = \cos(\phi_h)\sqrt{((x_d - x_r)\cos(\phi_h))^2 + ((y_d - y_r)\sin(\phi_h))^2} \tag{6.31}$$

where, $P_e[i]$ denotes the position error from the robot to the way point at i interval. ϕ_h denotes heading error from the yaw of the robot (ϕ_r) to the yaw of the desired position (ϕ_T). s_e is not real distance to the desired position but it denotes the forwarding distance error based on vehicle coordinate frame. Thus, the robot will rotate about z axis before it moves forward, if the desired position is on the sideway of the robot.

6.6.3 Position error estimation

From Fig.6.7, it exhibit that the route of the robot is presented as the dot line. It can detected by the odometry with the slip noise and s denotes the distance belong to the route. The error from the trajectory tracking is updated every i interval. To treat the wheel slip, the error will be

estimated as follows;

$$P_{e,es}[i,k] = P_{d,V}[i] - P_{r,h}[k] \tag{6.32}$$

$$P_{d,V}[i] = P_e[i] + P_{r,l}[i] \tag{6.33}$$

where, $P_{e,es}[i,k]$ denotes the estimate position error from the robot to the way point. $P_{d,V}[k]$ denotes the desired position based on vehicle coordinate frame. $P_{r,l}[i]$ and $P_{r,h}[k]$ denote the robot position based on vehicle coordinate frame of i and k intervals.

6.6.4 Controller design

To design the controller, the state space in Eq.(2.55) is represented in discrete multi sampling rate system as follows;

$$x_{ss}[i,k+1] = A_{d,ss}x_{ss}[i,k] + B_{d,ss}\tau[i,k] \tag{6.34}$$

$$x_{ss} = \begin{bmatrix} s & \phi_v & \theta_b & \dot{s} & \dot{\phi}_v & \dot{\theta}_b \end{bmatrix}^T \tag{6.35}$$

where, $A_{ss} = \begin{bmatrix} 0_{3\times3} & I_{3\times3} \\ -M_L^{-1}G_L & 0_{3\times3} \end{bmatrix}$, $B_{ss} = \begin{bmatrix} 0_{3\times2} \\ M_L^{-1}E \end{bmatrix}$, $A_{d,ss} = e^{A_{ss}T_u}$, and $B_{d,ss} = \int e^{A_{d,ss}\tau_s} d\tau_s B_{ss}$.

The discrete state space model with sampling interval T_u is given by

$$x_{ip}[k+1] = A_{d,ip}x_{ip}[k] + B_{d,ip}\tau[k] \tag{6.36}$$

$$A_{d,ip} = \begin{bmatrix} I_{3\times3} & T_u I_{3\times3} \\ T_u M_L^{-1}G_L & I_{3\times3} \end{bmatrix} \tag{6.37}$$

$$B_{d,ip} = \begin{bmatrix} 0_{3x3} \\ T_u M_L^{-1}E \end{bmatrix} \tag{6.38}$$

where, $x_{ip}[k] = \begin{bmatrix} x_1[k] & x_2[k] \end{bmatrix}^T$, $x_1[k] = P_{d,V}[k] - P_{r,l}[k]$, $\dot{P}_{d,V}[k] = 0$.

Input torque is given that

$$\tau[k] = -Kx_1[k] - F_1x_2[k] \tag{6.39}$$

where, K and F_1 is position tracking gain and balancing gain, subsequently.

Controller gain is derived using digital linear quadratic regulator (*DLQR*) by

$$Q = \mathrm{diag}[5, 1, 0.8, 0.05, 0.1, 1] \times 10^3 \tag{6.40}$$

$$R = \mathrm{diag}[10^4, 10^4] \tag{6.41}$$

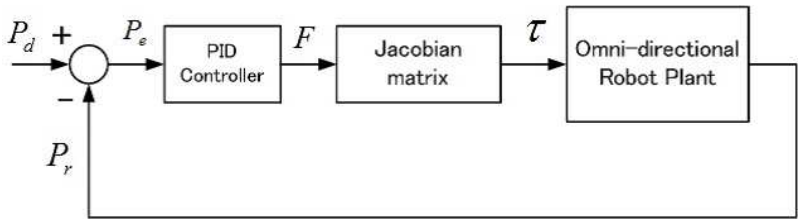

FIGURE 6.9: Vision feedback control with Jacobian matrix.

and feedback gain K_p and K_d are

$$K = \begin{bmatrix} 0.4351 & -0.2217 \\ 0.4351 & 0.2217 \end{bmatrix} \tag{6.42}$$

$$F_1 = \begin{bmatrix} 1.3328 & 0.5548 & -0.0843 & 0.2023 \\ 1.3328 & 0.5548 & 0.0843 & 0.2023 \end{bmatrix} \tag{6.43}$$

6.7 Simulation result

6.7.1 MRC vs Vision control system

This simulation presents the comparison of multi-rate control and vision feedback control. It demonstrates by the omni-directional robot and the vision feedback control is designed as Fig.6.9. The performance of both control systems is considered based on step response. The position reference is given as solid blue line in Fig.6.10 and the responses of the vision control and the multi-rate control are given as solid red line and dashed line, respectively.

The preliminary of this simulation is given that the multi-control system is presented in the previous sections and the vision feedback control is designed as Fig.6.9. The sampling interval of the vision control system equals with T_V. The proportional and derivative gains are defined as Eq.(6.26) and Eq.(6.27) and the integral gain is zero. Fig.6.10 deals the trajectory and the motion of the omni-directional robot. The motion of vision feedback control obtains the overshoot and oscillation motions because the sampled rate of the vision system is low. Then, the simulation result can confirm that the performance of the multi-rate control is greater than the vision feedback control.

6.7.2 Effectiveness of position estimator

This section shows the simulation of MRDC with position estimator in Fig.6.5 and the conventional MRC system without position estimator in Fig.**??** at various values of slip noise. The slip noise is added as global positioning uncertainty, which is described in Eq.(6.5). The

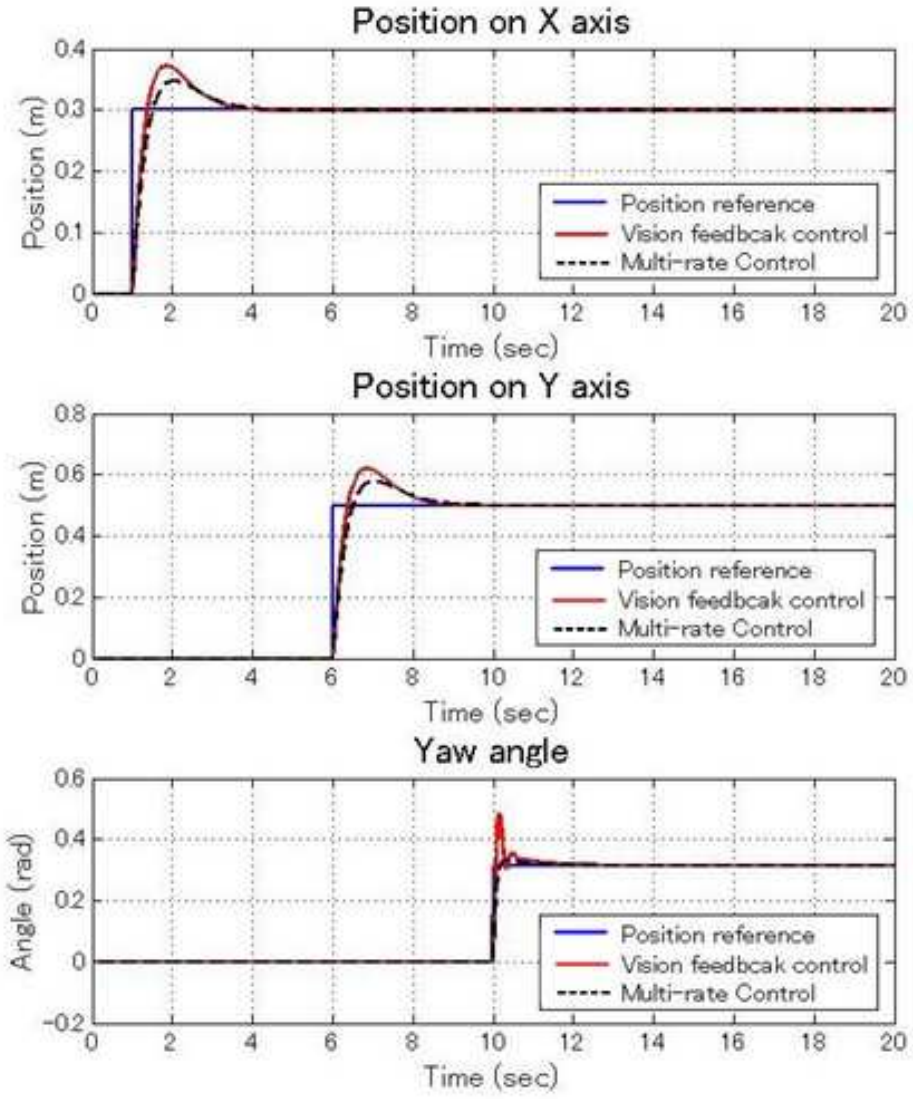

FIGURE 6.10: Motion of omni-directional robot using vision feedback control and multi-rate control system.

conventional MRC system without position estimator in Fig.**??** is designed based on the concept of multi-rate control in [18], which involves the robot position from intelligent space and odometry and the robot position from both sources are directly used to control the robot.

To analyze the effectiveness of position estimator and wheel slip, the robot motion is observed at non-slip motion and slip motion. Then, the slip model and the feedback gain are defined that the slip model is given as constant value such that $s_L = \begin{bmatrix} 0 & 0 & 0 \end{bmatrix}^T$ and $s_L = \begin{bmatrix} 1.3 & 1.3 & 1.3 \end{bmatrix}^T$. For controller gain of MRDC with position estimator, it seems PD controller and K_p and K_d are defined as Eq. (**??**)-(**??**). On the other hands, PID controller in Fig.**??** should consist of K_p, K_i and K_d. In order to compare the result with MRDC with position estimator, K_i is given as zero. K_p and K_d also equal Eq. (**??**)-(**??**). The step response of translation motion is shown in Fig.6.11 that black dash line is reference position Blue center

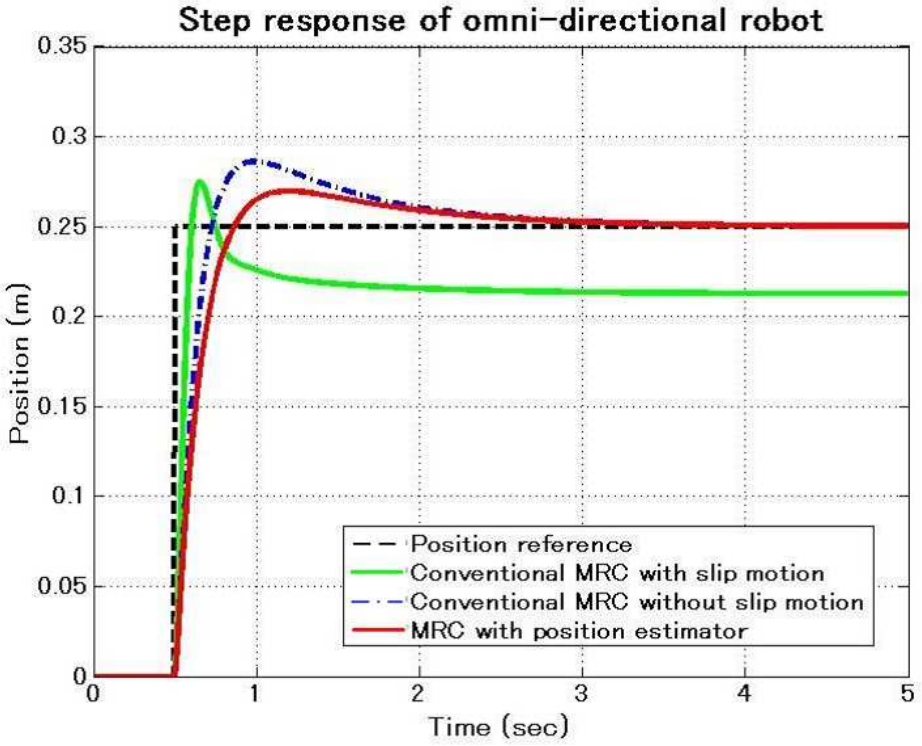

FIGURE 6.11: The step response of MRDC with position estimator and conventional MRC without position estimator.

and green solid lines denote the step response of the conventional MRC at $s_L = \begin{bmatrix} 0 & 0 & 0 \end{bmatrix}^T$ and $s_L = \begin{bmatrix} 1.3 & 1.3 & 1.3 \end{bmatrix}^T$, respectively.

As result, the wheel slip has the effectiveness to the responsibility of the conventional MRC without position estimator. When the wheel slip does not appear, the robot can perform to reference position successfully. If wheel slip appear, the robot can not perform to reference position. On the other words, MRDC with position estimator can control the robot to reference position with slip and non-slip cases. The effectiveness of the position estimator can treat the problem of global positioning error and the step response of MRDC with position estimator does not vary on wheel slip because it is treated by position estimator.

6.8 Experiment result

This section introduces the experiment result of multi-rate control based on the omni-directional robot and the inverted pendulum robot. The results are presented as follows;

6.8.1 Experiment on Wheeled Inverted Pendulum Robot

Fig.6.12 exhibits the motion of the inverted pendulum robot, which is performed by the multi-rate control system. Fig.6.13 shows the motion of the robot while it tracks the trajectory. The robot can track the trajectory, successfully. The result deals robot motion with trajectory that blue line denotes trajectory and red line denotes robot position, which is detected by the intelligent space, respectively. Fig.6.12(a) illustrates that the motions of the inverted pendulum robot in XY plane perturbs because the robot has to balance itself while it changes the direction or confines the position. To exhibit the successful of the trajectory tracking, Fig.6.12(b) deals the trajectory and the robot position in time domain. It shows that the robot can perform to track the trajectory, successfully.

6.8.2 Experiment on Omni-directional Robot

From the control system in Fig.6.5, omni-directional robot is performed in configuration space as shown in Fig.6.14. Trajectory is designed as center line, and then way point is defined on trajectory and it is presented instead of desired position (P_d). After that it is moved on the trajectory with 0.25 m/s., the robot is performed to track it. Robot position is computed by rotary encoders and intelligent space. They are recored to compare accuracy. To show the motion, Fig.6.15 illustrates the robot motion while it tracks the trajectory, which is shown in top view and perspective view. The left and right columns denote the top and perspective views, subsequently. The result deals robot motion with trajectory , where center line denotes trajectory. Dash line and solid line denotes robot position, which is detected by rotary encoders and intelligent space, respectively. Fig.6.14 shows that the position of robot by intelligent space is high accuracy than rotary encoder because the effective of wheel slip. If local controller uses only robot position by rotary encoders, the trajectory tracking may not approach to the desired position in space. The result exhibits that robot can track the trajectory successfully with a small error.

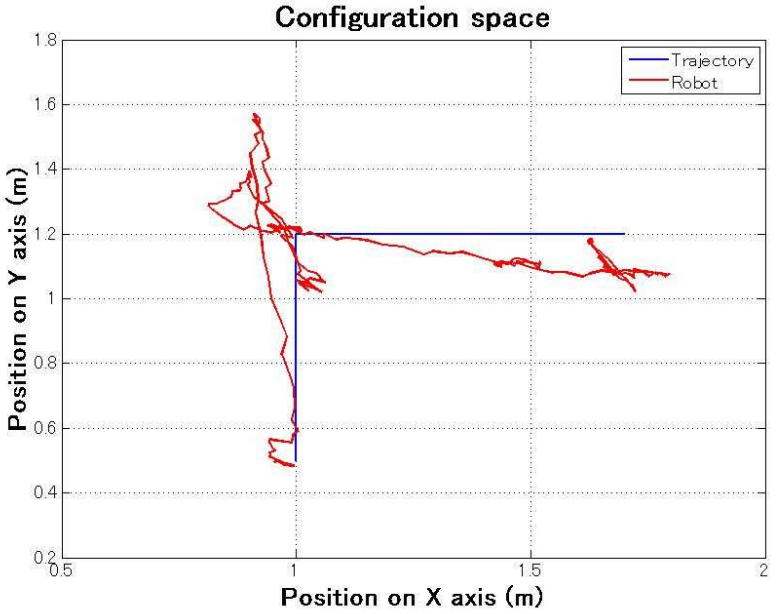

(a) Position of the inverted pendulum robot in XY plane.

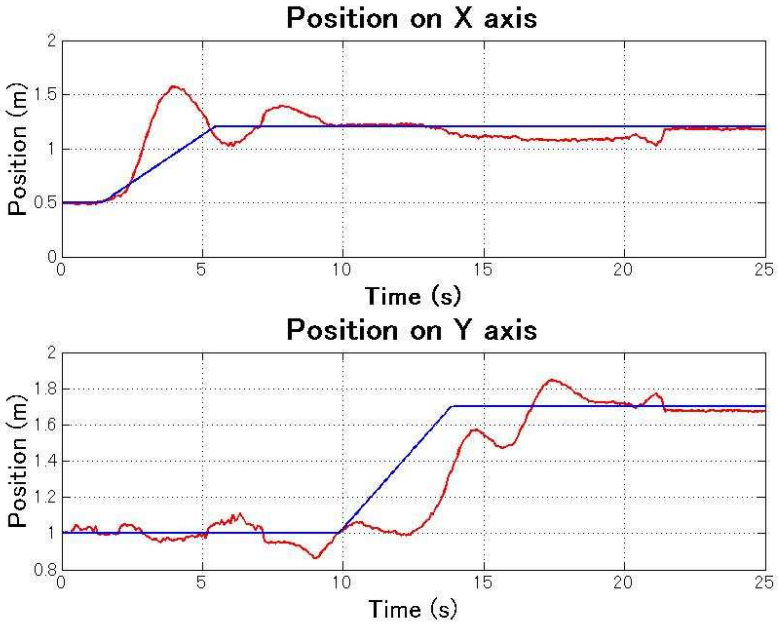

(b) Position of the inverted pendulum robot in time domain.

FIGURE 6.12: Robot's system and sampled data.

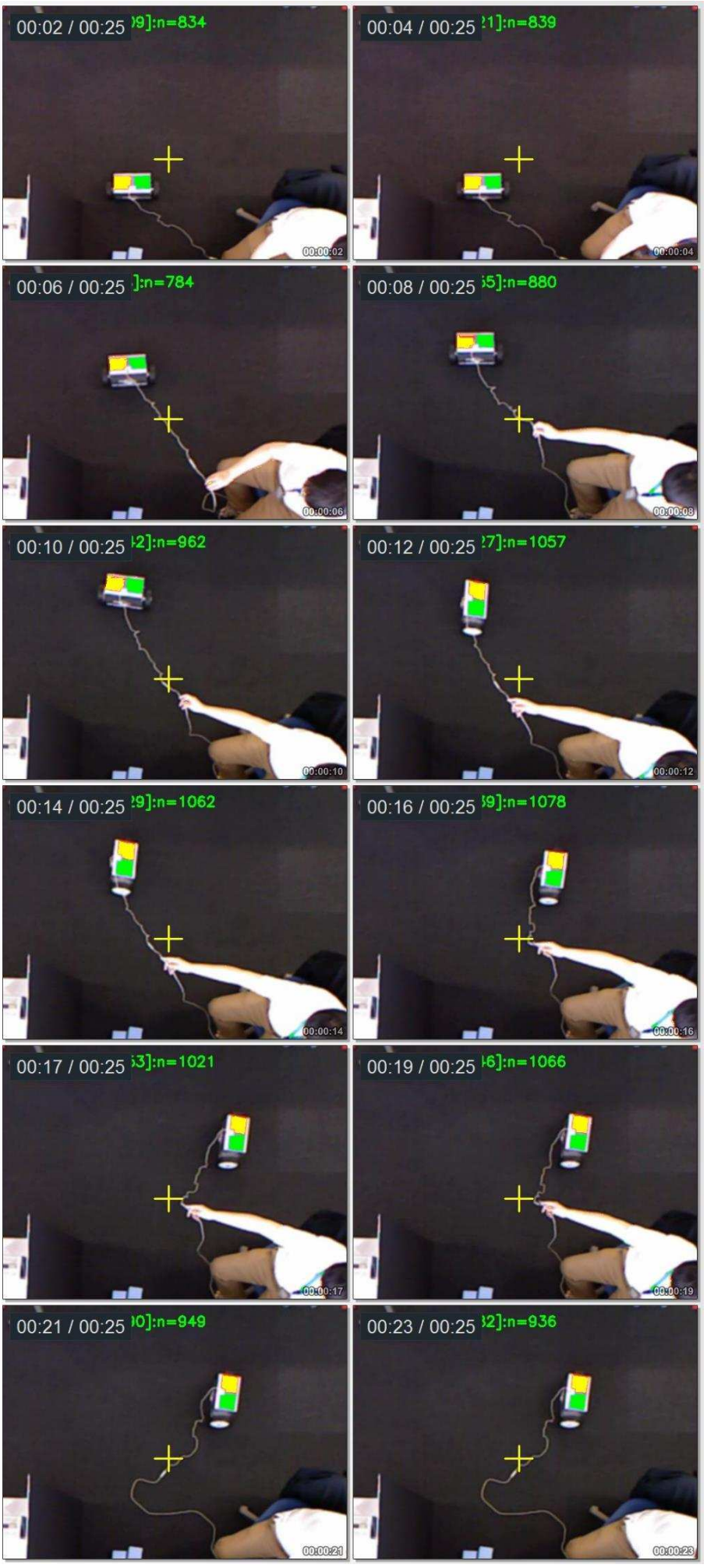
00:02 / 00:25
00:04 / 00:25
00:06 / 00:25
00:08 / 00:25
00:10 / 00:25
00:12 / 00:25
00:14 / 00:25
00:16 / 00:25
00:17 / 00:25
00:19 / 00:25
00:21 / 00:25
00:23 / 00:25

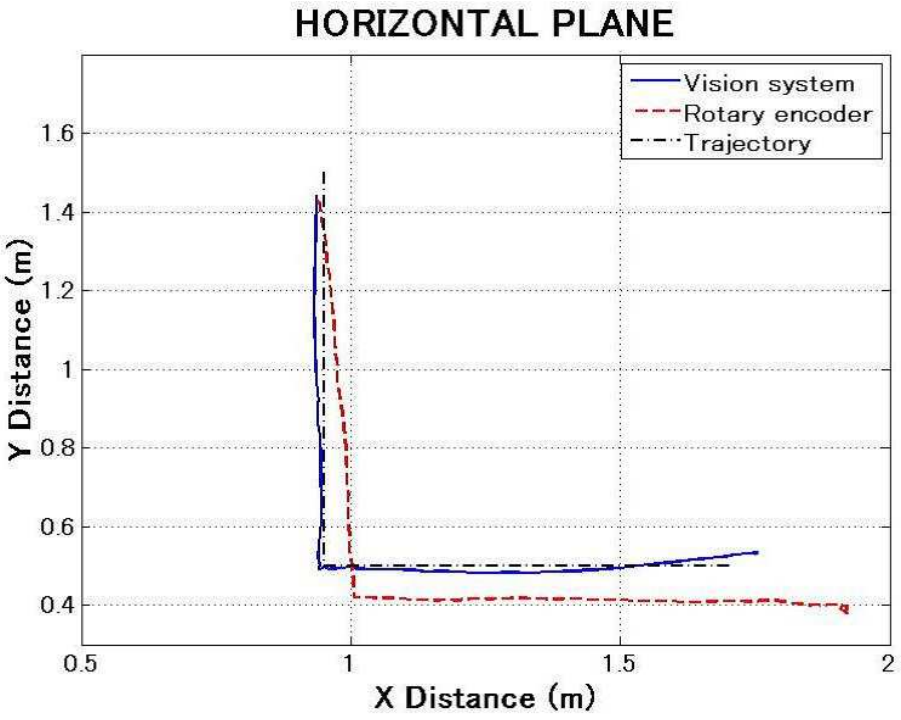

FIGURE 6.14: The experiment result of trajectory tracking using multi-rate discrete control when way point speed is 0.25 m/s..

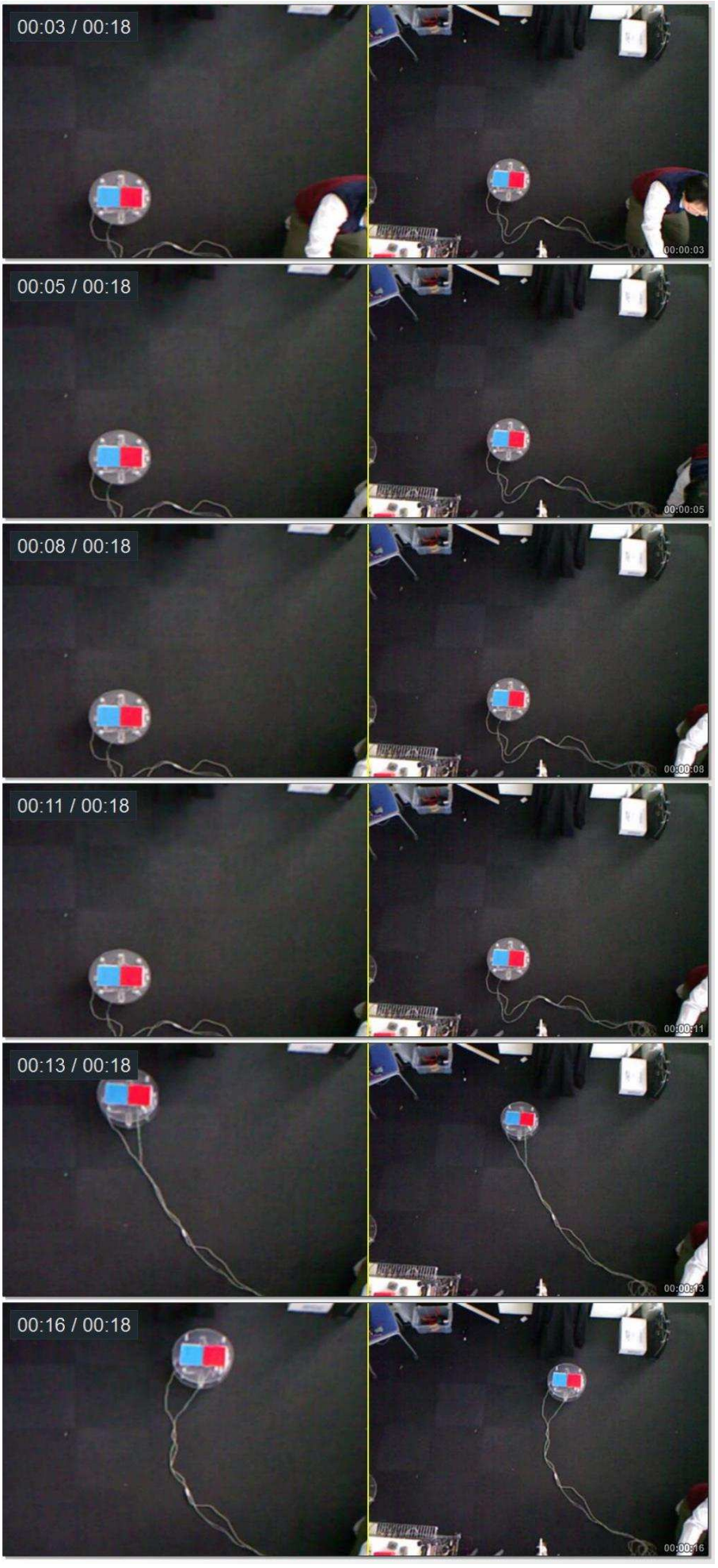

FIGURE 6.15: Motion of omni-directional robot in top view and perspective view.

Chapter 7

Conclusion

This thesis treated some problems for development of vehicle robots such as unknown system parameters, friction in mechanical system, global positioning error, and multi-rate sampling interval. They are benefits to improve the motion of the robots in indoor space. In previous chapters exhibit the principle knowledges, the new methodologies, and experiments and this chapter concludes the results of them. It is organized as follows:

7.1 System Identification and Friction Compensation

Many researchers studied about system identification for dynamic system, who prefer ARX model as model reference but it may not suitable corresponding to actual condition. Then, this study introduces another model such as ARMAX model with new assumption considering the uncertainties of actuator and sensor measurement. As the result, the identification results can be admired. The position and tilt angle errors in Fig.4.5 exhibits that the friction compensation successfully improve the control performance and the friction compensation using the friction estimate of the ARMAX model performs better than ARX model result and general feedback control, however the errors are remained a little. Therefore, we confirm that ARMAX model with high frequency error is suitable in practically more than ARX model in order to identify wheeled inverted pendulum robot system.

7.2 Localization

This study approaches the localization with perspective view The localization result shows a robot and objects in space. The size configuration space is 2.5×2.0 m. and image scale in

domain of pixel is 513 × 363 pixel. The scale of configuration image seems linear scale that horizontal scale is 0.00487 m./pixel and vertical scale is 0.00551 m./pixel.

7.3 Multi-rate Discrete Control

Multi-rate discrete control system for omni-directional robot in intelligent space is designed with position estimation, which estimates robot position by the position from localization and rotary encoders. Fig.6.4(b) illustrates comparison of estimate position, actual position, and position from localization and rotary encoders. The estimate position seems similar with the actual as same as the position from localization but the sampling interval is higher. The control systems for the inverted pendulum robot and omni-directional robot are different that the motion of the inverted pendulum robot is bounded. Then, the inverted pendulum robot may not tract to the trajectory as described in Fig.6.2, if the control system is designed based on Jacobian matrix. Then, the trajectory tracking algorithm is established to derive the distance error from the robot to the desired position and the result of the trajectory tracking is presented Fig.6.12 and 6.13. On the other hands, the control system for the omni-directional robot can perform to track the trajectory by Jacobain matrix and the result is shown in Fig.6.14-6.15. The results shows the robots can perform to track the trajectory successfully and they deal trajectory, position of robot by localization and rotary encoders. The position from rotary encoders is not high precision because the effective of wheel slip.

List of Publications

International Journal

[1] Danai Phaoharuhansa and Akira Shimada, Friction Compensation for Two Wheeled Inverted Pendulum Robot Using System Identification, *International Journal of Advances in Science and Technology (IJAST'2014)* , ISSN 2348-5426.

International Conference

[1] Danai Phaoharuhansa and Akira Shimada, Obstacle Avoidance for Multi-link Inverted Pendulum Robot using Virtual Impedance, *the 7th SEATUC symposium*, Bangkok, Thailand, 2012.

[2] Danai Phaoharuhansa and Akira Shimada, Trajectory Tracking for Wheeled Inverted Pendulum Robot Using Tilt Angle Control, *the 39th Annual Conference of the IEEE Industrial Electronics Society (IECON2013)*, Vienna, Austria, 2013.

[3] Danai Phaoharuhansa and Akira Shimada, Multi-rate Discrete Control for Omni-directional Robot in Intelligent Space, *SICE Annual Conference 2014*, Hokkaido, Japan, 2014.

Domestic Conference

[1] Danai Phaoharuhansa and Akira Shimada, Control on Inverted Pendulum Robot with Unknown Parameters and Disturbance, *the 30th Annual Conference of the Robotic Society of Japan (RSJ)*, Sapporo, Japan, 2012.

[2] Danai Phaoharuhansa and Akira Shimada, Position Control on Wheeled Inverted Pendulum Robot, *IEEJ Technical Meeting, IIC-13-115 MEC-13-115*, Chiba, Japan, 2013

List of Contributions

International Conference

[1] Akira Shimada and Danai Phaoharuhansa, An Adaptive Disturbance Observer Design on Mechatronic Systems, *2012 International Conference on Advanced Mechatronic Systems*, pp. 320-322, Tokyo, Japan, 2012.

Domestic Conference

[1] Koutaro Tsuboi, Danai Phaoharuhansa, Akira Shimada, Position Control of Combined Inverted Pendulums, *IEEJ Technical Meeting, IIC-13-116 MEC-13-116*, Chiba, Japan, 2013 [Japanese]

[2] Yutaka Okubo, Danai Phaoharuhansa, Akira Shimada, Transportation Control by Omni-directional Robots, *IEEJ Technical Meeting, IIC-13-123 MEC-13-123*, Chiba, Japan, 2013 [Japanese]

[3] Mousen Ri, Danai Phaoharuhansa, Akira Shimada, Cooperative System for Transportation Control Using Omni-directional Robots, *IEEJ Technical Meeting, IIC-13-124 MEC-13-124*, Chiba, Japan, 2013 [Japanese]

[4] Koutaro Tsuboi, Danai Phaoharuhansa, Akira Shimada, Friction Compensation for Two Wheeled Inverted Pendulum Robot Using System Identification, *Adaptive Disturbance Observer on Inverted Pendulum*, the 31th Annual Conference of the Robotic Society of Japan (RSJ), Tokyo, Japan, 2013. [Japanese]

[5] Yutaka Okubo, Danai Paoharuhansa, Ri Mousen, Akira Shimada, A Proposition of System Design for Omni-directional Robot, *IEEJ Technical Meeting, MEC-14-077*, Tokyo, Japan, 2014 [Japanese]

[6] Mousen Ri, Danai Phaoharuhansa, Misaki Tsuchimoto, Akira Shimada, Object Transportation Assist System using the Omni-vehicle, *IEEJ Technical Meeting*, Tokyo, Japan, 2014 [Japanese]

Bibliography

[1] Lennart Ljung. *System Identification : Theory for The Users, second edition*. PTR Prentice Hall Information and System Science Serires, 2009.

[2] Zexiang Li Richard M. Murray and S. Shankar Sastry. *A Mathematical Introduction to Robotic Manipulation*. CRC press, 1994.

[3] Stefan Brock. Identification of the parameters in inverted pendulum model. *the 7th International Workshop on Advance Motion Control (AMC'07)*, 2007.

[4] Chenglin Hu and Feng Wan. Parameter identification of a model with coulomb friction for a real inverted pendulum system. *in Proc. of the 9th IEEE international conference on Control and Decision Conference, CCDC09*, pages 818–823, 2009.

[5] A. Pattanapukdee O. Gomonwattanapanich and M. Mongkolwongrojn. Compensation and estimation of friction by using extended kalman filter. *International Joint Conference SICE-ICASE 2006*, pages 5032–5035, 2006.

[6] Suk-Kyo Hong Duckgee Park, Dongkyoung Chwa. An estimation and compensation of the friction in an inverted pendulum. *SICE-ICASE International Joint Conference*, 2006.

[7] Zhao Yixin He Qiang Huang Qiaoli Xiao Lin Qi Qian, Huang wei. System identification of the double inverted pendulum based on genetic algorithm. *the 2nd International Symposium on Systems and Control in Aerospace and Astronautics, 2008. ISSCAA 2008.*, 2008.

[8] Victor Semedo de Mattos Siqueira Hugo Tanzarella Teixeira and Celso Jose Munaro. Comparison of methods for estimation and compensation of friction applied to an inverted pendulum. *the proceeding of 7th International Conference on Control and Automation (ICCA)*, pages 818–823, 2011.

[9] Pongtorn Chunhacha and Taworn Benjanarasuth. Parameters tuning effects in the model predictive control of an inverted pendulum. *in Proc. of TENCON 2011 - 2011 IEEE Region 10 Conference*, pages 1080–1084, 2011.

[10] Danai Phaoharuhansa and Akira Shimada. Position control on wheeled inverted pendulum robot. *IEEJ Technical Meeting, IIC-13-115 MEC-13-115*, 2013.

[11] Seong Hee Jeong and Takayuki Takahashi. Wheeled inverted pendulum type assistant robot: inverted mobile, standing, and sitting motions. *in Proc. of IEEE/RSJ international conference on Intelligent Robots and System (IROS)*, pages 1932–1937, 2007.

[12] Seong Hee Jeong and Takayuki Takahashi. Stable and quick standing-sitting motion of i-pentar by whole-body motion with force control. *in Proc. of IEEE/RSJ international conference on Intelligent Robots and System (IROS)*, pages 199–204, 2009.

[13] Hyung-Jik Lee and Seul Jung. Gyro sensor drift compensation by kalman filter to control a mobile inverted pendulum robot system. *IEEE International Conference on Industrial Technology, 2009. ICIT 2009.*, 2009.

[14] Kazuhiro Yubai Masahiro Kawakita and Junji Hirai. The multi-rate sampling control for a reconfigurable robot. *the 11th IEEE International Conference on Control, Automation and Systems*, 2011.

[15] Akira Shimada and Danai Phaoharuhansa. An adaptive disturbance observer design on mechatronic systems. *2012 International Conference on Advanced Mechatronic Systems*, 2012.

[16] Chaisamorn Yongyai Akira Shimada. Motion control of inverted pendulum robots using a kalman filter based disturbance observer. *SICE-JCMSI, Vol.2, No.1,pp.50-55,2009-1*, 2009.

[17] Fujii Nobuyuki Yongyai Chaisamorn, Shimada Akira. Tilting angle control on inverted pendulum robots considering measurement noise. *IIC-09-138, IEEJ, 2009-3*, 2009.

[18] Douglas P. Glasson. Development and applications of multi-rate digital control. *Control systems magazine, IEEE Control Systems Society*, 1983.

[19] Hyun-Gu Lee Joo-Hyung Kim, Jeong-Eom Lee and Gwi-Tae Park. Identification and control for an unknown robot in intelligent space. *The 18th IEEE International Symposium on Robot and Human Interactive Communication*, 2009.

[20] Robert Holmberg and Oussama Khatib. Development and control of a holonomic mobile robot for mobile manipulation tasks. *International Journal of Robotics Research, vol. 19, pp. 1066-1074.*, 2014.

[21] Danai Phaoharuhansa and Akira Shimada. Control on inverted pendulum robot with unknown parameters and disturbance. *the 30th Annual Conference of the Robotic Society of Japan (RSJ)*, 2012.

[22] Mazayoshi Tomizuka. Multi-rate control for motion control applications. *the 8th IEEE International Workshop on Advanced Motion Control (AMC '04)*, 2004.

[23] Akira Shimada Koutaro Tsuboi, Danai Phaoharuhansa. Position control of combined inverted pendulums. *IEEJ Technical Meeting, IIC-13-116 MEC-13-116*, 2013.

[24] Chris Urmson Michael Darms, Paul Rybski. Classification and tracking of dynamic objects with multiple sensors for autonomous driving in urban environments. *2008 IEEE Intelligent Vehicles Symposium,*, pages 1197 – 1202, 2008.

[25] Yoshkazu Suita Mitsuhiro Ryuman Hiroyulu Sogo Shoichiro Fujisawa, Tom Yamamoto and Takeo Yoshida. Development of path tracking control for omni-directional mobile robot using visual servo system. *The 27th Annual Conference of the IEEE Industrial Electronics Society*, 2001.

[26] Danai Phaoharuhansa and Akira Shimada. Trajectory tracking for wheeled inverted pendulum robot using tilt angle control. *the 39th Annual Conference of the IEEE Industrial Electronics Society (IECON2013)*, 2013.

[27] Swee Leong Tan and Jason Gu. Investigation of trajectory tracking control algorithms for autonomous mobile platforms: Theory and simulation. *Proceeding of International Conference on Mechatronics and Automation*, 2005.

[28] Jiang Chang and Qingxin Meng. Trajectory tracking control of nonholonomic wheeled mobile robots. *Proceeding of International conference on Information and Automation*, 2010.

[29] Miguel Torres Jose-Luis Peralta and Marcelo Guarini. Trajectory prediction of multiple robocup f-180 autonomous mobile robots for perception-latency compensation. *IEEE 3rd Latin American Robotics Symposium (LARS '06)*, 2006.

[30] Hyun-il Kwon Jong-hyeon Kim Chang-hun Lee M. Latif Anjum Kwang-soo Kim Jaehong Park, Wonsang Hwang and Dong il Dan Cho. High performance vision tracking system for mobile robot using sensor data fusion with kalman filter. *the 2010 IEEE/RSJ International Conference on Intelligent Robots and Systems*, 2010.

[31] Danai Phaoharuhansa and Akira Shimada. Obstacle avoidance for multi-link inverted pendulum robot using virtual impedance. *the 7th SEATUC symposium*, 2012.

[32] Danai Phaoharuhansa and Akira Shimada. Multi-rate discrete control for omni-directional robot in intelligent space. *SICE Annual Conference*, 2014.

[33] Hiroshi Fujimoto Yafei Wang, Binh Minh Nguyen and Yoichi Hori. Vision based multi-rate estimation and control of body slip angle for electric vehicles. *the 38th Annual*

Conference on IEEE Industrial Electronics Society (IECON 2012), pages 4278 – 4283, 2012.

[34] Akira Shimada Yutaka Okubo, Danai Phaoharuhansa. Transportation control by omni-directional robots. *IEEJ Technical Meeting, IIC-13-123 MEC-13-123*, 2013.

[35] Akira Shimada Yutaka Okubo, Danai Phaoharuhansa. A proposition of system design for omni-directional robot. *IEEJ Technical Meeting, MEC-14-077*, 2014.

[36] Yasuhiro Ota. Partner robots - from development to implementation -. *2010 3rd Conference on Human System Interactions (HSI)*, 2010.

[37] Akira Shimada Mousen Ri, Danai Phaoharuhansa. Cooperative system for transportation control using omni-directional robots. *IEEJ Technical Meeting, IIC-13-124 MEC-13-124*, 2014.

[38] Misaki Tsuchimoto Akira Shimada Mousen Ri, Danai Phaoharuhansa. Object transportation assist system using the omni-vehicle. *IEEJ Technical Meeting*, 2014.

[39] Toyota company. Toyota personal mobility, 2014. URL http://www.toyota-global.com/innovation/personal_mobility/.

[40] Wen-Chung Chang and Ping-Rung Chu. An intelligent space for mobile robot navigation with on-line calibrated vision sensors. *the 11th international Conference Control, Automation, Robotics and Vision*, 2010.

[41] Hideki Hashimoto Joo-Ho Lee, Noriaki Ando. Design policy of intelligent space. *The proceeding of IEEE International Conference on System, Man, and Cybernatics*, 1999.

[42] Mariana Rampinelli and Daniel Pizarro. Implementation of an intelligent space for localizing controlling a robotic wheelchair. *2012 ISSNIP Biosignals and Biorobotics Conference : Biosignals and Robotics for Better and Safer Living (BRC)*, 2012.

[43] CHRISTOPHER R. BAKER and JOHN M. DOLAN. Street smarts for boss. *IEEE Robotics and Automation Magazine*, pages 78–87, 2009. ISSN 1070-9932.

[44] Thomas Emter and Andreas Stein. Identification and control for an unknown robot in intelligent space. *the 18th IEEE International Symposium on Robot and Human Interactive Communication*, 2009.

[45] Yuechao Wang Xiaokang Song and Zhenwei Wu. Kinematical model-based yaw calculation for an all-terrain mobile robot. *IEEE/ASME International Conference on Advanced Intelligent Mechatronics, 2008.*, pages 274–279, 2008.

[46] Jer-Jia Sheu Shou-Tao Peng and Chau-Chin Chang. A control scheme for automatic path tracking of vehicles subject to wheel slip constraint. *Proceedings of the 2004 American Control Conference, 2004.*, 1:804 – 809, 2004.

[47] Hyoung-Jin Kang Inyong Hwang Daegun Hong, Paljoo Yoon and Kunsoo Huh. Wheel slip control systems utilizing the estimated tire force. *Proceedings of the 2006 American Control Conference*, 2006.

[48] Michihiro Yamashita and Tadashi Soeda. Development of a new traction control method to suppress wheel-slip of electric locomotives. *Electrical Systems for Aircraft, Railway and Ship Propulsion (ESARS)*, 2012.

[49] Jr. Walter T. Higgins. A comparison of complementary. *IEEE Transactions on Aeorspace and Electronic System*, AES-11(3):321–325, 1975.

[50] Li Chuntao Cao Dong, Qu Qiang. Research of attitude estimation of uav based on information fusion of complementary filter. *2009 Forth International Conference on Computer Sciences and Converence Information Technology*, pages 1290–1293, 2009.

[51] Richard T. BAILLIE. Predictions from armax models. *Journal of Econometrics 12 (1980)*, pages 365–374, 1980.

[52] Richard Szeliski. *Computer Vision: Algorithms and Applications*. Springer, 2011.